Climate Dynamics (1988) 2:205—260

Climate Dynamics

The dynamical range of global circulations — I

Gareth P Williams

Geophysical Fluid Dynamics Laboratory/NOAA, Princeton University, Princeton, New Jersey 08542, USA

Abstract. The dynamical range of atmospheric circulations is examined by integrating a global circulation model (GCM) over a wide range of parameter values. We study the influence of rotation rate on moist and dry atmospheres with regular, drag-free, and interior-heated surfaces in Part I, and on axisymmetric, oblique, and diurnally heated moist atmospheres in Part II. Despite their variety, the circulations are composed of only a few elementary forms whose existence, scale, and mix alter as the parameters vary. These elements can be interpreted in terms of standard symmetric-Hadley (SH) and quasi-geostrophic (QG) theories. The natural-Hadley (NH) circulation consists of a polar jet and a hemispheric direct cell, such as occur in slowly rotating SH flows, together with Rossby waves generated by moist convection and barotropic cascades. The quasi-Hadley (QH) circulation consists of a tropical westerly jet and a narrow direct cell, such as occur in the low-latitude part of rapidly rotating SH flows, together with Rossby waves generated by baroclinic instabilities in the neighboring midlatitude part of the SH flows; it occurs only in moist atmospheres. The two QG circulations represent the two extremes of eddy momentum flux produced during eddy cycles — the special form of enstrophy cascade describing nonlinear baroclinically unstable wave growth and barotropic wave dispersion. The QG_γ element has a latitudinally asymmetric wave dispersion that gives a poleward, jet-traversing momentum transport, while QG_β has a symmetric wave dispersion that gives a jet-converging momentum transport. Both elements have a westerly jet and three cells. (In Part II, we describe the solstitial symmetric-Hadley, the QG-Hadley, the diurnally modified NH, and the Halley circulations.) In moist atmospheres, NH circulations exist in the rotational low range ($\Omega^* = 0$–$\frac{1}{4}$); overlapping QG_γ and QH elements in the midrange ($\Omega^* = \frac{1}{2}$–1); and QG_γ, QG_β, and QH elements in the high range ($\Omega^* = 2$–8); here $\Omega^* = \Omega/\Omega_E$ is the rotation rate normalized by the terrestrial value. In dry atmospheres, circulations follow a similar progression but have a simpler blend because they lack a QH element. Kinetic energy peaks at $\Omega^* = \frac{1}{8}$ in the moist, Hadley-dominated atmospheres but at $\Omega^* = \frac{1}{2}$ in the dry, QG-dominated atmospheres. Instability-generated Rossby waves propagate equatorward more easily in the westerlies of the diabatically driven (moist) Hadley cell than in the easterlies of the eddy-induced (dry) direct cell. Temperatures vary from almost barotropic at $\Omega^* = 0$ to almost radiative-convective at $\Omega^* = 8$, while maintaining almost constant global means. In modified-surface systems, freeslip conditions eliminate the QH element from a moist atmosphere and allow strong deep easterlies to arise in low latitudes to balance the strongly barotropic westerly jets that occur in midlatitudes. In a regular dry atmosphere, enhanced surface heating in low latitudes imitates latent heating and produces a tropical circulation resembling that of the moist QH element. Overall, circulation theory works well in explaining the GCM states but does not, as yet, describe the interactions among elements or reveal how jet scales are determined, nor explain phenomena at the extremes of the parameter range.

1 Introduction

In this paper (to be published in two parts), we generate a comprehensive set of circulations by varying some of the fundamental external parameters and primary internal factors that control the dynamics of a terrestrial global circulation model (GCM). The solutions are developed for two pur-

poses: (1) to study basic circulation dynamics; and (2), to define the parametric variability of circulations. By altering the size, strength, and mix of the eddies, jets, and cells in a variety of flow forms, we hope to developed further insight into how they arise and interact. By developing a wide range of circulations, we hope to gain perspective on the parametric circumstance of Earth's climate and to broaden the data base from which we extrapolate in theorizing about other planets and other climates (Hunt 1979a, b, 1982). To generate as complete a circulation set as possible, we evaluate moist, dry, axisymmetric, oblique, and diurnal model atmospheres over a wide range of rotation rates: $\Omega^* = 0$–8, where $\Omega^* = \Omega/\Omega_E$ is normalized by the terrestrial value.

For the set to be meaningful, the GCM must be valid at all parameter values. We believe this to be so, although we cannot prove it. The GCM has some known limitations, such as the non-universal boundary-layer and radiation formulations, but these do not affect the fundamental structure of the flows. We also assume, in presenting the solutions, the hypothesis that circulation variability is limited to the mix of a few elementary components that can be understood in terms of regular quasi-geostrophic (QG) and Hadley theories. The interpretation of the solutions in terms of these theories is essentially qualitative — just as it is for the terrestrial ($\Omega^* = 1$) case (Held and Hoskins 1985).

The modern view of the terrestrial circulation is still based on the explanation summarized by Lorenz (1967, 1969): that in low latitudes, the time-averaged flow is mainly the product of thermal forcing (as suggested by Palmén) and described by quasi-Hadley (QH) theories; that in midlatitudes, the time- and zonal-averaged flow is essentially the product of forcing by the large-scale eddies (as suggested by Eady, Rossby and Starr) and described by QG theories; and that the two flows and regions interact extensively. In the Northern Hemisphere, strong orographically driven standing waves complicate this view (Wallace and Lau 1985), but we ignore surface inhomogeneities in this paper. The outstanding circulation issue posed by Lorenz in 1969 concerned the role of the eddies in forming and maintaining the angular-momentum characteristics: why is the eddy-momentum transport mainly poleward; what is the basic state with which the eddies interact; what form does the idealized symmetric-Hadley (SH) state take and how does it relate to the natural state? Some of these questions have been resolved and new ones have emerged.

A variety of theories has been developed to describe various aspects of Earth's circulation but a global theory for the flow as a whole, in terms of closure schemes or simple models, is still lacking (Held and Hoskins 1985). Some of these theories also form the basis for describing the various GCM states and are reviewed in § 3. For low latitudes, the SH and wave-propagation theories help explain the mean flow and eddies, respectively, but the two have yet to be combined. Although the correct SH state has been known for a decade (Schneider 1977, Held and Hou 1980), its connection with the basic state felt by the eddies remains obscure. For midlatitudes, the ideas of QG turbulence have given insight into the nonlinear aspects of eddy behavior, revealing a potential-enstrophy spectral cascade towards zonality and barotropy (Rhines 1977); but Earth's sparse eddy sources, narrow spectral range, and strong Ekman-dissipation limit the direct application of the theory. Instead, the simpler spatial cascades associated with the eddy cycles of nonlinear baroclinic instability have proven to be more useful in understanding the eddy heat and angular-momentum fluxes (Simmons and Hoskins 1978, 1980).

Theories concerned with eddy-mean flow interactions have benefitted from being reformulated in terms of the transformed Eulerian mean (TEM) equations. These use the Eliassen-Palm (**E**) or eddy potential vorticity flux as the fundamental measure, rather than the individual eddy heat and momentum fluxes (Andrews and McIntyre 1976). The TEM formulism is advantageous because it directly links the eddy flux with the eddy propagation, and the mean-flow forcing with the divergence of the eddy flux. However, given that the eddy-mean flow interaction is a tightly coupled, two-way process and is partly an artifact of the averaging, the description of circulations (especially turbulent ones) in terms of eddy propagation and flow forcing may be inherently limited (Andrews 1985).

Using the **E** flux to analyze the nonlinear development of baroclinic instability, in so-called eddy-cycle studies, gives a direct view of how the planetary waves generated by the midlatitudinal instability propagate equatorward to influence and end up in the subtropical upper troposphere (Edmon et al. 1980). The poleward eddy-momentum transport of the atmosphere results from the dispersion of the instability-generated Rossby waves and not from the character of the instability itself. Large-scale Rossby waves on a sphere prefer to disperse equatorward, thereby transferring easterly momentum equatorward or, equivalently,

westerly momentum poleward. Calculations with a forced-eddy barotropic model produce the same eddy-momentum transports, thus confirming the unimportance of the character of the instability (Williams 1978, Fig. 3). These nonlinear studies have essentially answered the eddy-momentum issue raised by Lorenz: the poleward transport is caused by the asymmetry of large-scale wave dispersion on a (β-varying) sphere.

Although many questions remain about how these propagating waves interact with the tropical flow and moist convection — this is now the major circulation issue — preliminary explanations mark the emergence of a global circulation theory (Held and Hoskins 1985). The nonlinear-instability studies also imply that closure theories must describe both the midlatitudinal instability mixing and the low-latitudinal wave mixing. Closure theories must also account for the QG and Hadley mean flows. Because large-scale atmospheric motions have a localized forcing, it may be possible to devise ad-hoc closure schemes that are simpler than the fundamental, direct-interaction scheme needed for fully developed planetary turbulence (Salmon 1982). Partial closure schemes that treat the baroclinic component implicitly and the barotropic component explicity are also useful for addressing propagation issues (Williams 1978).

Other major issues are raised by our GCM solutions. In particular, we need to explain how jet widths are determined, how multiple jets interact, and (for solstitial states) how eddies behave in the nonlinear baroclinic instabilities of low-latitude easterly jets. The planets also raise circulation issues (Leovy 1985, Rossow 1985, Williams 1985) and our GCM study was prompted, in part, by parametric studies with simpler barotropic and quasi-geostrophic models that sought to explain the formative processes and terrestrial connection of Jupiter's circulation (Williams 1978, 1979a, b). These studies showed that Jupiter's zonal flow is similar to that of a larger, faster-spinning Earth in midlatitudes, a conclusion extended to low latitudes by the GCM studies (Williams and Holloway 1982). This suggests that the GCM oblique states could be relevant to Saturn and Uranus; the diurnal (low Ω^*) states, to Venus and Titan; and the dry states, to Mars. In Part II, we compare the GCM and planetary states to see if the planets provide useful data for testing the circulation theories.

For the GCM to be general enough for planetary extrapolation, complete enough for terrestrial relevance, and simple enough for theoretical interpretation, we select a moist atmosphere with a zonally symmetric swamp surface and solar insolation; but options are retained. For their ability to describe fully the state of any circulation, in any parametric or physical region, we adhere to the traditional methods of analysis. Thus the description of the solutions focusses on the (time- and longitude-averaged) zonal and meridional flows (the jets and cells), the temperature, and the eddy fields defined by the heat and angular-momentum fluxes. (The preliminary publication in Williams and Holloway (1982) gave instantaneous flow fields only.) Further analysis using the TEM formalism was not possible at the time of computation and this limits our interpretation.

The calculations were made on a TI-ASC computer during 1980–1982 and some solutions are compromised by the computational limits of that era. The presentation begins in § 2 with a description of the basic model and the computational procedure. Section 3 reviews the theories used in defining the circulation elements and in understanding the solutions. Section 4 describes and explains the circulations that arise in the moist model atmosphere as Ω^* varies from 0 to 8. Section 5 does the same for a dry atmosphere, partly to expose the role of latent-heat release in the moist system. Section 6 examines the role of the momentum and heat sources by removing the surface drag and boosting the surface heating. Part II of the paper continues our discussion of circulation dynamics and parametric variability by examining the axisymmetric, oblique, and diurnal moist atmospheres, and the planetary relevance of the GCM solutions.

2 Model physics and equations

Our basic GCM is a version of the so-called swamp A-physics model devised by Holloway and Manabe (1971), updated numerically to incorporate the spectral transforms and implicit time-differencing procedures of Gordon and Stern (1982). Model options allow for the inclusion of seasonal heating (Manabe and Holloway 1975) or diurnal heating (Holloway, unpublished) and the exclusion of latent heating or longitudinal variation. Although the dynamical equations are well defined, the radiative equations involve complex empirical recipes that cannot be documented here.

2.1 System of equations

The primitive equations of motion for a thin hydrostatic atmosphere have horizontal-momentum tendencies that can be written as

$$\frac{\partial \mathbf{v}}{\partial t} = -(\zeta+f)\,\mathbf{k}\times\mathbf{v} - \dot{\sigma}\frac{\partial \mathbf{v}}{\partial \sigma} - \nabla(\Phi+\tfrac{1}{2}\,\mathbf{v}\cdot\mathbf{v}) - RT\nabla(lnp_s) + \mathbf{F}_{\mathbf{v}} \quad (1)$$

with $\sigma(=p/p_s)$, ∇, $\mathbf{k}$, Φ, R, and $\mathbf{F}$ denoting the vertical co-ordinate, spherical horizontal operator, unit vertical vector, geopotential height, gas constant, and diffusion operator, respectively. For a convenient description of all equations and symbols, see Miyakoda (1973) and Haltiner and Williams (1980). For numerical purposes, Eq. (1) is transformed into the (scalar) vorticity (ζ) and divergence (D) equations:

$$\frac{\partial \zeta}{\partial t} = \mathbf{k}\cdot\nabla\times\mathbf{S},\quad \frac{\partial D}{\partial t} = \nabla\cdot\mathbf{S} \quad (2)$$

where $\zeta=\mathbf{k}\cdot\nabla\times\mathbf{v}$, $D=\nabla\cdot\mathbf{v}$, and where $\mathbf{S}$ symbolizes terms on the right side of Eq. (1).

The equations for the temperature and the mixing ratio of water vapor are:

$$\frac{\partial T}{\partial t} = -\mathbf{v}\cdot\nabla T - \dot{\sigma}\frac{\partial T}{\partial \sigma} + \frac{\kappa T\omega}{p} + \frac{Q}{c_p} + F_T \quad (3)$$

$$\frac{\partial r}{\partial t} = -\mathbf{v}\cdot\nabla r - \dot{\sigma}\frac{\partial r}{\partial \sigma} + C + F_r \quad (4)$$

where c_p is the specific heat and $\kappa=R/c_p$, and where $Q(T,r,I)$ and $C(T,r)$ denote the sources or sinks of heat and moisture, with I symbolizing the dependence on insolation.

The mass-conservation equation gives, on vertically averaging, the surface-pressure equation

$$\frac{\partial}{\partial t} lnp_s = -\tilde{\mathbf{v}}\cdot\nabla(lnp_s) - \nabla\cdot\tilde{\mathbf{v}} \quad (5)$$

and, on vertically integrating, a diagnostic for the sigma velocity, $\dot{\sigma}=D\sigma/Dt$:

$$\dot{\sigma} = [\sigma\tilde{\mathbf{v}} - \hat{\mathbf{v}}]\cdot\nabla(lnp_s) + [\sigma\tilde{D} - \hat{D}] \quad (6)$$

where $\hat{(\,)} = \int_0^{\sigma} (\,)\,d\sigma$ and $\tilde{(\,)} = \int_0^{1} (\,)\,d\sigma$ denote the vertical integral and the vertical average. The boundary condition $\dot{\sigma}=0$ at $\sigma=0$ and 1 has been imposed and implies that the top of the atmosphere reflects energy. The pressure velocity $\omega=Dp/Dt$ approximates $-w$ (the vertical velocity), and can be calculated from the identity:

$$\omega = p\left[\frac{\dot{\sigma}}{\sigma} + (\mathbf{v}-\tilde{\mathbf{v}})\cdot\nabla(lnp_s) - \tilde{D}\right] \quad (7)$$

This system of equations for predicting the basic variables ζ, D, T, r, and lnp_s, and the auxiliary variables $\dot{\sigma}$, $\mathbf{v}$, and ω, is completed by an expression for the hydrostatic balance and by writing the velocity in terms of the stream function (ψ) and the velocity potential (χ):

$$\frac{\partial \Phi}{\partial \sigma} = -\frac{RT}{\sigma},\quad \mathbf{v} = \mathbf{k}\times\nabla\psi + \nabla\chi \quad (8)$$

where $\zeta=\nabla^2\psi$, $D=\nabla^2\chi$. The Laplacian operator has spherical harmonics as eigenfunctions and these form the natural basis functions for solving the equations.

2.2 Heat and moisture exchanges

The sources (and sinks) in Eqs. (3) and (4) may be written as

$$Q = Q_* + \delta_m Q_m + \delta_d Q_d + Q_i,\quad C = -P_* - \delta_m P_m \quad (9)$$

according to Manabe et al. (1965). The small-scale latent and sensible heating, Q_m and Q_d, are produced by the moist and dry convective adjustment of air that is hydrostatically unstable and, in the moist case, saturated; δ_m and δ_d are their Kronecker switches. The large-scale condensation heating, Q_*, and precipitation, P_*, occur in saturated (denoted by $_*$) but stable air; here $Q_*=L\cdot P_*$ for the latent-heat coefficient L. Evaporation, E, from the swamp surface provides the only source of vapor via the vertical mixing F_r^V (see Eq. (14)). The term Q_i denotes the radiative heating induced by the insolation.

Small-scale convection occurs when the atmosphere is absolutely unstable ($\delta_d=1$): when the lapse rate, $\Gamma\equiv-\partial T/\partial z$, exceeds the dry adiabatic value $\Gamma_d=g/c_p$. Dry convective adjustment involves resetting T in the vertical in such a way that the potential-temperature gradient, $\partial\Theta/\partial p$, vanishes while conserving the dry static energy $c_p\int Tdp$. Adjusting the lapse rate of the dry adiabat simulates the strong thermal mixing produced by dry convection in the free atmosphere, but ig-

nores the momentum mixing. (When moisture is omitted from the model, we adjust to a hypothetical moist adiabat.)

Small-scale condensation occurs when the atmosphere is conditionally unstable and saturated ($\delta_m = 1$): when $\Gamma_d > \Gamma \geqslant \Gamma_m$ and $r \geqslant r_*$. The moist-adiabatic lapse rate is given by $\Gamma_m = \Gamma_d[1 + r_* L/RT][1 + \varepsilon L^2 r_*/c_p RT^2]^{-1}$ and the Clausius-Clapeyron law determines the saturated mixing ratio $r_*(T)$, where $\varepsilon = 0.622$ is the ratio of the molecular weights of water vapor and dry air. The moist convective adjustment then resets T in the vertical in such a way that $\partial\Theta_e/\partial p$ vanishes while conserving the moist static energy $\int (c_p T + Lr)dp$, where $\Theta_e = \Theta \exp(Lr_*/c_p T)$ defines the equivalent potential temperature. This produces a precipitation rate $P_m = (r - r_*)/\Delta t$ over the time step Δt. The moist adjustment stabilizes the lapse rate, condenses the water vapor, and releases and transfers the latent heat upward to create a warm core in the upper troposphere and a cold core in the lower troposphere, thereby converting potential energy into kinetic energy and representing fundamental aspects of the tropical circulation (Manabe, Holloway, and Stone 1970).

Large-scale condensation occurs when the atmosphere is completely stable and saturated: when $\Gamma < \Gamma_m$ and $r > r_*$. Precipitation then decreases the mixing ratio by $P_* = [r - r_*][1 + \varepsilon L^2 r_*/c_p RT^2]^{-1}$ and increases the temperature by $L \cdot P_*/c_p$.

2.3 Radiative heating

The temperature change due to radiative transfer, symbolized by Q_i in Eq. (9), is calculated using the integration procedures for the long- and shortwave Schwarzschild transfer equations devised by Manabe and Strickler (1964) and Manabe and Wetherald (1967).

For solar radiation, the Schwarzschild equation ought to be solved with parameters for the cloud distribution, reflectivity and absorptivity, as well as for the cosine of the zenith angle of the sun, the optical thickness of ozone, the mixing ratio of water vapor, and the surface albedo. But instead, the transfer is calculated by assigning reflectivities and transmissivities to the scattering layers of cloud and gas.

For terrestrial radiation, three gases are taken into consideration: water vapor, carbon dioxide, and ozone. The distribution of water vapor is computed from Eq. (4) for the troposphere and assumed to connect smoothly to a small constant stratospheric value of 3×10^{-6}. (In the dry model, the climatological moisture is prescribed in tabular form.) The mixing ratio of carbon dioxide is assumed to be constant everywhere at 0.456×10^{-3}, while the ozone mixing ratio is prescribed as a function of latitude and height. The net result (at $\Omega^* = 1$) is that in the stratosphere ozone heats (by solar absorption) and carbon dioxide cools (by thermal emission), while in the troposphere water vapor and carbon dioxide heat (by solar absorption) and water vapor cools (by thermal emission).

The solar radiation at the top of the atmosphere is specified as a function of latitude only and is based on the annual-mean zenith angle at each latitude. The annual-mean cloud distribution is specified as a function of latitude at three heights (high, middle, and low). The swamp and cloud albedos are specified as a function of latitude. Diurnal and seasonal variations in the zenith angle are added to the GCM in Part II.

2.4 Grid and surface exchanges

The horizontal diffusion of all fields is represented by the scale-selective biharmonic operator, thus:

$$(F_\zeta^H, F_D^H) = -\kappa_H \left(\nabla^2 + \frac{2}{a^2}\right)^2 (\zeta, D),$$
$$(F_T^H, F_r^H) = -\kappa_H \nabla^4 (T, r) \tag{10}$$

where $\kappa_H = 1 \times 10^4$ km^4 s^{-1}. This empirical value of the diffusion coefficient — derived from experience with weather and climate models — is used for all integrations, even though it may not be optimal at all Ω^*. The formulation works well, but its validity when $\Omega^* \to 0$ is unknown.

The vertical diffusion of vorticity and divergence is derived from the (downward) momentum fluxes:

$$F_\zeta^V = \mathbf{k} \cdot \nabla \times \mathbf{F}_v^V, \quad F_D^V = \nabla \cdot \mathbf{F}_v^V \tag{11}$$

$$(F_u^V, F_v^V) = \frac{1}{\rho} \frac{\partial}{\partial z} (\tau_\lambda, \tau_\theta),$$

$$(\tau_\lambda, \tau_\theta) = \rho \kappa_V \frac{\partial}{\partial z} (u, v) \tag{12}$$

Invoking the mixing-layer hypothesis for a neutrally stratified atmosphere, we select a simple planetary-boundary-layer (PBL) model based on

a constant-flux Prandtl layer and a superposed Ekman layer, defining $\kappa_V = l^2 |\partial \mathbf{v}/\partial z|$ where l is the mixing length with the simple vertical form $l = \kappa_0 z$ for $0 < z \leqslant z_P$, $l = \kappa_0 z_P (z_E - z)/(z_E - z_P)$ for $z_P < z < z_E$, and $l = 0$ for $z \geqslant z_E$. The heights of the Prandtl and Ekman boundary layers are fixed at $z_P = 75$ m and $z_E = 2.5$ km, respectively, and the value of the von-Kármán constant is $\kappa_0 = 0.4$. The same mixing-length formulation is used for the diffusion and (upward) flux of sensible heat and moisture:

$$F_T^V = -\frac{1}{\rho c_p}\frac{\partial H}{\partial z}, \quad H = -\rho c_p \kappa_V \frac{\partial}{\partial z}(T + \Gamma_d z) \tag{13}$$

$$F_r^V = -\frac{1}{\rho}\frac{\partial E}{\partial z}, \quad E = -\rho \kappa_V \frac{\partial r}{\partial z} \tag{14}$$

At the surface level (denoted by s) the stress and upward fluxes of heat and moisture are defined by:

$$\tau_\lambda^s = \rho c_D |\mathbf{v}| u, \quad \tau_\theta^s = \rho c_D |\mathbf{v}| v \tag{15}$$

$$E_s = \rho c_D |\mathbf{v}| [r_*(T_s) - r],$$

$$H_s = \rho c_p c_D |\mathbf{v}| [T_s - T\sigma^{-\kappa}] \tag{16}$$

where ρ, c_D, $\mathbf{v}$, T, r, σ are evaluated at the lowest level, $z = z_P$, and where $|\mathbf{v}|$ has a lower bound of 1 m s^{-1}. For $z_P = 75$ m and a smooth swamp surface, the drag coefficient c_D equals 1×10^{-3}. The shallow swamp acts only as a source of moisture (via the evaporation, E_s) and has no heat capacity. The surface temperature is thus given by the balance requirement

$$bT_s^4 + H_s + LE_s - (1 - A_s)I_s - F_s^\downarrow - Q_e = 0 \tag{17}$$

where b, A_s, I_s, $F_s^\downarrow$, and Q_e denote the Stefan-Boltzmann constant, the surface albedo, the insolation reaching the surface (after reduction by the atmospheric albedo, A_a), the downward flux of terrestrial radiation, and a sublayer heat source (normally zero), respectively. The albedo A_a varies from 0.3 in low latitudes to 0.35 in midlatitudes and to 0.4 near the pole, while A_s varies from 0.06 to 0.1 to 0.4 (Smagorinsky 1963, Table A2). No ice-albedo feedbacks are incorporated: our swamp has antifreeze.

At the top of the atmosphere, we specify a solar constant of 1.92 ly min^{-1} and assume the downward long-wave radiation to be zero.

2.5 *Non-universal model features*

As a representation of Earth's atmosphere, the GCM has significant deficiencies. For example, it omits land surfaces and ocean transports, it does not forecast the cloud, carbon dioxide and ozone distributions, and it has no snowcover or ice-albedo feedbacks. The imposed distributions of the minor gases, clouds, and albedo in the radiation calculation relate only to the $\Omega^* = 1$ state and at other Ω^* produce only a relative forcing and circulation. But for our purposes any reasonable thermodynamical forcing suffices and the strong tuning of the radiative heating to conditions at $\Omega^* = 1$ at least provides a realistic reference state.

A more troublesome non-universality having a more direct dynamical impact lies in the PBL formulation. In the GCM, the PBL is assumed to be neutrally stable so that only mechanical mixing occurs and the associated Prandtl- and Ekman-layer depths are fixed at empirical values. This prescription provides a reasonable first approximation for $\Omega^* = 1$ studies. Although a formulation with $z_E \sim \Omega^{-1}$ would be more appropriate for an Ω^*-varying GCM, even it fails at low Ω^*. Given such limitations, we decided not to make the PBL formulation a function of Ω^*. Thus the PBL parameters, like the radiation ones, are fixed at their $\Omega^* = 1$ values. This is not a satisfying compromise to make but it does eliminate the great inconvenience of having to make the vertical grid spacing a function of Ω^*. We believe that these PBL limitations mainly affect the surface winds and do not significantly influence circulation structure.

2.6 *Numerical algorithms*

The numerical integration of the GCM uses finite differencing in the vertical, spectral transforms in the horizontal, and semi-implicit differencing in time — for details, see Gordon and Stern (1982).

In the time scheme, the linear components of the equations are integrated implicitly to dampen and slow the gravity waves, thereby allowing a five-fold increase in the time step. This feature may be less desirable at low Ω^* because the gravity waves then play a more fundamental role, but the issue is not explored. A Robert time filter with a coefficient of 0.01 prevents the time-splitting instability in all solutions except the axisymmetric ones — where a value of 0.04 is needed.

The model has nine levels in the vertical, with two in the boundary layer, two in the stratos-

phere, and five in the troposphere. The variables ζ, D, T, r, Φ, ω are defined at $\sigma = 0.025$, 0.095, 0.205, 0.350, 0.515, 0.680, 0.830, 0.940, 0.990 which, for $p_s = 1000$ mb, correspond to the pressure levels seen in, e.g., Fig. 2. Vertical gradients and the $\dot{\sigma}$ velocity are calculated at half levels, starting at the surface where $\dot{\sigma} = 0$.

The GCM uses surface spherical harmonics to represent the horizontal distributions of the basic fields and the spectral transform method to convert their nonlinear products from physical to spectral form. In this spectral representation, all variables are expanded (at each level) as

$$Z(\lambda, \theta, t) = \sum_{m=-M}^{M} \sum_{n=|m|}^{|m|+M} Z_n^m(t)\, Y_n^m(\lambda, \theta) \qquad (18)$$

where Z_n^m are the time-dependent coefficients, and $Y_n^m = P_n^m(\sin\theta)\, e^{im\lambda}$ are the spherical harmonics based on associated Legendre polynomials of degree n and order m in latitude (θ) and on trigonometric functions in longitude (λ). M denotes a rhomboidal wavenumber truncation in which each zonal wavenumber, m, has the same number of latitudinal modes, whose wavenumber is $n - |m|$.

To evaluate the nonlinear advection and the local physical processes, the spectral coefficients are transformed onto at least $N_\lambda = 3M + 1$ longitudinal gridpoints to ensure exact alias-free Fourier transforms and onto at least $N_\theta = (5M+1)/2$ Gaussian-latitude gridpoints, θ_j — which are given by the zeros of $P_{N_\theta}(\sin\theta_j) = 0$ and are almost equally spaced — to ensure an exact Gaussian quadrature of the Legendre transform. The nonlinear products, such as $u\zeta$, are evaluated on the Gaussian grid and then transformed back to the spectral domain — where their horizontal derivatives may be treated analytically — using a Gaussian quadrature transform

$$Z_n^m = \sum_{j=1}^{N_\theta} W_j(\theta_j)\, Z_m(\theta_j)\, P_n^m(\sin\theta_j) \qquad (19)$$

for the Fourier coefficient Z_m that involves a summation over the N_θ Gaussian latitudes with the Gaussian weights W_j ($\simeq \cos\theta_j \cdot \Delta\theta_j$).

For our idealized problems, a sector of a hemisphere suffices as an integration domain. Sector models involve only $M/2$ latitudinal modes and M/I_λ longitudinal modes, where I_λ is the number of sectors. They are equivalent to having a freeslip equatorial boundary and a periodicity over $2\pi/I_\lambda$ longitude. (In Part II, solstitial states are evaluated with a two-hemisphere crescent.) In our calculations we use $M = 15$, 30, and 42 to provide low, medium and high resolutions. These resolutions allow $I_\lambda = 3$ and the division of a hemisphere into 120° sectors — domains that provide a good representation of longitudinal activity and whose computational economy makes this study feasible. The R42 system (rhomboidal truncation with $M = 42$) uses 53 gridpoints between the equator and pole and 43 gridpoints over 120° of longitude, giving spacings of $\Delta\theta \simeq 1.7°$ and $\Delta\lambda \simeq 2.8°$. Table 1 lists the characteristics of the various resolutions and domains used in obtaining the various solutions.

Table 1. Spectral and grid characteristics of the models

System	Resolution	Sector Width	Hemispheres	N_θ[b]	$\Delta\theta$	N_λ[b]	$\Delta\lambda$	Δt (mins)	Main solution series
A	R15[a]	120°	1	20	4.5°	16	7.5°	30	Non-diurnal
B	R15	120°	2	40	4.5°	16	7.5°	30	Oblique
C	R15	360°	1	20	4.5°	48	7.5°	30	Diurnal
D	R30	120°	1	40	2.2°	32	3.7°	20	Dry
E	R42	120°	1	53	1.7°	43	2.8°	15	Moist
F	R42	9°	1	53	1.7°	10	0.9°	10	Axi-symmetric
G	FD[c]	≡360°	≡1	64	≡1.5°	128	≡3.0°	15	Quasi-geostrophic

[a] R15 denotes a rhomboidally truncated representation with 15 zonal waves over 360° of longitude, or 5 waves over 120°. All GCMs have 9 vertical levels

[b] N_θ = number of latitudinal gridpoints per hemisphere (or globe in system B); N_λ = number of longitudinal gridpoints per sector

[c] FD denotes a finite-difference representation. The QG_2 model has two vertical levels and a hemisphere-size β-plane

To analyze the solutions, the data on the Gaussian grid is converted to the uniform latitude-longitude grid of the diagnostics routine.

2.7 Computational range and procedure

Calculations are made for the range of parameter values and resolutions listed in the various integral tables. In Part I, we create the MOIST(Ω^*), DRY(Ω^*), SURFACE SLIP, ENHANCED HEATING, and QUASI-GEOSTROPHIC sets to examine the influence of rotation, moisture, surface drag, surface heating, and Coriolis gradient (β) on circulation dynamics. In Part II, the AXISYMMETRIC(Ω^*), OBLIQUE(Ω^*, θ_P), DIURNAL(low Ω^*), and HIGH CLOUD sets examine the role of longitudinal variation, obliquity, diurnal heating, and cloud opacity.

The initial condition adopted in all calculations is that of a resting atmosphere at a temperature of 288 K. Integrations begin with an R15 resolution and continue with the preferred higher resolution (R30, R42) until the global integrals equilibrate. The periods of integration range from 1 to 3 years (see Tables) with the longer times occurring in the lower Ω^* cases and involving dynamical rather than thermodynamical variations — perhaps because of insufficient dissipation. The time-mean equilibrium states are defined by averaging 30–90 days of data (using 1 value per day) for the high-resolution cases, and 100–200 days of data (using 1 value per 5 days) for the low-resolution cases.

3 Circulation dynamics

Circulations are usually described in terms of jets, cells, and eddies, and are interpreted in terms of an eddy-mean flow interaction that involves two coupled processes: the action of the mean-state on the genesis, development, and propagation of the eddies; and the action of the eddies on the development of the mean-state. To be complete, interpretations must consider both processes, preferably simultaneously, and also consider contributions from the diabatic heating and the diffusion.

The GCM states involve interactions between regions as well as between eddies and mean flows and it is then useful to define the circulations in terms of local "elements" — each one consisting of a jet, 1–3 cells, and characteristic eddy fluxes. These elements are isolated from the solutions and are based on the standard Hadley and QG theories reviewed in § 3.1 and 3.2. An isomorphism between these two classes of theory is described briefly in § 3.3. To emphasize the limits of any interpretation based on elementary GCM diagnostics, we review the traditional and transformed formalisms for eddy-mean flow processes in § 3.4. These suggest that the elements and the interactions among elements could be defined more fundamentally than in this paper.

3.1 Hadley dynamics

Hadley modes, driven by the diabatic heating, contribute strongly to the mean state of many circulations but they remain poorly understood. Only the symmetric-Hadley (SH) state has been theoretically defined and then only recently. Hadley states subjected to internally or externally generated planetary waves have been isolated qualitatively from the GCM solutions in the form of natural-Hadley (NH) or quasi-Hadley (QH) elements, but they lack a theoretical definition.

Symmetric-Hadley (SH) theory. The present understanding of SH circulations comes from the incisive geometric argument of Schneider (1977) and Held and Hou (1980). According to this theory, steady-state SH circulations exist in a balance between a momentum wind plus Hadley cell in lower latitudes and a thermal wind in higher latitudes. The system is driven by a solar heating that tries to create a temperature field $T_E(\theta, z)$ in a radiative-convective equilibrium, with a baroclinicity Δ_H and a static stability Δ_V; here, both quantities are normalized by the global mean temperature T_0 in a Boussinesq atmosphere of depth H. The baroclinicity produces a westerly thermal wind, given by

$$\left(fu_E + \frac{u_E^2}{a}\tan\theta\right) = -\left(\frac{gH}{aT_0}\right)\frac{\partial T_E}{\partial\theta},$$

that exists freely in higher latitudes.

In lower latitudes, however, such a thermal wind exceeds the maximum flow allowed under angular-momentum conservation — the so-called momentum wind, $u_M = a\Omega\sin^2\theta/\cos\theta$ — and cannot generally exist. Consequently, a Hadley cell arises in lower latitudes to reduce the baroclinicity and to maintain consistent zonal winds. Angular momentum is then conserved by the zonal wind associated with the upper, poleward-flowing

branch of the Hadley cell that rises at the equator, so that $u(\theta, H) = u_M(\theta)$. In the lower branch, the surface drag leads to a near-vanishing wind, so that $u(\theta, 0) = u_s(\theta) \simeq 0$. The shear, $u_M - u_s$, in this quasi-inviscid atmosphere induces — via the inverse of the thermal-wind balance — a "dynamical-temperature" field, T_D, that deviates significantly from T_E. This heat imbalance drives the Hadley cell, setting its strength and latitudinal extent θ_H.

From the thermal-wind balance, the conservation of heat, and the upper-level conservation of angular momentum, the SH theory predicts the cell width, the vertically averaged heat and momentum fluxes, the position of the upper-level jet, and the distribution of the surface winds; all (when nondimensionalized) as universal functions of the external Rossby number $R_E = gH\Delta_H/(a\Omega)^2$. Although it seems surprising that such a simple theory for a nonlinear meridional circulation should yield so many simple results, the situation is not unique: the β-turbulence theory produces similar insights and even possesses an isomorphism with the SH theory — see § 3.3.

For $R_E \ll 1$, the theory predicts that the Hadley cell extends to the core of a tropical jet, close to the latitude where u_E and u_M interact, to $\theta_H = (\frac{5}{3} R_E)^{1/2}$ — about 30° for Earth. Although the cell reduces the tropical baroclinicity to near zero, its weak overturning fails to alter the static stability, S, from its radiative-convective value Δ_V. As R_E increases, circulations switch from geostrophy to cyclostrophy near $\Omega^* = \frac{1}{2}$ (and $\theta_H = 55°$), a rate at which the GCM is baroclinically unstable. For $R_E \gg 1$, the theory predicts that the Hadley cell extends to the core of a polar jet at $\theta_H = 1 - 3/8R_E$ — about 90° for Venus. The strong heat transport of the cell at low Ω^* reduces the global baroclinicity to near zero and its strong overturning controls the static stability, so that $S \simeq O(\Delta_H/3)$. A third of the radiative heating goes into the vertical transport, the rest into the horizontal transport.

The numerical SH studies of Held and Hou (1980), while confirming the basic predictions of the theory, show that the geometric argument, because of its integral character and its neglect of the internal structure, oversimplifies the meshing of the thermal and momentum winds at θ_H. They reveal that a second jet occurs just poleward of θ_H when the vertical mixing is weak. (This second jet also occurs in the AXISYMMETRIC solutions with high Ω^*.) The weak friction prevents the development of symmetric instabilities. The SH state is an intrinsic circulation mode, even though it is prone to symmetric, baroclinic, and barotropic instabilities.

The SH mode is useful for defining the NH and QH elements and for interpreting the AXISYMMETRIC circulations (in Part II). However, some of the SH theoretical assumptions are not always met in the parametric and physical range encompassed by the GCM solutions. For example, for the thermal-wind (dynamic-temperature) balance to hold requires that $fu \gg \nabla \cdot (\mathbf{v}v)$ over most of the Hadley cell, a condition that may not hold when the cell is confined to the equatorial region. Thus the $R_E \to 0$ limit of the theory may be approached when $\Omega^* = 8$ (and $\theta_H = 5°$). A strong surface drag, a steady state, and a single vertical scale are also crucial. The SH theory applies, at best, only to flows close to the equinoctial limit in which the heating is symmetrical about the equator. In Part II, we modify the geometric argument for the solstitial limit in which the hottest region lies at the summer pole.

The natural-Hadley (NH) element. The closest an atmosphere comes to realizing an SH state is when the rotation rate is low enough ($\Omega^* < \frac{1}{4}$) to exclude baroclinic instability. Then natural-Hadley (NH) circulations exist that can be thought of as a combination of an SH($R_E > 1$) mode and momentum-transporting planetary waves (Fig. 1, col. 4). In moist atmospheres, the waves are generated by the convective eddies that transfer heat upward and momentum downward at the equator, and by barotropic cascades in the polar jet. The wave propagation results in a latitudinally uniform eddy kinetic energy (Fig. 5h and i) and in equatorial westerlies. In dry atmospheres, the waves are confined to the jet region and the equatorial westerlies are much weaker.

The mean flow of the NH element, as isolated from the GCM low-Ω^* solutions, has most of the characteristics of the SH($R_E > 1$) mode: a polar jet with dual momentum and thermal winds, a low baroclinicity, and a wide Hadley cell whose extent increases as Ω^* decreases. In the dry case, the cell has a broader upward flow but the same amplitude as in the moist case, as theory predicts. To understand the eddy transports requires a theoretical study of how planetary waves propagate in the modified beta field $\tilde{\beta} = \beta - u_{yy}$ provided by the u_M and u_E winds of the SH($R_E > 1$) state. Waves cannot propagate at the tropopause until they modify the SH state because $\tilde{\beta} = 0$ in the u_M wind. At low Ω^*, only the zonal flow and the largest waves are stable to the wave-wave resonances that energize the eddies (Baines 1976). Because the NH

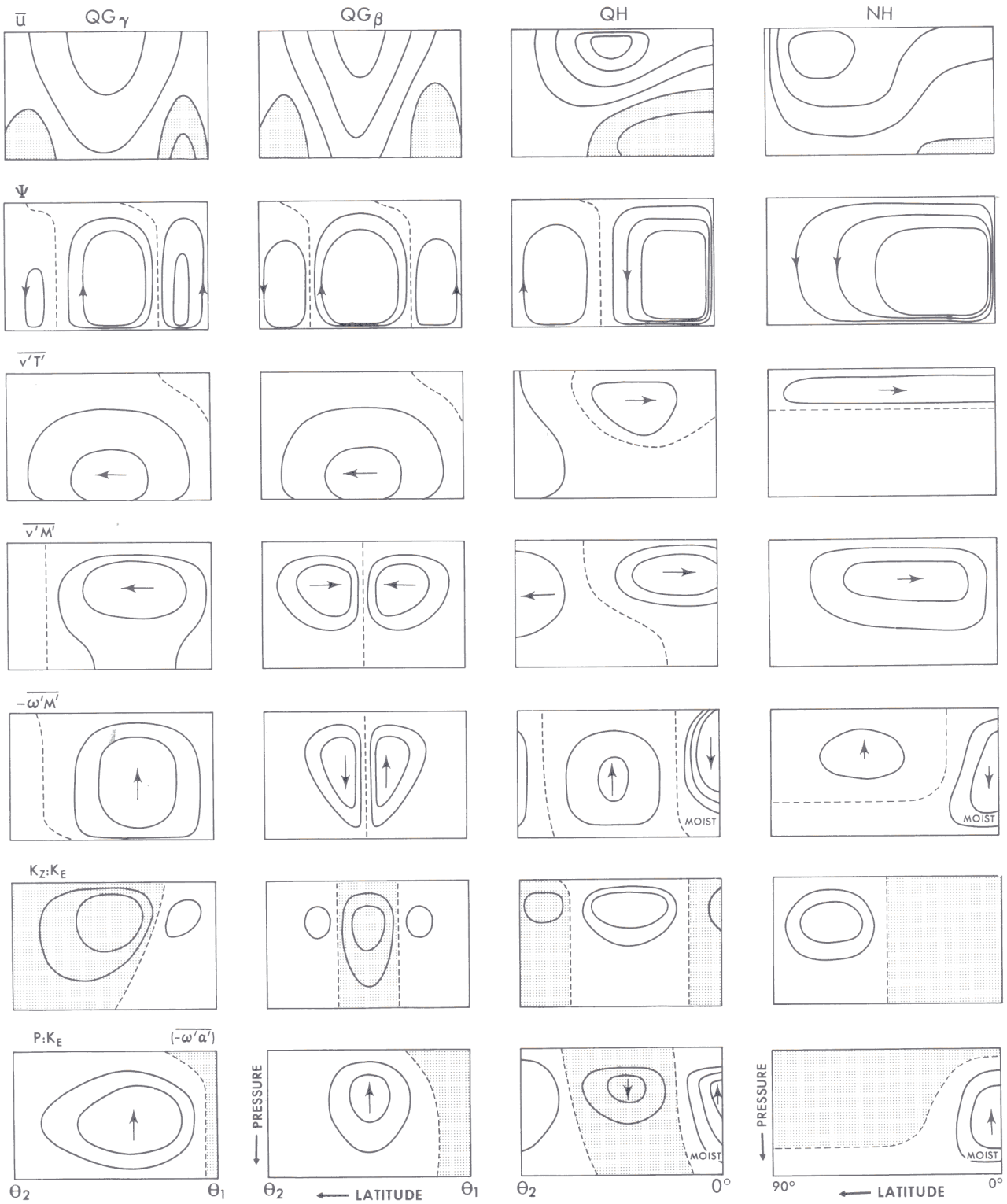

Fig. 1. Schematic summary of the quasi-geostrophic (QG_γ and QG_β), quasi-Hadley (QH), and natural-Hadley (NH) circulation elements in terms of their mean flows and eddy fluxes. Here $\bar{u}$ is the mean zonal wind, $\bar{\Psi}$ the mean stream function, $\overline{v'T'}$ the mean meridional eddy heat transport, $\overline{v'M'}$ the mean meridional momentum transport, $-\overline{\omega'M'}$ the mean vertical momentum transport, $K_Z:K_E$ the barotropic energy conversion, and $P:K_E$ the baroclinic energy conversion (see text for details). *Shading* denotes negative values

eddy transports, with their export of easterly momentum from source regions and their weak up-gradient heat transfer, are typical of Rossby waves (Dickinson 1978) and because Rossby waves are the major waveform at $\Omega^* = 1$ (Hayashi 1974), we consider the NH eddies to be low-Ω^* planetary waves.

The Quasi-Hadley (QH) element. A Hadley mode also exists when the baroclinic instability is active. Such quasi-Hadley (QH) modes are easily identified in GCM solutions with a high Ω^* because they are then confined more to low latitudes and the adjacent instability is smaller, weaker, and confined more to midlatitudes. The MOIST(4) solution provides the clearest definition of the QH element shown in Fig. 1, col. 3. The QH element does not occur in dry atmospheres because the dry Hadley mode is uniform and easily overwhelmed by the eddy-induced QG circulation. But in moist atmospheres the QH element survives because the confined upward flow gives the Hadley cell a greater robustness.

The QH element in Fig. 1 has a strong Hadley cell extending to the core of a strong westerly jet and a weak Ferrel cell coinciding with the surface westerlies needed to balance the strong easterly trade winds. The planetary eddies behave like Rossby waves by transporting heat and momentum mainly equatorward. They are generated by a neighboring baroclinic instability and by the convective eddies that transport heat upward and momentum downward at the equator. The QH element can be thought of as the tropical part of an SH($R_E < 1$) circulation subjected to externally and internally generated waves, in contrast to the view of the NH element as a full SH($R_E > 1$) circulation subjected to internally generated waves. The structure and scale of the QH westerly jet and Hadley cell are consistent with those produced by the interplay of the u_M wind and the subtropical part of the u_E wind in the SH($R_E < 1$) state.

To explain the easterly trade winds, eddy transports, and Ferrel cell requires a theory describing the instability of the u_E wind of the SH($R_E < 1$) circulations and the subsequent propagation and absorption of the dispersing Rossby waves in the u_M wind. Existing theory for Earth shows that the observed mean winds (at $\Omega^* = 1$) have a critical latitude in their easterlies that blocks the equatorward wave propagation (Held and Hoskins 1985). In the QH element, however, waves can propagate aloft in the westerlies because the easterly trade winds are never deep enough to block them. Wave propagation differs in a dry atmosphere: the QH westerlies do not form and the QG eddies induce a weak direct cell and weak, deep, blocking easterlies — the waves deposit enough easterly momentum to prevent further transmission and to trap the instability.

The QH and NH elements have much in common because of their similar wave forms and their common SH background — only R_E varies. Comparing them indicates that the QH easterly trade winds can be attributed to changes induced by the adjacent baroclinic instability.

3.2 *Quasi-geostrophic dynamics*

QG processes control the eddy fluxes and the eddy-induced mean flows of GCM states with $\Omega^* \geqslant \frac{1}{4}$. Thus we can use linear baroclinic instability theory to explain eddy origin and scale, and nonlinear baroclinic instability theory to explain eddy evolution and fluxes. The latter theory leads us to define $QG_{\gamma,\beta}$ elements in terms of eddy cycles involving the growth, decay and propagation of eddies. Eddy cycles are a special (inhomogeneous) form of enstrophy cascade. The general (homogeneous) cascades of QG turbulence theory give further insight into how planetary eddies behave and how zonal flows develop a barotropic component.

Linear baroclinic instability. Baroclinic instability is the main source of transient variability in circulations with $\Omega^* \geqslant \frac{1}{4}$. The instability is produced by baroclinicity at the lower surface and by sign changes in the internal gradient of mean potential vorticity, $\bar{q}_\theta$. The two-level quasi-geostrophic (QG_2) model describes the internal instability of waves that extend over the scale height, H. The QG_2 instabilities occur when the eddy size, vertical shear (between the layers), and baroclinicity exceed the minimum critical values $L_c = 2.4\pi L_R$, $U_c = 0.5\,\beta L_R^2$, and $\Delta T_c = \beta f Y L_R^2 R^{-1}$, shown in Table 2 for Ω^* ranging from 1/4 to 4; here $L_R = NH/f$ is the Rossby radius, β the Coriolis gradient, and Y the channel width. When $\Omega^* = \frac{1}{4}$, L_c greatly exceeds the Earth's radius and an instability occurs only if the baroclinicity

Table 2. Minimum values of the critical eddy size, vertical shear, and baroclinicity for instability in the QG_2 model

Ω^*	L_c (10^3 km)	$2U_c$ (ms^{-1})	ΔT_c (K)
4	1.5	2.5	35
1	6.0	10.0	35
¼	24.0	40.0	35

greatly exceeds ΔT_c. Such values ($\simeq 150$ K) are not realized, so the atmosphere is effectively stable to a deep instability when $\Omega^* = \frac{1}{4}$. Although the QG_2 eddies become larger and stronger as Ω^* decreases, they eventually become extinct because the domain becomes too small to support them.

Atmospheric instabilities do not experience the sharp QG_2 long-wave cutoff but, rather, disappear gradually over a transitional range near $\Omega^* = \frac{1}{4}$ by becoming shallower and less efficient (Held 1978). Such instabilities are influenced more by the surface baroclinicity than by the internal $\bar{q}_\theta$, and are described by Charney's (1947) model. Waves destabilized by the surface baroclinicity penetrate to the height $h = H^2 u_z/\beta L_R^2$ if $h < H$, otherwise they end at the tropopause. The value of h decreases as Ω^* decreases, so shallow instabilities occur naturally in the transitional Ω^* range. The horizontal scale of the shallow instabilities, $l = Nh/f = Hu_z/\beta L_R$, is dependent on β and the shear, unlike the instabilities of depth H which asymptote to a scale proportional to L_R alone. For a given baroclinicity, the linear growth rate $\sigma_i = 0.3\ (g\Theta_y/N\Theta_0)$ is virtually independent of the rotation rate and so most GCM flows have similar dynamical time scales. The basic state on which the instability grows lies somewhere between the SH and zonal-mean states. These ideas hold for the GCM because the static stability (fixed in the theory) is mainly controlled by radiation and convection, not by the instability.

The eddy heat transport produced by Charney's linear instability is confined to lower levels and is down-gradient (poleward and upward). An eddy momentum transport occurs only if a lateral shear or non-β sphericity effects are present, but its behavior does not follow simple rules (Simmons 1974, Hollingsworth 1975, Held and Andrews 1983). When $\Omega^* = 1$, the eddy momentum flux $\overline{v'u'}$ produced by a linear instability tends to peak at lower levels and to converge onto the core of a jet lying in midlatitudes (or on a β-plane), and to traverse poleward across a jet lying in high latitudes (Simmons and Hoskins 1976). On Earth, however, the flux peaks aloft and traverses poleward across a midlatitude jet. To understand the terrestrial flux clearly requires a nonlinear theory and a spherical domain; linear theory and the midlatitude β-plane give an inadequate guide. The vertical fluxes of momentum and heat correspond systematically with the horizontal ones because of the close correlation between v and w: thus a converging $\overline{v'u'}$ flux has a bimodal $\overline{w'u'}$, with upward (downward) and poleward (equatorward) transports coinciding.

Most linear instabilities induce three meridional cells, with the central Ferrel cell dominating and coinciding with the peak eddy energy. These cells arise to restore the thermal wind balance and are forced by meridional variations in the eddy heat flux convergence and by vertical variations in the eddy momentum flux convergence (see Eq. (23) below). The former dominates for linear modes and accelerates the westerly jet near the surface.

Nonlinear baroclinic instability: eddy cycles. The original integrations of the dry, spherical GCM equations first revealed the character of nonlinear baroclinic instability (Smagorinsky 1963, Smagorinsky et al. 1965). They showed that the time-averaged momentum fluxes obtained by following eddy development through cycles of growth and decay differ radically from those of linear theory but closely match the observed. More detailed analyses of such "eddy cycles" indicate that, for a specified zonal flow, linear theory applies for the first few days, with the midlatitudinal eddy energy growing exponentially at all heights but transporting heat poleward mainly at low levels (Simmons and Hoskins 1978, 1980; Edmon et al. 1980). After 6 days, the unstable wave eliminates the surface temperature gradient and the low-level growth ceases. The upper-level eddy energy, fed by the upward wave radiation, continues to grow until about day 8. Then the upper-level troughs develop a SW–NE tilt and generate the planetary waves that propagate into the subtropics and produce a large poleward momentum flux. During this barotropic decay phase of the instability, the eddy kinetic energy is converted into zonal kinetic energy. Averaged over the cycle, the momentum flux is poleward and strongest aloft, in agreement with observation.

Similar cycles occur in barotropic models with a forced-eddy source representing the instability (Williams 1978, § 7a, b). The momentum flux generated by the wave dispersion in the baroclinic and forced-barotropic eddy cycles has no connection with the flux associated with the linear instability. The dominance of the upper-level mixing in nonlinear flows means that the complexity of the mixing in the instability can be ignored when studying the interaction between the propagating waves and the Hadley cell and convection.

Although the sequence of events in the eddy cycle can be explained in terms of linear growth, nonlinear cessation of growth, wave propagation and wave absorption in subtropical enstrophy-dissipating critical layers, the overall eddy fluxes

cannot be expressed simply in terms of the time-averaged basic fields. Thus the poleward eddy fluxes of Earth's atmosphere and the GCM at $\Omega^* = 1$ can only be understood in terms of an eddy-cycle scenario involving baroclinic instability and barotropic wave dispersion. Consequently, we try to describe all GCM states in terms of standard elements whose fluxes are, or could be, understood in terms of eddy cycles. Simpler interpretations, especially those based on linear or midlatitude β-plane theories, could be misleading. Unfortunately, however, existing eddy-cycle scenarios do not provide complete explanations because they are based on arbitrarily specified zonal flows and do not equilibrate. Eddy cycles based on the SH state would be less ambiguous, self-consistent, and more closely related to statistically steady states. They might then, for example, explain what determines the lateral scale of a jet — assumed to be close to L_R in the above calculations.

The QG_γ, QG_β elements. The two quasi-geostrophic elements used in describing the GCM states represent the two extremes — as measured by the eddy momentum flux — between which most QG flows lie (Fig. 1, cols. 1 and 2). The QG_γ element idealizes flows with momentum transports that are poleward-traversing ($\overline{v'M'} > 0$) and monotonically upward ($-\overline{\omega'M'} > 0$). Its zonal flow consists of a westerly jet and peripheral, low-level easterlies that together give a zero net surface torque. The meridional flow consists of a dominant Ferrel cell and a pair of weak direct cells — the polar one sometimes vanishes. The eddy heat transport is entirely poleward ($\overline{v'T'} > 0$) and is strongest at lower levels. The eddies are energized by the potential energy conversion ($\{P:K_E\} > 0$) and they support the mean zonal flow ($\{K_Z:K_E\} < 0$).

The QG_γ element corresponds to the flow produced in the *nonlinear* baroclinic instability calculations described above. The QG_γ fluxes can be understood only in terms of an eddy-cycle scenario: the linear instability phase gives the poleward heat flux at lower levels, while the wave dispersion phase gives the poleward momentum flux at upper levels. The eddies induce the three cells and the surface wind variation. The momentum flux is poleward because *large* planetary waves disperse asymmetrically from midlatitudes and favor equatorward propagation. To understand the QG_γ element better it would be useful to evaluate linear and nonlinear baroclinic instability on the *equatorial* β-plane because it allows an asymmetric wave dispersion.

The QG_β element in Fig. 1 idealizes flows with the converging lateral and bimodal vertical eddy momentum transports. Otherwise the element generally resembles QG_γ. The fluxes do, however, produce a sharper jet and deeper easterlies. The QG_β flow corresponds to the flow produced by nonlinear baroclinic instability calculations on a midlatitude β-plane. No eddy-cycle calculations have yet been made for such a flow on a sphere but it seems reasonable to assume that the converging momentum flux occurs because the wave dispersion is symmetrical, with equal propagation towards equator and pole. Symmetrical dispersion can occur on a sphere only if β is relatively constant across the element, a condition favored by narrower jets, smaller eddies, and lower latitudes, i.e., by the high-Ω^* states. Consequently, the QG_β element (like the QH) cannot exist on its own on a sphere, but the QG_γ (like the NH) can. It should now be obvious that the γ and β subscripts symbolize the asymmetric and symmetric sphericity effects associated with variable and uniform Coriolis gradients.

In the GCM solutions, for example, the QG_γ element exists on its own in the DRY(1) flow and as the poleward partner of a QG_β element in the DRY(2) flow. In the MOIST(1) state, the QG_γ element partners and interacts with a tropical QH element by inducing its eddy fluxes. In the MOIST(2) state, a QG_β element lies in midlatitudes between a polar QG_γ element and a tropical QH element. The various elements interact with each other and the underlying zonal flows are created in ways that need to be examined by calculating the eddy cycles of unstable SH states at various Ω^*.

Geostrophic turbulence. Nonlinear baroclinic instability, with its conversion of potential energy to kinetic energy, describes a special form of potential enstrophy cascade, and eddy cycles, with their limited spectral representation (e.g., $k_\lambda = 6$, 12, 18 ...), provide an idealized, wave-like description of these special cascades. The most general form of enstrophy cascade is described by QG turbulence theory, a theory that gives insight into how large-amplitude eddies generally evolve, interact, equilibrate, and dissipate and how eddy cascades generate the planetary waves that give zonal flows a barotropic component and a distinct lateral scale.

Eddy evolution in homogeneous, two-dimensional, barotropic β-turbulence can be anticipated from the energy and enstrophy conservation constraints. The latter predominates, causing enstrophy to cascade to smaller scales and energy to de-

cascade to larger scales, giving ever-larger eddies and ever-thinner shear layers. Eddies forced at some wavenumber k_0 produce an enstrophy-flux subrange with a k^{-3} spectrum and a vanishing energy transfer in $k>k_0$, plus an energy-flux subrange with a $k^{-5/3}$ spectrum and a vanishing enstrophy transfer in $k<k_0$ (Kraichnan 1967). This phenomenological theory fails to predict the strong vorticity concentrations and the steeper (up to k^{-6}) enstrophy inertial-range spectra seen in numerical studies, mainly because it treats vorticity like a passive scalar and ignores the subtle influence of vorticity advection on the flow (Basdevant et al. 1981).

The Coriolis gradient β does not influence the conservation constraints but it does alter the cascade rates and directions. When eddies become large enough to be affected by β they become coherent and propagate as Rossby wave packets (Rhines 1975). The waves and turbulence interact when the nonlinear and β terms become comparable, i.e., when the wave steepness $\varepsilon=\beta L^2/U$ approaches unity for eddies of size L and speed U. The wavenumber $k_\beta=(\beta/U)^{1/2}$ separates the wave and turbulence regimes. The wave transition is abrupt because the wave-dispersion relation $\omega_\beta=\beta k^{-1}\cos\phi$ and the turbulence-dispersion relation $\omega_\varepsilon=Uk$ between the frequency and the wavenumber have opposite slopes; here ϕ is the angle between the wave vector and the longitudinal axis.

In other words, the turbulent energy decascade, towards small k and small ω, does not continue into the wave regime because Rossby waves have a large ω associated with a small k. The eddies are not blocked uniformly at the transition and they do not remain isotropic because the wave-dispersion relation is anisotropic. To continue the transfer of energy to lower frequency, the eddies alter the direction of the wave vectors and reduce ω_β by shrinking their meridional scale and expanding their zonal scale. This leads to longitudinally oriented eddies, waves, and currents. In this way, the wave-dispersion relation interrupts the migration of the eddies to small k and small ω, to create the resonant triads that focus the energy into zonal currents of scale $L_\beta=\pi k_\beta^{-1}$.

Similarly, eddy evolution in three-dimensional, baroclinic flows is controlled by the total energy and potential enstrophy invariants that can be written in spectral form, for the QG_2 model (Salmon 1982), as

$$\frac{d}{dt}\sum_k [BT(k)+BC(k)]=0 \qquad (20a)$$

$$\frac{d}{dt}\sum_k [k^2 BT(k)+(k^2+k_R^2)\,BC(k)]=0 \qquad (20b)$$

BT being the barotropic kinetic energy, BC the potential energy plus baroclinic kinetic energy, and k_R the Rossby deformation wavenumber. Because of the constant k_R^2 factor, there is no enstrophy constraint on the transfer of baroclinic energy towards smaller scales when $k<k_R$. Consequently, only barotropic energy cascades to the largest horizontal scales and baroclinic energy moves towards the k_R scale from either smaller or larger eddies. A distinct change occurs in the dynamics at k_R: when $k>k_R$, the two layers act independently and two-dimensionally; when $k<k_R$, the layers lock together and behave like a single barotropic fluid. Barotropic-baroclinic interaction is effective only at k_R and is asymmetric in that baroclinic flows can generate barotropic flows, but not vice-versa.

Thus, QG turbulence, by cascading potential enstrophy upward through spectral space, determines eddy development, converts baroclinic energy into barotropic energy and turbulence into waves, and produces large-scale flows favoring zonality and barotropy. The cascade ends with the weak dissipation of potential enstrophy at small scales and, if drag exists, of barotropic energy at large scales. The Coriolis gradient β influences both the barotropic up-scale cascade — at k_β — and the baroclinic down-scale cascade (energy conversion) — at k_R. The key role of β in jet formation is illustrated by the QG_2 calculations described in the Appendix. The complete theory of geostrophic turbulence is given in Rhines' (1977) synthesis of ocean dynamics.

As regards atmospheric relevance, the QG turbulence theory is limited mainly by its insistence on spatial homogeneity. The atmosphere (at $\Omega^*=1$) has sparse energy sources, so eddies tend to spread out spatially as much as spectrally and thereby violate the conditions under which cascades occur. This is the main reason for doubting the existence of an energy decascade (and its spectral laws) in Earth's atmosphere. Identifying processes in the atmosphere is made difficult by the narrow spectral range of the motions in which $k_R\sim k_\beta$. The presence of a Hadley mode and a deep boundary layer also complicate matters by modifying the energy propagation and by making the energy dissipation comparable with the enstrophy dissipation. The main results of QG turbulence theory — the k_R and k_β transitions and the tendency to zonality and barotropy — may apply more to less-dissipative, more-homoge-

neously energized systems like the ocean, Jupiter or the high-Ω^* GCM states.

Identifying which processes actually control the lateral scale of the jets in a particular GCM state remains difficult, however. Although baroclinic and barotropic jets lie close to L_R and L_β in scale, respectively, examples of jets evolving from L_R to L_β in scale have been found in computations (Williams 1979b, Figs. 13 and 14). Jet widths also depend on the domain size, wave dispersion, and the Hadley mode.

3.3 Isomorphic dynamics: relation between β-turbulence and symmetric-Hadley circulations

Symmetric-Hadley circulations exist in a balance (described in § 3.1) between the momentum wind and the equilibrium thermal wind, between u_M and u_E. When the u_E wind is baroclinically unstable, eddies develop and energy cascades in ways described in some cases by QG- or β-turbulence theory. The eddies of β-turbulence also exist in a balance (described in § 3.2), a balance between the turbulent and wave regimes. Strangely, these SH and β-turbulence balances are isomorphic and so the two basic theories underlying our understanding of planetary circulations are structurally related.

The isomorphism exists between the angular velocity and latitude range of the SH current and the frequency and scale of the β-turbulence eddies. For the SH system, relationships of the form $\omega_M = L(f/a)$ and $\omega_E = L^{-1}(afR_E)$ exist between the angular frequencies (u/L) of the momentum and thermal winds and the distance (L) from the equator. Heat and momentum are transferred in the low-L region but stop (almost) where $\omega_M = \omega_E$, at $L_H = aR_E^{1/2}$. For β-turbulence, relationships of the form $\omega_\beta = L(\beta)$ and $\omega_\varepsilon = L^{-1}(U)$ exist between the wave and turbulence frequencies (ω) and scales (L). Energy decascades at small L but stops (almost) where $\omega_\beta = \omega_\varepsilon$, at $L_\beta = (U/\beta)^{1/2}$. Thus, there is a clear correspondence between the SH items (ω_M, ω_E, L_H) and the β-turbulence items (ω_β, ω_ε, L_β), with (afR_E) and U measuring the respective forcings (with the former also determining the latter in baroclinically unstable atmospheres), and fa^{-1} and β the respective inhibitors. Anisotropic frequency factors, $\omega_\beta(\phi)$ and $\omega_M(z)$, complicate the transitions in both balances.

3.4 Diagnostic dynamics

The interpretation of circulations also depends upon which fields and formalisms are used to define the elements and the eddy-mean flow interactions. The diagnostic equations can be formulated in different ways because of the ambiguities raised by two tight couplings: that between the eddies and the mean flow and that between the vertical shear and the horizontal temperature gradient. The definition of the eddy-mean flow interactions, such as occur in the eddy cycles and elements, is considered to be more fundamental and direct when given in terms of the **E** (Eliassen-Palm) flux of the transformed Eulerian mean (TEM) equations because it captures the essential duality of the exchange (Andrews 1985). We now summarize the traditional equations which underlie our interpretation of the GCM solutions, and the transformed equations which reveal the limitations of that interpretation.

Equation formalisms. The traditional and transformed (*) formalisms, labeled (a) and (b), may be written at the QG β-plane level of approximation (for simplicity) following Edmon et al. (1980) as

$$\bar{u}_t = f_0\bar{v} - (\overline{v'u'})_y + \bar{F},\ \bar{\Theta}_t = -\bar{\omega}\Theta_p^0 - (\overline{v'\Theta'})_y + \bar{Q} \tag{21a}$$

$$\bar{u}_t = \bar{f}_0\bar{v}^* + \nabla\cdot\mathbf{E} + \bar{F},\ \bar{\Theta}_t = -\bar{\omega}^*\Theta_p^0 + \bar{Q} \tag{21b}$$

for the mean zonal flow and potential temperature, where

$$\mathbf{E} = (-\overline{v'u'}, f_0(\overline{v'\Theta'})/\Theta_p^0) \tag{22}$$

and ∇ are meridional (y,p) vectors; and as

$$f_0^2\Psi_{pp} + \hat{R}(|\Theta_p^0|\Psi_y)_y = f_0(\overline{u'v'})_{yp} - \hat{R}(\overline{v'\Theta'})_{yy} + \hat{R}\bar{Q}_y - f_0\bar{F}_p \tag{23a}$$

$$f_0^2\Psi_{pp}^* + \hat{R}(|\Theta_p^0|\Psi_y^*)_y = f_0(\nabla\cdot\mathbf{E})_p + \hat{R}\bar{Q}_y - f_0\bar{F}_p \tag{23b}$$

for the meridional and residual-meridional (*) circulations, where

$$\bar{v} = \Psi_p,\ \bar{\omega} = -\Psi_y \tag{24a}$$

$$\bar{v}^* = \bar{v} - ((\overline{v'\Theta'})/\Theta_p^0)_p = \Psi_p^*,\quad \bar{\omega}^* = \bar{\omega} + ((\overline{v'\Theta'})/\Theta_p^0)_y = -\Psi_y^* \tag{24b}$$

and $\Psi = 0$, $\Psi^* = -(\overline{v'\Theta'})/\Theta_p^0$ at the surface. Here Q and F symbolize the heating and friction, $\Theta^0(p)$ is a reference distribution, and $\hat{R} = R\sigma^{\kappa-1}p_s^{-1}$. Equation (23a, b) comes from differentiating Eq. (21a, b) for substitution in the thermal-wind balance: $f_0\bar{u}_p = \hat{R}\bar{\Theta}_y$.

These equations may be replaced or augmented by those of the q formalism for the mean potential vorticity ($\bar{q}$) and eddy potential enstrophy $(\overline{q'})^2$, together with those for $\bar{\Theta}$ and $(\overline{\Theta'})^2$ at the surface. The traditional and transformed versions are

$$\bar{q}_t + (\overline{v'q'})_y = \bar{S},\ (\overline{q'})^2_t + (\overline{v'q'})\bar{q}_y = \overline{S'q'} \qquad (25a)$$

$$\bar{q}_t + (\nabla \cdot \mathbf{E})_y = \bar{S},\ A_t + \nabla \cdot \mathbf{E} = \bar{S}^* \qquad (25b)$$

where $q' = v'_x - u'_y + f_0(\Theta'/\Theta^0_p)_p$, $\nabla \cdot \mathbf{E} \equiv \overline{v'q'}$, $S = S(Q,F)$, and where $A = (\overline{q'})^2/2\bar{q}_y$ is the activity density for small weak eddies. Both forms of Eq. (25) are capable of describing the two-way, eddy-mean flow processes through the dual role played by the $\overline{v'q'}$ flux. The q field and its parent, the Ertel potential vorticity $q_E = (f+\zeta)\nabla\rho/\rho$, are the fundamental field variables for circulations and can be used to extend diagnostics to longitudinally dependent mean states (Plumb 1986). Although u and Θ are linked and are given by q in the free atmosphere, they are independent in the boundary layer and worth analyzing separately.

Of the traditional and transformed formalisms for exchanges among the eddy and mean potential and kinetic energies (P_E, P_Z, K_E, K_Z), we present (for brevity) only the K_E equation — the main indicator of eddy genesis and development in the traditional case. Both systems have the form (Plumb 1983)

$$\frac{\partial K_E}{\partial t} = \{K_Z : K_E\} + \{P_E : K_E\} - \nabla \cdot \mathbf{G}(K_E) + \overline{\mathbf{v}' \cdot \mathbf{F}'} \qquad (26)$$

where the conversions from the mean-kinetic and eddy-potential energies are

$$\{K_Z : K_E\} = \bar{u}(\overline{v'u'})_y,\ \{P_E : K_E\} = -\hat{R}\,\overline{\omega'\Theta'} \qquad (27a)$$

$$\{K_Z : K_E\}^* = \bar{u}\,\nabla \cdot \mathbf{E},\ \{P_E : K_E\}^* = -\hat{R}(\overline{\mathbf{v}'\Theta'}) \cdot \nabla\bar{\Theta}/\Theta^0_p \qquad (27b)$$

and the energy fluxes are

$$\mathbf{G}(K_E) = \overline{\mathbf{v}'(\Phi' + \bar{u}u')} \qquad (28a)$$

$$\mathbf{G}(K_E)^* = \overline{\mathbf{v}'\Phi'} - \bar{u}\mathbf{E} \qquad (28b)$$

with $\mathbf{v} = (v, \omega)$ and $K_E = [(\overline{u'})^2 + (\overline{v'})^2]/2$. The other eddy source, the conversion from mean-potential energy to eddy-potential energy in the P_E and P_Z equations, has the form

$$\{P_Z : P_E\} = -\hat{R}\,\overline{v'\Theta'}\,\bar{\Theta}_y/\Theta^0_p \qquad (29a)$$

$$\{P_Z : P_E\}^* = 0 \qquad (29b)$$

Thus there is only one mean-to-eddy conversion in the transformed system: $\{K_Z : K_E\}^*$.

Equation interpretation. The transformed equations capture the duality of the eddy-mean flow interaction in basic terms: the flux divergence $\nabla \cdot \mathbf{E}$ appears both as a source of wave activity (Eq. 25b) and as a forcing of the mean state (Eqs. 21b and 23b), and its connection with the $\overline{v'q'}$ flux makes it a more fundamental item than the individual $\overline{v'u'}$ and $\overline{v'\Theta'}$ fluxes. The $\mathbf{E}$ flux itself gives a direct view of wave propagation in the meridional plane: for waves in a WKB zonal flow, the direction of $\mathbf{E}$ gives the sense of the wave propagation via the connection $\mathbf{E} = A\mathbf{c}_g$ with the activity density and the group velocity. Equation (25b), relating $\nabla \cdot \mathbf{E}$ to wave transience and nonconservation, gives a simpler view of how waves propagate in a complex zonal flow than does the $\partial K_E/\partial t$ equation because it lacks complex conversion terms. Waves prefer to propagate into regions with a large positive refractive index, $m^2 = [\bar{q}_y(\bar{u}-c)^{-1} - k^2]\Theta^0_p f_0^{-2}$. The $\mathbf{E}$ field is mainly used in eddy-cycle calculations to relate the eddy fluxes to the baroclinic instabilities and the dispersing planetary waves. But it is not known if the $\mathbf{E}$ field maintains its advantages when multiple wave fields emanate from multiple sources to interact with each other and with the mean flow, as they do in the high-Ω^* states.

The normal and residual meridional circulations forced by the eddies, heating, and friction are described by Eq. (23a, b). The circulations arise to re-establish the thermal wind balance, in whose absence the forcing would change $\bar{u}$ and $\bar{\Theta}$ separately. In the traditional formalism it is difficult to gauge the overall effect of the eddy fluxes on $\bar{u}_t$ and $\bar{\Theta}_t$ because the ageostrophic circulation terms in Eq. (21a) are not independent of those fluxes — as Eq. (23a) shows. For example, in Earth's atmosphere, the Ferrel cell arises entirely as a response to the upper-tropospheric eddy momentum flux: $f_0\bar{v} = -(\overline{u'v'})_y$. In the transformed formalism, the residual circulation is designed to remove explicit eddy effects on $\bar{\Theta}_t$. Then $\bar{u}_t$ depends on $\nabla \cdot \mathbf{E}$ and on a residual circulation whose elliptic, space-emanating character varies, rather complicatedly, as $\nabla^{-2}(\nabla \cdot \mathbf{E})_p$. Thus the $\mathbf{E}$ field is not that simple a guide to eddy-mean flow interactions. (The q formalism in Eq. (25) avoids the difficulties associated with the ageostrophic

circulation, but it does not reveal how $\bar{u}$ and $\bar{\Theta}$ change in time.)

In the transformed energy cycle, the only mean-to-eddy conversion occurs via an expanded $\{K_Z{:}K_E\}^*$ term than can be split into the traditional barotropic and baroclinic conversions, Eq. (27). The energy flux term $\mathbf{G}(K_E)^*$ introduces an extra energy flow between the surface and the internal kinetic energy that is useful for representing the influence of surface temperature gradients on baroclinic instabilities. This term also implies that a non-zero value for the divergence of the geopotential flux ($\overline{v'\Phi'}$), the traditional indicator of wave propagation, does not necessarily indicate a piling up of wave activity: the mean and eddy terms, the fluxes and conversions are all too interdependent. Moreover, simple examples reveal that neither energy-cycle formalism describes processes in a causal or sequential manner, that both have ambiguities for individual conversions and flux divergences (Plumb 1983).

Thus, the transformed formalism allows a more fundamental (but not simple) description of the eddy-mean flow interactions and provides a new diagnostic for relating the eddy transports to the eddy propagation. It also reveals that no form of energy "conversion" and energy "flux" is an accurate indicator of eddy "genesis" and eddy "propagation". The main disadvantage of the formalism is that it overemphasizes the role of $(\overline{v'\Theta'})_p$ in changing the zonal flow — the process only redistributes momentum in the vertical.

Given, however, the nonavailability of the transformed formalism at the time of computation, our GCM analysis must rely on just the traditional elementary fluxes of heat, momentum and geopotential to give a preliminary measure of eddy genesis, eddy forcing, and eddy propagation in a few standard elements. We leave to future studies the task of redefining the elements and their interactions in terms of eddy-cycle scenarios involving the $\mathbf{E}$ and $\nabla \cdot \mathbf{E}$ fields. Completely new diagnostics are needed for the cyclostrophic, baroclinically stable, diurnally heated circulations prevalent at low Ω^*.

3.5 Summary of theory

Although theoretical developments have brought us close to a good understanding of Earth's ($\Omega^* = 1$) atmospheric motions (Held and Hoskins 1985), circulation theory is far from complete and must be extended if it is to deal with motions over a wider parameter range. Explanations begin with the symmetric-Hadley theory and how a nonuniform radiative heating creates a jet at the edge of a Hadley cell. The natural-Hadley and quasi-Hadley elements then describe the effect of neutral waves on the SH mode at low and high Ω^*, while nonlinear QG theory describes the effect of instabilities in the SH jet in terms of eddy-cycle scenarios. QG turbulence theory indicates that these eddy cycles are a special form of enstrophy cascade and hence give a fundamental description; it also explains why certain jets develop a barotropic component and a distinct lateral scale. The $\mathrm{QG}_{\gamma,\beta}$ elements describe the limiting forms of eddy cycle. Closed descriptions of circulations, using the $\bar{u}_t$, $\bar{\Theta}_t$, $(\overline{q'})_t^2$ and Ψ equations, appear to be feasible — at least at the QG level.

4 MOIST(Ω^*) circulations

We now consider the first set of GCM solutions, defined in the classical manner (Smagorinsky et al. 1965) using the time- and zonal-averaged mean fields and eddy fluxes. This MOIST(Ω^*) set describes how the circulations of moist atmospheres vary with the rotation rate. To obtain a full range of flows, we take eight values of Ω^*, spaced in factors of 2 from 1/16 to 8, with supplementary values at $\Omega^* = 0$ and 3/4 (Table 3). The numerical resolutions, R42 for $\Omega^* \geqslant 1$ and R30 for $\Omega^* \leqslant 3/4$, are accurate except perhaps at $\Omega^* = 8$ where the baroclinic eddies and cells are very small. The computational domain, a 120° sector, gives a good representation of most circulations but may cause minor shifts in the parameter dependence when the eddies are domain size, at $\Omega^* \leqslant 1/2$.

We begin by outlining how the mean fields and eddy fluxes vary over $\Omega^* = 0$–8, and follow with a detailed description and interpretation of the circulations in three Ω^* subranges. The Ω^* range splits naturally into subranges, each with its own characteristic flows: the baroclinically stable low range ($\Omega^* = 0$–1/4), the large eddy midrange ($\Omega^* = 1/2$–1), and the small eddy high range ($\Omega^* = 2$–8). The MOIST(Ω^*) set undergoes transitions: (a) when the zonal flow becomes singular, near $\Omega^* = 0$; (b) when cyclostrophy becomes important, near $\Omega^* = 1/2$; (c) when instabilities become shallow at the long-wave cutoff, near $\Omega^* = 1/4$; and (d) when the radiative-convective state is approached at the short-wave cutoff, near $\Omega^* = 8$.

For conciseness we use expressions such as "the MOIST(4) $\mathrm{QG}_\beta(25°)$ jet" to refer, for example, to a zonal flow centered at $\theta = 25°$ and having

Table 3. MOIST Circulations: energy, heat, and momentum integrals

Case		Energy						Heat					Momentum				
Ω^*	Δ	τ_I	K_Z	K_E	$P{:}K_Z$	$P{:}K_E$	$K_Z{:}K_E$	T^a	r^a	RAD	$v'T'^{d}$	$-\omega'T'$	Max[b] torque	$v'M'$	$-\omega'M'$	Max $\lvert u\rvert$	Max $\lvert v\rvert$
8V[c]	E		19	9	26	83	− 2	251.1	6.5	−827	89	114	17	5	− 84	17	0.7
8	E	634	60	10	44	98	3	253.7	7.0	−837	132	141	26	19	−153	62	1.5
4	E	359	77	25	80	219	− 1	253.6	5.0	−868	256	374	−44	99	−120	47	1.9
2	E	319	97	47	89	258	− 9	254.2	3.6	−903	344	483	45	146	− 4	46	2.6
1	E	319	183	65	106	224	− 41	253.6	2.9	−944	384	452	−77	564	146	52	4.7
¾	D	379	213	55	123	237	− 58	253.8	2.9	−956	387	464	−71	482	239	56	4.3
½	D	989	286	51	20	290	−112	253.6	2.8	−966	459	589	−78	362	300	68	4.3
¼	D	969	556	35	146	130	42	253.9	2.9	−940	207	313	− 7	−164	−186	77	2.6
⅛	D	979	571	30	173	48	95	254.1	2.7	−925	115	142	− 6	−296	−256	86	4.2
1/16	D	909	286	21	162	36	51	253.1	2.0	−921	309	132	− 8	−179	− 70	81	7.6
0	D	449	12	14	118	54	0	252.4	1.8	−927	8	106	− 0.6	− 14	− 11	2	11.6
Units		Days	$J\ kg^{-1}$		$10^{-6}\ W\ kg^{-1}$			K	cm water	$10^{-8}\ Ks^{-1}$	$10^1\ J\ m\ kg^{-1}\ s^{-1}$	$10^{-2}\ W\ m^{-2}$	$m^2\ s^{-2}$	$10^5\ kg^2\ m^{-2}\ s^{-2}$	10^2	$m\ s^{-1}$	

[a] Instantaneous values; all others are time averaged
[b] Integrals are global means (not totals) but Max is local value
[c] Variant is low kinetic energy phase of solution at $\Omega^* = 8$
[d] Eddy heat and momentum transports are denoted symbolically; sphericity factors are involved in actual calculations

τ_I denotes integration period
Δ denotes domain and resolution (see Table 1)
RAD denotes radiative heating rate

the eddy fluxes of a QG_β element in a moist atmosphere with $\Omega^* = 4$. Describing the circulations in terms of the idealized regional elements greatly simplifies their presentation, but — like the eddy-mean description — has inherent limitations. The correlations among the various fields are best seen by imposing a transparency of the $\bar{u}$ field upon the other figures.

4.1 The MOIST(Ω^*) progression (Figs. 2–11)

The atmospheres evolve from isothermal initial states into statistically equilibrated, troposphere-stratosphere systems in much the same way at all Ω^*. In a typical history, the global-mean kinetic energy fluctuates over a small range: for example, from 9 to 12 units when $\Omega^* = 4$. In the only atypical history, at $\Omega^* = 8$, this integral varies substantially, from 2 to 10 units, with the lower values occurring for shorter intervals. For this case, we define a typical average over a 90-day interval and a variant average, dubbed LOW K.E. in Fig. 11, over a 20-day interval.

The mean fields. The mean zonal flow in Fig. 2 goes from a single jet in the low range to overlapping jets in the midrange and to multiple jets in the high range. The axis of the strongest jet moves equatorward as Ω^* increases, first in the NH element at low Ω^* and then in the QH element at higher Ω^*. Easterlies separate the multiple jets in midlatitudes and form trade winds in low latitudes when baroclinic instabilities occur. The meridional flow in Fig. 3 goes from a single, subhemispheric Hadley cell in the low range to a pair of Hadley and Ferrel cells in the midrange and to multiple direct and indirect cells in the high range. The Ferrel cells, induced by baroclinic instabilities and correlated with jet cores and surface westerlies, become narrower with increasing Ω^* in keeping with the eddy scale L_R. The Hadley cell — the main direct cell — varies more weakly with rotation because of baroclinicity changes in the SH scale $\theta_H \sim \Delta_H^{1/2}\Omega^{-1}$.

The baroclinicity in Fig. 4 ranges from the small value (10 K) produced by the strong cell transport at $\Omega^* = 0$ to the strong value (55 K) allowed by the narrower cell at $\Omega^* = ¼$, to the moderate value (35 K) produced when the large eddies take over in the midrange, and to the very strong value (90 K) allowed by the small eddies when radiative-convective equilibrium is approached in the high range. The tropical tropopause extends from the equator to 30° latitude in the mid- and high ranges, where moist convection controls the lapse rate, but approaches the pole in the low range where cell overturning controls the static stability — in agreement with SH theory.

The eddy fields. The eddy kinetic energy in the low range is generated by the moist convection

($\{P:K_E\}>0$) and by the barotropic cascades ($\{K_Z:K_E\}>0$) in the polar jet and is confined to the tropics and the upper troposphere (Fig. 5). The midrange eddies, generated mainly by baroclinic instability, are the most energetic and extensive but are excluded (almost) from the easterly trade winds. Although the eddies are larger at $\Omega^*=\frac{1}{2}$, they are stronger at $\Omega^*=1$ because the Hadley region is narrower and gives the eddies more room to develop at the higher rotation rate. (In the DRY(Ω^*) set all eddy properties peak at $\Omega^*=\frac{1}{2}$ because the Hadley mode is weak in the absence of moisture.) The high-range eddies have energy maxima in each of the various jets but in the $\Omega^*=8$ limit are again confined to the upper and tropical troposphere. The MOIST(8) eddies, energized more by convection than baroclinicity, are actually weaker than those at $\Omega^*=0$.

The eddy heat fluxes in Figs. 6 and 7 become organized with the onset, at $\Omega^*=\frac{1}{4}$, of a shallow baroclinic instability that gives poleward and upward transports in the lower troposphere. (A very shallow instability occurs at $\Omega^*=\frac{1}{8}$ but is so weak that we regard the MOIST($\frac{1}{8}$) flow as stable.) The heat fluxes become strong and deep in the midrange and remain monotonically poleward and upward even when generated by multiple instabilities in the high range. Although eddies transport heat continuously poleward, without limitation across the various easterlies and westerlies, their momentum fluxes are local (see below). Thus the multiple jets appear to interact baroclinically (via overlapping heat fluxes) but not barotropically — the easterlies block the barotropic wave dispersion. Waves do propagate aloft, however, into the subtropics and produce equatorward and downward heat fluxes that become more confined as Ω^* increases (cf. Hayashi 1974). Moist convection produces an upward heat transport at the equator that also becomes more confined as Ω^* increases. (The vertical heat flux is represented approximately, but accurately, by the baroclinic conversion $-\overline{\omega'\alpha'}$.)

The eddy momentum fluxes in the low range in Figs. 8 and 9 are equatorward and downward and are associated with the planetary waves generated by the equatorial convection. Such fluxes are confined to low latitudes when instabilities arise in the higher ranges. The midrange fluxes mainly traverse poleward and upward across the jet in midlatitudes, but the high-range fluxes are more local, converging laterally on the midlatitude jets and traversing the high-latitude jets. Bimodal vertical fluxes usually coincide with converging lateral fluxes but the behaviour of this ageostrophic item becomes more erratic as geostrophy strengthens at higher Ω^*. The geopotential fluxes $\overline{v'\Phi'}$ show that, in the high range, energy is strongly redistributed in the vertical but does not propagate far laterally — only to the jet boundaries (not shown, but see Figs. 24 and 25).

The synoptic fields. The 500-mb geopotential heights in Fig. 10 show that the circulations have the same synoptic character as the QG_2 circulations discussed in the Appendix because the tropical jets do not show at this level. The contours progress from being zonally aligned in the low range — waves appear only near the 300-mb level when $\Omega^*=\frac{1}{4}$ — to having regular waves in the midrange and multiple, less-regular concentrations in the high range. Blocking highs occasionally appear between the tropical and midlatitude jets in the MOIST(2) case (cf. Fig. 13 of Williams 1979b). Details of the MOIST(1) vertical motions, fronts, and cyclone families are given in an earlier high-resolution study (Manabe, Smagorinsky, Holloway, and Stone 1970, hereafter MSHS70).

Convective (tropical, warm-core, cyclonic) storms occur in the high-range circulations because of their high surface temperatures and in models with fixed surface temperatures (Manabe, Holloway, and Stone 1970, hereafter MHS70). In the MOIST(4) solution convective storms originate in the region of zero zonal flow at $\theta=15°$, mature rapidly, and migrate to midlatitudes. These storms are exaggerated versions of the convective eddies that convert potential energy into kinetic energy at the equator. Convective adjustment gives these humid towers a moist adiabatic lapse rate, a warm core and strong upward flow above 800 mb and a cold core below. These 3000-km-wide cyclones are most pronounced in the lower troposphere where they produce a 20-mb drop in the surface pressure and a 10 K rise in the 500-mb temperature. They have little effect on the global circulation.

4.2 The low-range circulations

Looking at the solutions in more detail, we see that the low-range zonal flows vary between a tight polar jet at $\Omega^*=\frac{1}{16}$ and a broad midlatitude jet at $\Omega^*=\frac{1}{4}$ (Fig. 2g–i). The flow amplitude, however, remains constant at $80\ \mathrm{m\ s^{-1}}$ and closely matches the value of the momentum wind u_M at the latitude of the jet core. (Note that $a\Omega=60\ \mathrm{m\ s^{-1}}$ when $\Omega^*=\frac{1}{8}$.) The low-range Hadley cell extends to the jet core and becomes

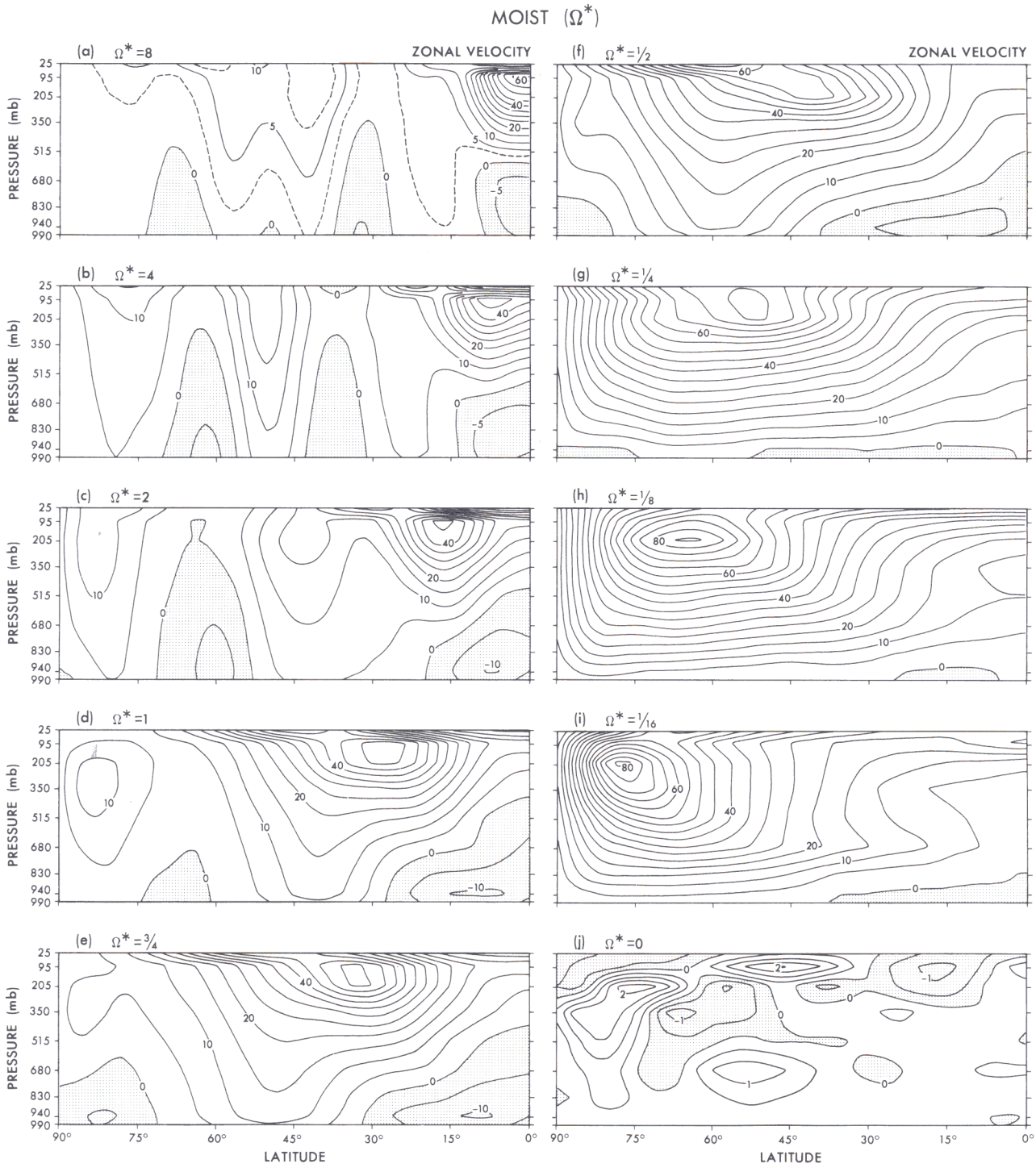

Fig. 2. Meridional distribution of the mean zonal wind for the MOIST model with $\Omega^* = 0$–8. Units: m s^{-1}

narrower as Ω^* increases (Fig. 3g–j). Cell upflow is confined to the equator (as in SH theory) but cell downflow has complex tilts and, at $\Omega^* = \frac{1}{4}$, a strong disruption induced by the shallow instability (cf. Hunt 1979a). The gain in the surface baroclinicity comes mainly from a drop in the high-latitude temperatures; the equatorial surface temperatures remain close to 300 K for $\Omega^* = 0$–2 (Fig. 4). The MOIST($\frac{1}{4}$) eddy heat flux shows that the shallow instability lies below 700 mb and is cen-

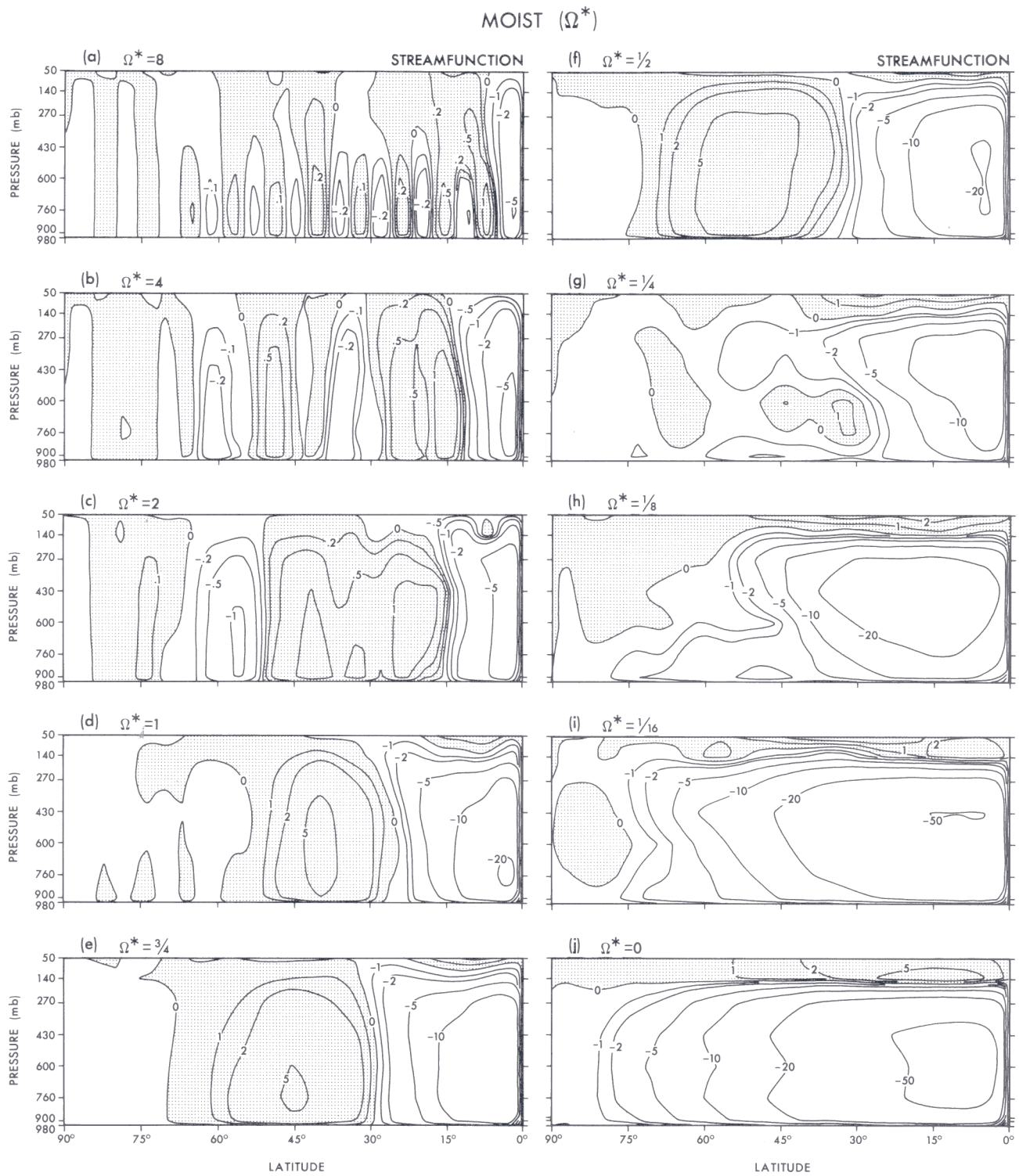

Fig. 3. Meridional distribution of the mean stream function for the MOIST model with $\Omega^* = 0$–8. Units: 10^{13} g s^{-1}

tered near the jet axis at $\theta = 50°$ (Fig. 6g). The MOIST(¼) equatorward momentum flux has the same extent as the Hadley cell and arises from waves propagating in the modified momentum wind (Fig. 8g).

Low-range circulations closely resemble the

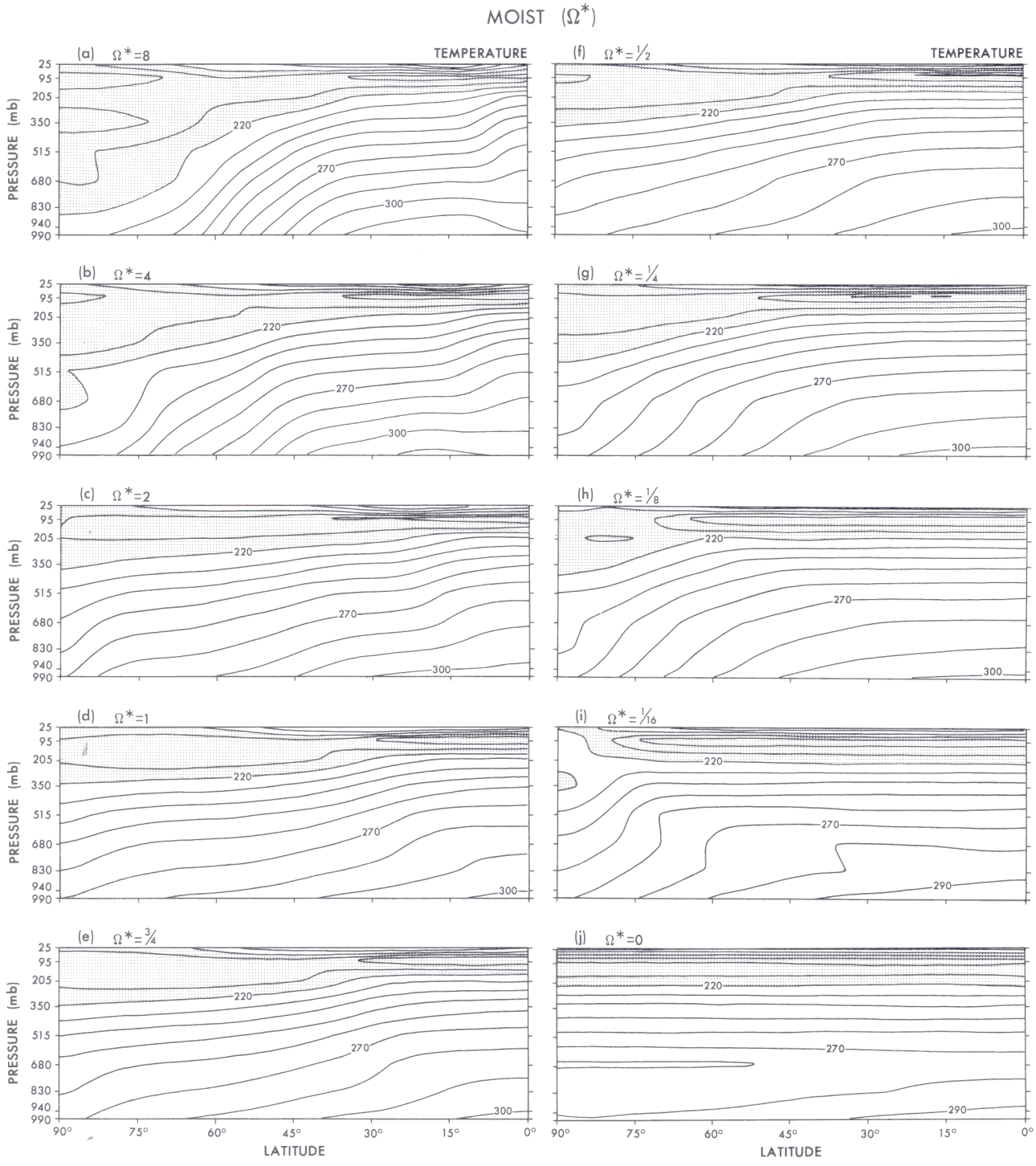

Fig. 4. Meridional distribution of the mean temperature for the MOIST model with $\Omega^* = 0$–8. Units: K

idealized NH element of Fig. 1 and have many of the features and the Ω^* dependence described by the SH($R_E > 1$) theory: a jet with a thermal wind on its poleward side and a momentum wind on its equatorward side; a Hadley cell that extends to the jet core; temperature gradients that are small in the cell but strong outside it. The GCM differs from the theory by having equatorial westerlies —

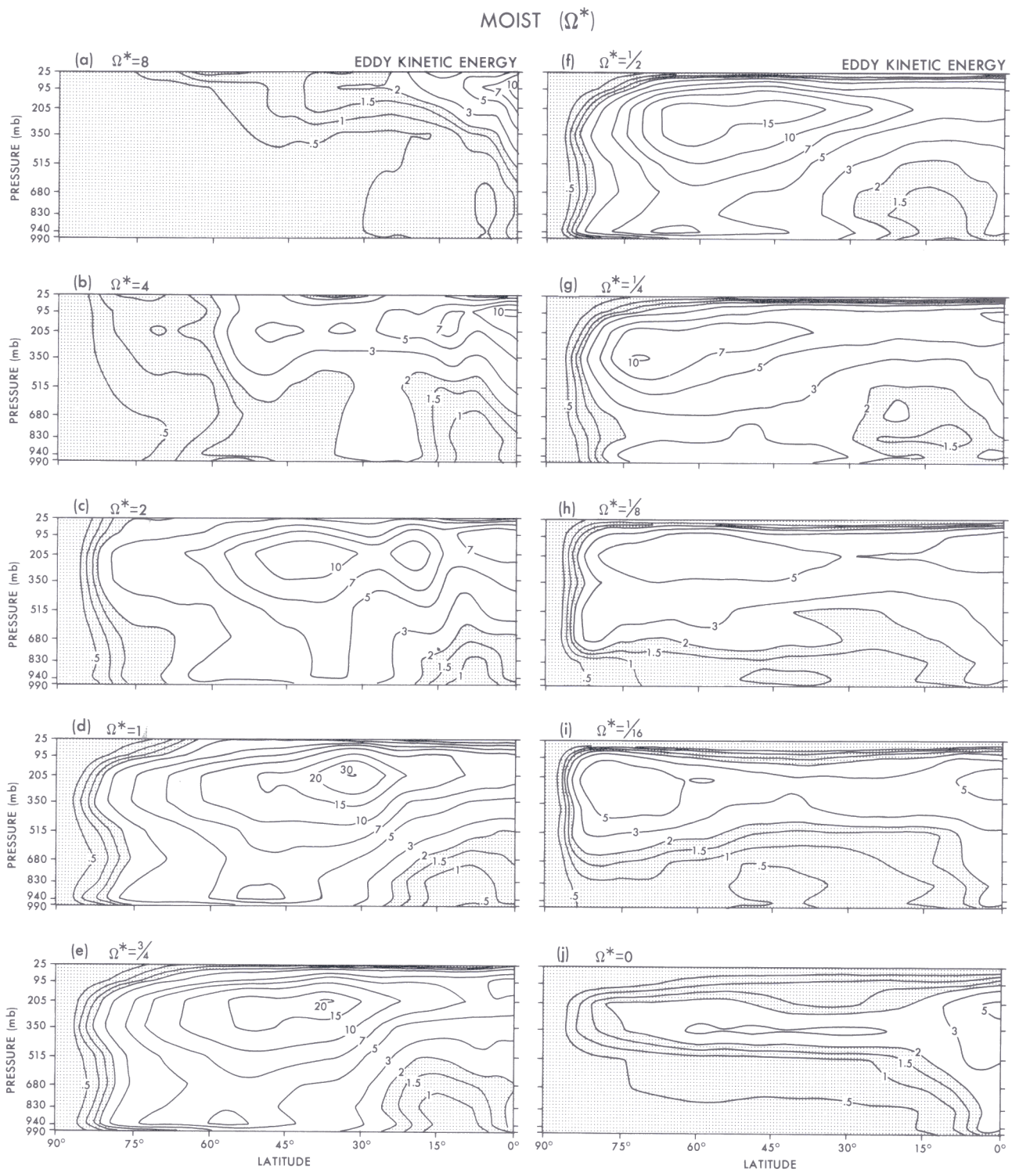

Fig. 5. Meridional distribution of the mean eddy kinetic energy for the MOIST model with $\Omega^* = 0$–8. Units: 10 J kg^{-1}

produced by propagating planetary waves — and complex cell downflows — produced by vertical variations in the meshing of the thermal and momentum winds.

4.3 The midrange circulations

The midrange jets in Fig. 2d–f consist of a midlatitudinal QG_γ component that extends over the re-

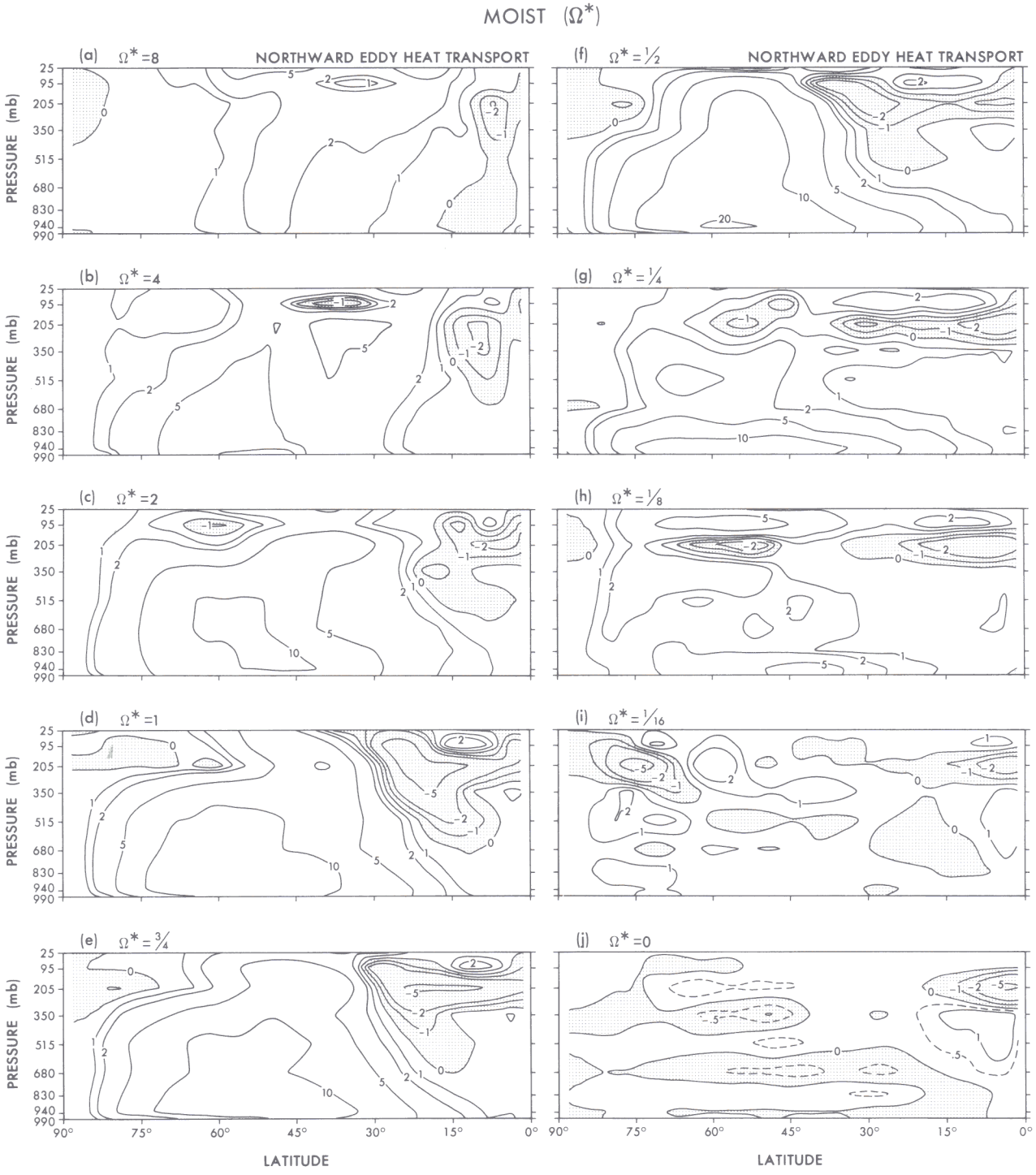

Fig. 6. Meridional distribution of the mean northward transport of heat by the eddies in the MOIST model with $\Omega^* = 0$–8. Units: 10^3 J m kg^{-1} s^{-1}

gion with surface westerlies, and of a subtropical QH component that extends from the equator to the jet core. Both components move equatorward as Ω^* increases but the jet maintains a near-constant amplitude (50 m s^{-1}). Easterly trade winds are induced by the baroclinic instability and produce surface torques that are an order of magnitude stronger than those of the stable low-range flows (Table 3).

The meridional circulations in Fig. 3d–f have

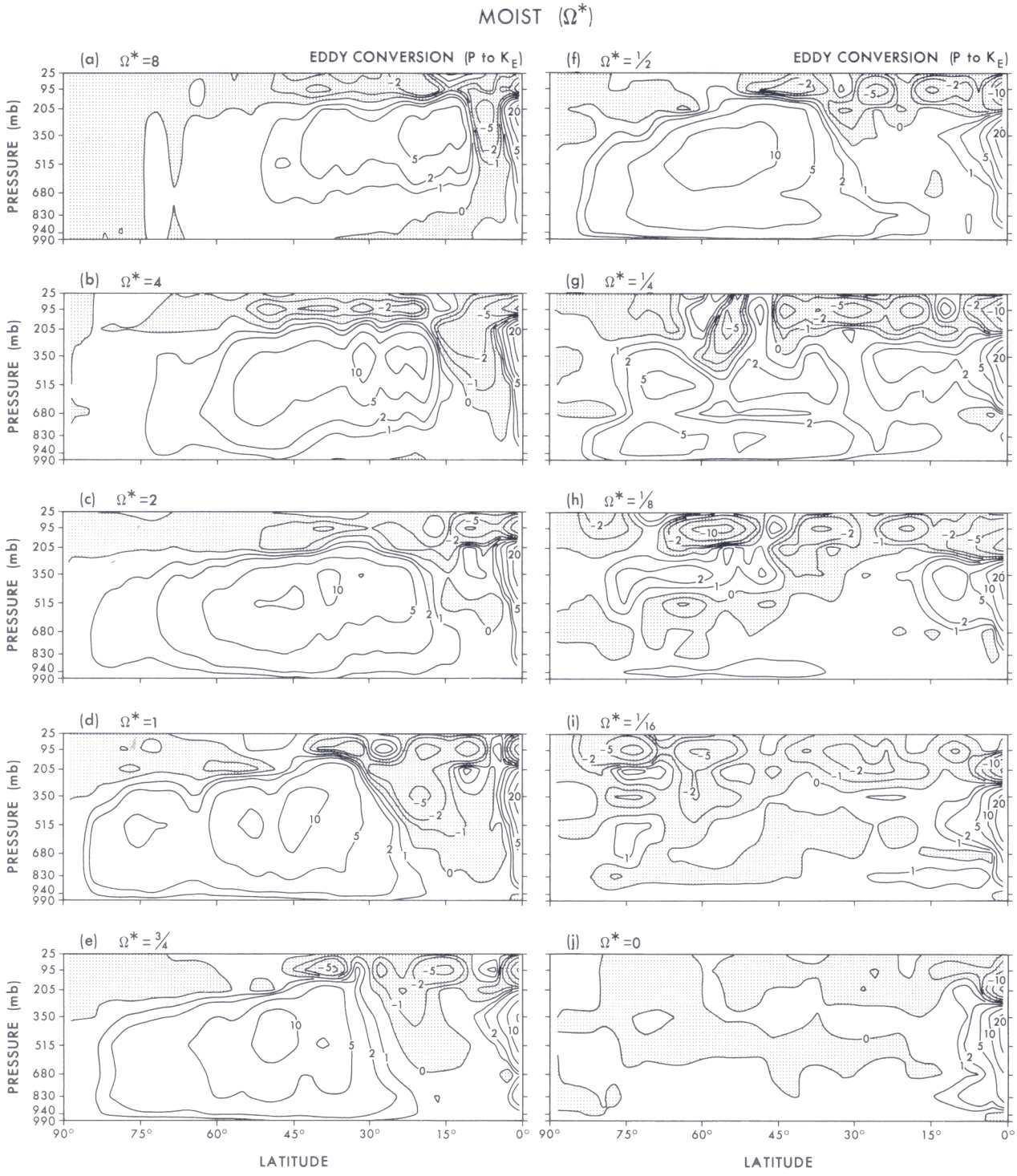

Fig. 7. Meridional distribution of the mean baroclinic energy conversion by the eddies in the MOIST model with $\Omega^* = 0$–8 (parallels the vertical eddy heat transport). Units: 10^{-4} W kg^{-1}

only two cells because the waves generated by the instability propagate only equatorward. (In the DRY(1) case the low-latitude easterlies inhibit the equatorward propagation and three cells develop.) The midrange Hadley cell is very strong because of the high moisture level produced by the swamp surface (Table 3). It does not quite reach the jet core (as it does in the SH flows) because of

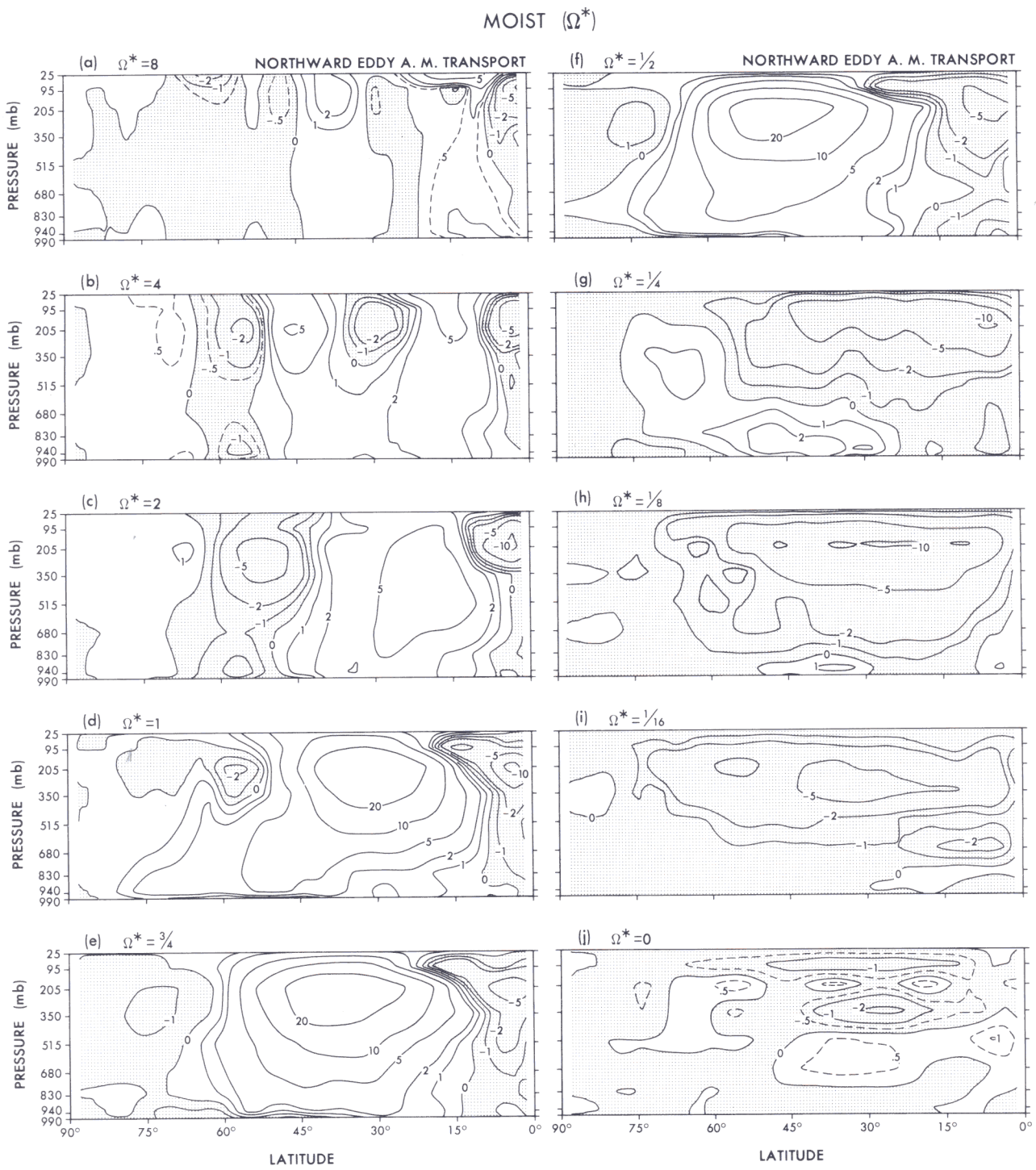

Fig. 8. Meridional distribution of the mean northward transport of angular momentum by the eddies in the MOIST model with $\Omega^* = 0$–8. Units: 10^7 m^3 s^{-2}

the eddy effects. The Ferrel cell extends over the unstable QG part of the jet and halves its width across the midrange in keeping with the eddy scale L_R.

The temperature fields remain almost invariant across the midrange (Fig. 4d–f). The onset of the strong instability reduces the surface baroclinicity from 55 K at $\Omega^* = \frac{1}{4}$ to a constant 35-K mi-

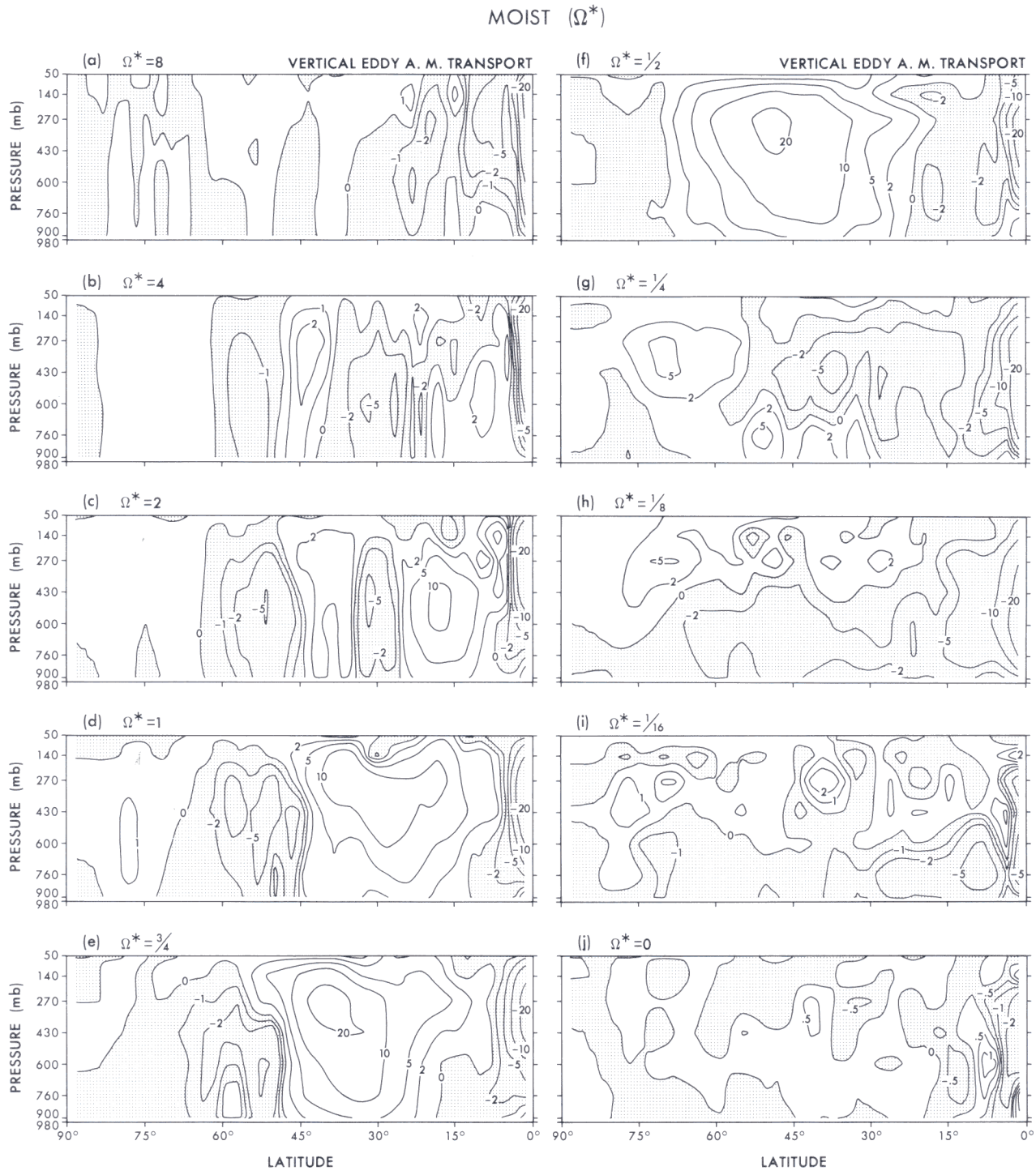

Fig. 9. Meridional distribution of the mean vertical transport of angular momentum by the eddies in the MOIST model with $\Omega^* = 0$–8. Units: 10^4 kg s^{-2}

drange value. Eddy transport is offset by cell transport, but the net remains the same despite changes in the eddy and cell sizes.

The subtropical heat flux components in Fig. 6d–f reveal that the instability penetrates (and perhaps drives) the easterly trade winds at low levels and that the Rossby waves propagate in the tropical westerlies at high levels. The momentum fluxes in Fig. 8d–f show that the eddies accelerate the poleside (QG_γ) part of the jet plus the equato-

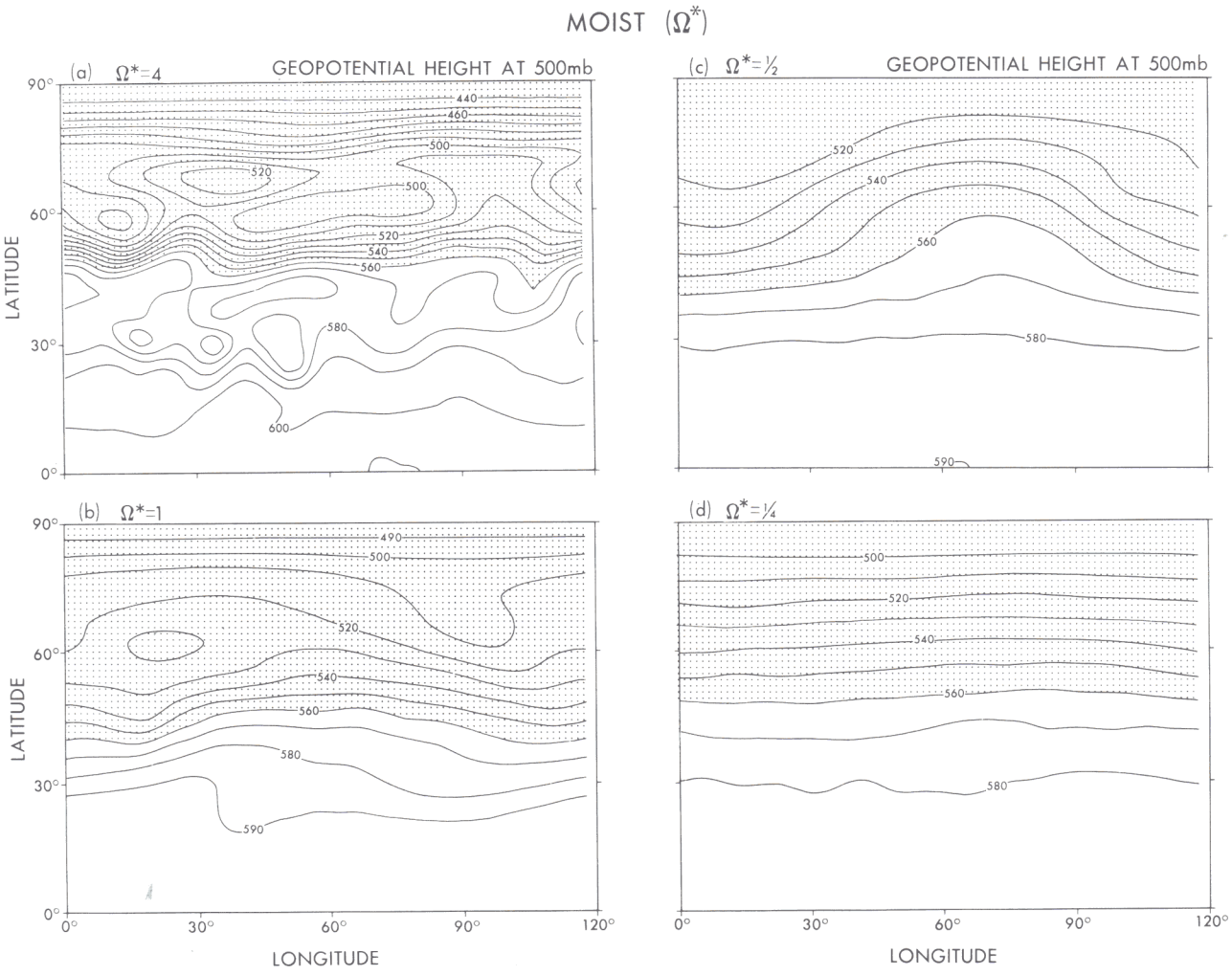

Fig. 10. Latitude-longitude distribution of the instantaneous 500-mb geopotential height for the MOIST model with $\Omega^* = ¼$–4. Units: 10 m

rial westerlies, but decelerate the subtropical (QH) part of the jet. The vertical momentum fluxes in Fig. 9d–f reveal that subtle ageostrophic changes occur in the midlatitude flows over the midrange: at $\Omega^* = ½$ the eddies transport momentum only upwards into the jet core, but at $\Omega^* = 1$ they also transport it downward on the poleward side of the jet. Such bimodal fluxes do not occur in the DRY midrange and may be an early indication that the MOIST(1) flow is close to a transition.

Midrange circulations are essentially a mix of QG_γ and QH elements. Although it may be equally valid to regard them as a type unto themselves, we prefer to regard them as a hybrid because the two components separate out at higher Ω^* and because the DRY midrange flows contain only the QG_γ element. When Ω^* increases to midrange values, the low-range NH jet becomes baroclinically unstable in its thermal wind section, producing eddies that alter the zonal flow, induce a Ferrel cell, propagate into the momentum wind, strengthen the Hadley cell and thereby drive the easterly trade winds. The diabatically driven part of the Hadley circulation dominates low latitudes and controls the extent of the QG_γ element. The baroclinic eddy fluxes show the QG_γ element exists in $\theta > 30°$, the QH element in $\theta < 30°$.

The interaction between the two elements or between the eddies and the mean flows cannot be defined precisely from the GCM state, but it could be from eddy cycles based on the SH state. (The eddy cycle of Simmons and Hoskins, 1978, lacks a Hadley component.) The elements and regions are linked by the interplay of the u_E and u_M winds that underlie the mean flow and by the ex-

change of eddies. The QG_γ element influences the QH element by imposing waves on it; QH influences QG_γ by controlling the wave dispersion. In the DRY midrange, however, the waves eliminate the Hadley mode.

4.4 The high-range circulations

Increasing Ω^* from 1 to 2 in Fig. 2c causes the zonal flow to split into a $QG_\beta(40°)$ jet and a QH(15°) jet. (AXISYMMETRIC flows also split into two jets in this range; see Part II.) When Ω^* increases to 4, these jets narrow and move equatorward to form the $QG_\beta(25°)$ and QH(10°) jets and allow extra $QG_\beta(50°)$ and $QG_\gamma(75°)$ jets in higher latitudes (Fig. 2b; cf. Hunt 1979a). When $\Omega^* = 8$, the QH jet narrows further, moves right to the equator, develops an oscillatory amplitude (cf. Fig. 11), and is accompanied by one polar QG_γ and three midlatitudinal QG_β jets. The QH jet gives the strongest flow (50 m s^{-1}) throughout the high range while overlying a near-constant (5 m s^{-1}) easterly trade wind. The QG_β jet that abuts the QH jet at $\Omega^* = 2$ and 4 is the weakest jet but is real nonetheless: $\overline{\omega'\alpha'}$ shows that a baroclinic instability occurs in its zone. The jet widths decrease with Ω^*, but not as linearly as the eddies, so the controlling process remains unclear.

The main Ferrel cell in Fig. 2b and 2c is actually wider in the high range than in the midrange because it has two parts: one associated with the baroclinic instability, the other with the Hadley mode (cf. the AXISYMMETRIC(2) cells in Part II). The Ferrel part of the QH mode is more apparent at $\Omega^* = 8$ because then the QG cells all lie below 500 mb. These shallow narrow cells are the signature of linear instabilities near the short-wave cutoff. Small eddies are easily dissipated by the Ekman layer and fail to develop beyond the first eddy-cycle phase. Deeper cells do occur, however, in the variant state (see § 4.5). Normally a QG jet has three cells; but two QG jets will share a common direct cell in their common easterly buffer and so have a total of five cells, while n QG jets have $(2n+1)$ cells.

With the decline in the width and efficiency of the cells and eddies, the surface baroclinicity increases from 45 K to 90 K over the high range, mainly through the cooling of higher latitudes (Fig. 4a–c). The equator remains close to 300 K. The hottest region, however, moves from the equator to the subtropics ($\theta \sim 15°$), just as it does in the AXISYMMETRIC and SURFACE SLIP (but not DRY) high ranges. This hotspot is not correlated with cell subsidence and may be forced by the zonal flow via the thermal wind balance.

The high-range poleward heat flux in Fig. 6a–c develops a countergradient "hole" at the tropopause in midlatitudes. The hole occurs in easterly or weak westerly flows and reveals the existence of a critical level: "When a planetary wave is incident on a critical level from below, the associated heat flux vanishes discontinuously just above the level as a result of the absorption of the wave, according to linear theory" (Uryu 1980). Such a critical level barely exists at $\Omega^* = 1$.

The eddy momentum fluxes in Fig. 8a–c converge on all midlatitude jets, diverge from each QH jet, and traverse each polar jet. The converging fluxes are produced (presumably) by waves that disperse equally to the north and south because of their short wavelength and their confinement to narrow zones and high levels by the deep easterlies. Bimodal vertical fluxes coincide with converging lateral fluxes for the $QG_\beta(40°)$ jet at $\Omega^* = 2$ and for the $QG_\beta(50°)$ jet at $\Omega^* = 4$, but such correlations become weaker with increasing Ω^* (Fig. 9a–c). The MOIST(8) QH jet lies at the equator because of the momentum diffusion by the small Rossby waves and the subgrid-scale eddies. Even with greater numerical resolution this jet would lie very close to the equator, so this solution is not unrealistic.

High-range circulations thus consist of a tropical QH element, a polar QG_γ element, and multiple midlatitudinal QG_β elements. The circulations can be thought of as originating in baroclinically unstable $SH(R_E \gg 1)$ states. At high Ω^*, the SH momentum wind is confined to low latitudes and the thermal wind develops multiple instabilities because the eddy scale L_R is small. Nonlinear eddy development and wave propagation then generate multiple QG jets. Barotropic waves disperse from the jet cores in both directions but only penetrate neighboring jets in low latitudes, where they convert the Hadley flow into a QH element. The multiple QG elements transport heat smoothly poleward and upward by sharing common direct cells and easterlies. The localized momentum fluxes support the idea that separate elements exist but the continuous heat flow implies that the elements have soft boundaries, that they interact baroclinically if not barotropically, in keeping with Eq. (20). The dynamics of the MOIST(Ω^*) circulations are the dynamics of the QG, QH and NH elements, but a better understanding is needed of the element and eddy-mean flow interactions.

4.5 *The MOIST(8) variant circulation*

Singular circulations occur when $\Omega^* \to 0$ and $\Omega^* \to \infty$. The transition to the upper limit begins with the MOIST(8) case and its lack of a unique equilibrium. (The lower limit is discussed in Part II.) In the MOIST(8) variant phase in Fig. 11, the QH jet drops from 60 m s^{-1} to 15 m s^{-1} and the Hadley cell halves its amplitude, but without changes in width (see $\{P{:}K_Z\}$ in Table 3). The QG jets, cells, and instabilities, however, become stronger and deeper.

Why does the QH jet weaken so drastically and suddenly and then gradually re-establish itself? To answer this question we need a theory that explains what happens to circulations as $\Omega^* \to \infty$. Can cells exist at very high Ω^*, no matter how narrow they become, or do they degenerate into convection as the scale-separation diminishes? Does energy vacillate between the Hadley cell and the tropical convection, with the QH jet pulsating periodically, waving goodbye as it disappears into the near-hourly sunset?

To understand the oscillation of the QH jet, it would be useful to extend the SH theory to very high Ω^*. As noted in § 3.1, the SH theory breaks down when the Hadley cell becomes very narrow and the condition for a balanced flow, $\nabla \cdot (\mathbf{v}v)/fu_M \ll 1$, cannot be met (Held and Hou 1980). The critical value of θ_H appears to lie near 5° of latitude. The MOIST(8) case suggests that as $\Omega^* \to \infty$ the SH mode becomes symmetrically unstable, causing the momentum wind to oscillate before it finally vanishes.

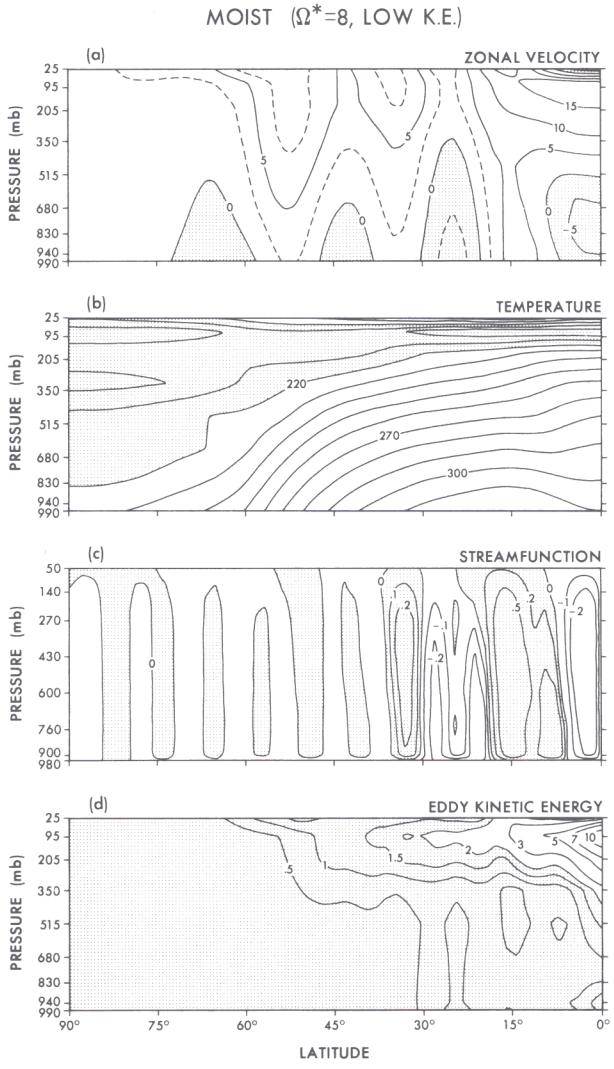

Fig. 11. Meridional distribution of the mean zonal wind, temperature, stream function and eddy kinetic energy for the MOIST model with $\Omega^* = 8$ during the variant phase of low kinetic energy. Units: m s^{-1}, K, 10^{13} g s^{-1}, 10 J kg^{-1} in (a)–(d), respectively

4.6 *The budgets and balances* (Table 3, Figs. 12–15)

The heat (moisture), momentum, and energy budgets and balances for the various MOIST(Ω^*) circulations involve dynamical variations on the standard $\Omega^* = 1$ theme of MSHS70. The thermal wind balance links the heat and momentum balances.

Heat. Although the meridional temperature fields vary considerably over $\Omega^* = 0$–8, compensations between the polar and equatorial regions, between the eddy and cell transports, and between the convection and radiation result in global values that range only weakly about the effective temperature, from 251 K to 254 K, and in cooling rates that vary by only 10% (Table 3). The dynamical redistribution of heat appears to have little net effect on the global mean temperature. The moisture amount varies considerably, from 2 cm to 7 cm of water, in response to changing surface temperatures; yet the radiative cooling in low latitudes remains nearly constant in Fig. 13a and 13c because of the compensation between the absorption and emission. Constant global temperatures thus result from a variety of compensations.

The meridional heat balance, represented by the equation

$$\bar{T}_t = -(\Gamma_d - \Gamma)\bar{w} - (\overline{v'T'})_y + \bar{Q} \qquad (32)$$

involves cell transport ($\Gamma < \Gamma_d$), eddy flux convergence, and diabatic heating and cooling. In the vertically averaged version in Fig. 12, the subgrid (S.G.) processes — convection and diffusion — are computed as a residual and generally match the radiative cooling in amplitude. Near the equator, however, the intensity of the convective heating far exceeds the radiative cooling rate because of the large moisture inflow and the concentrated latent-heat release in the convective towers. The Hadley cell imports the moisture in the lower troposphere and exports the released latent heat in the poleward flow aloft. Air subsiding in the Hadley cell heats the subtropics, suppresses convection, and is cooled by radiation. The large latitudinal variations in the cell heating are due to Gibbs-like oscillations set up by the sharp equatorial upflow; they occur when $\Omega^* = 0$, ½ and 1 but not when the whole cell is narrow, as in the MOIST(4) case, or when the upward flow is broad as in the DRY system.

In midlatitudes (QG regions), the compensation between the cell and eddy fluxes is strong and in the midrange is comparable to that between radiation and convection, with the Ferrel cell heating lower latitudes and cooling higher latitudes in response to the poleward eddy heat flux (Fig. 12b and 12c). When $\Omega^* = 0$ the Hadley subsi-

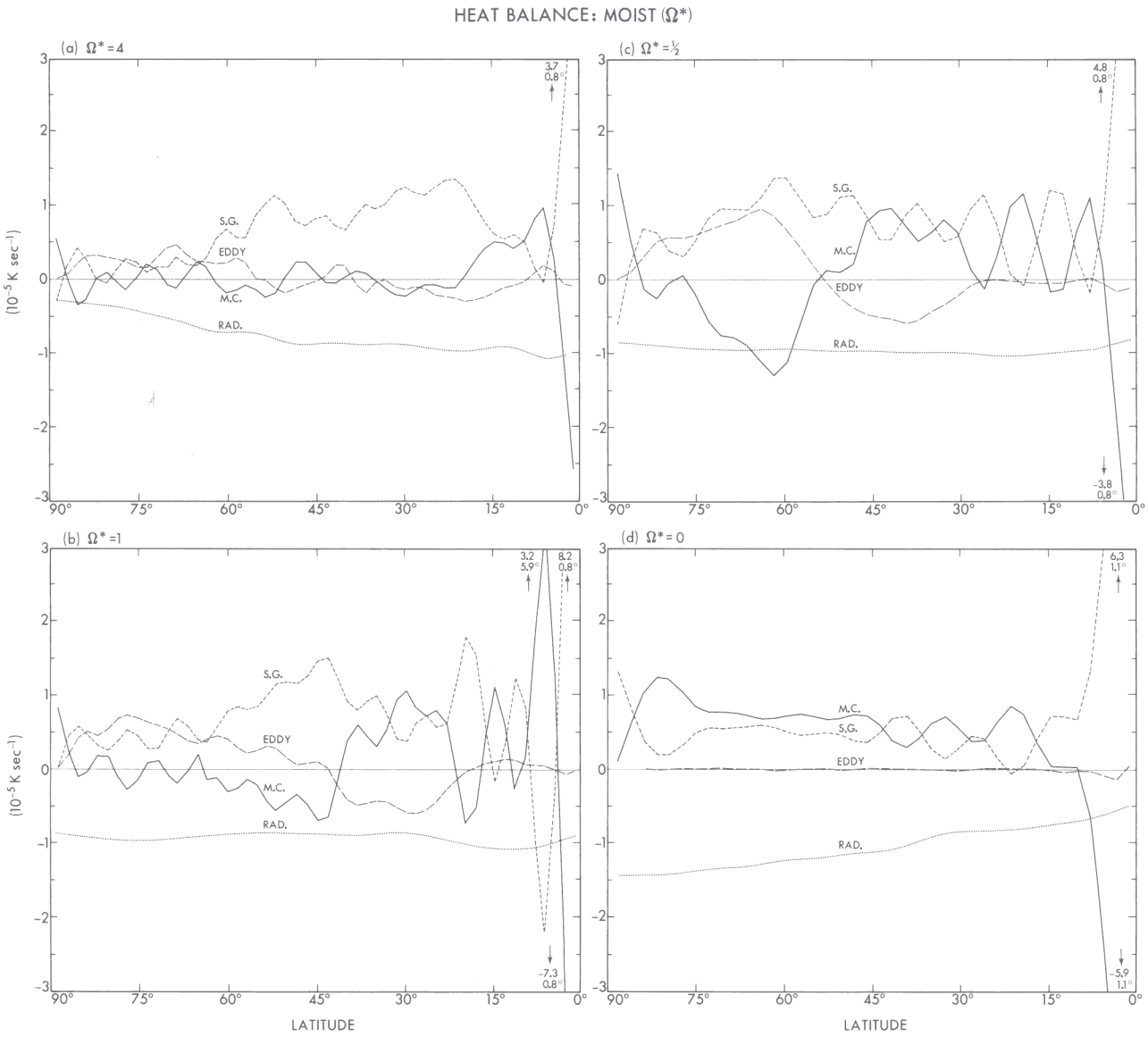

Fig. 12. Latitudinal distribution of the contributions to the mean rate of temperature change by the meridional circulation (M.C.), the radiation (RAD), the eddies (EDDY), and the subgrid-scale exchanges (S.G.) in the MOIST model with $\Omega^* = 0$, ½, 1, and 4

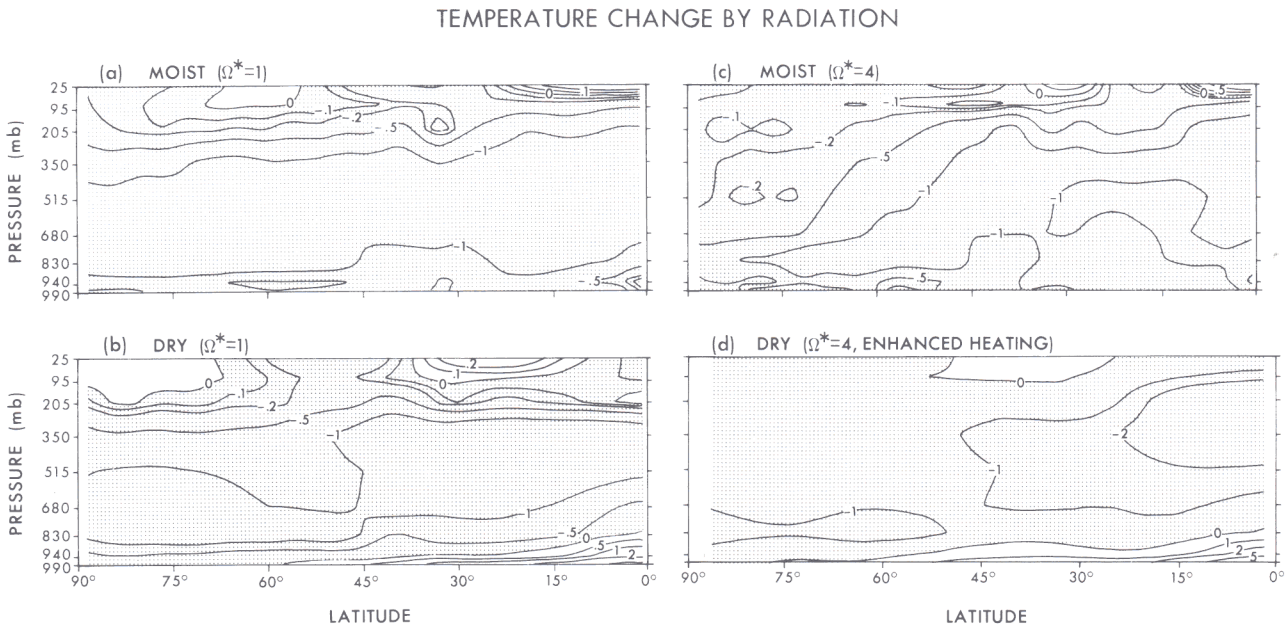

Fig. 13. Meridional distribution of the mean rate of temperature change due to radiation, for representative cases from the various sets. Units: 10^{-5} K s^{-1}

dence extends to the pole, with the advective and convective heating balancing the radiative cooling (Fig. 12d). When $\Omega^* = 4$ the dynamical heat transports are weak outside the Hadley region — except near the pole (Fig. 12a). Generally, the convection is deep (reaching up to 100 mb) near the equator but shallow (lying below 70 mb) in high latitudes and subsidence regions. In the Hadley cell the upper-level outflow exceeds the low-level inflow to cool the equator, while in the Ferrel cells the boundary-layer flux convergence dominates to heat the subsidence regions. The Ferrel heat transports are strong aloft only when large eddies induce a strong cell at $\Omega^* = \frac{1}{2}$. Thus compensations between the eddy and cell heat transports rarely occur at the same height.

As regards the radiation components in Fig. 13a and b, the thermal cooling by water vapor exceeds the solar heating by water vapor in tropospheric low latitudes by almost the same amount at $\Omega^* = 1$ and 4, despite large differences in the temperatures and the moisture contents. This large cooling decays rapidly with height at the tropopause and, when $\Omega^* = 4$, with latitude near the pole where the whole troposphere approaches a radiative equilibrium. In the stratosphere, a near balance between the solar heating by ozone and the thermal cooling by carbon dioxide and water vapor results in a weak heating in low latitudes and a weak cooling in midlatitudes.

Momentum. The surface torques in Table 3 are strongest in the midrange and an order of magnitude weaker in the low range. This variation illustrates how important the baroclinically unstable eddies are in determining the surface westerlies and easterly trade winds. The strongest mean meridional motions are eddy-induced in the midrange and diabatically forced at $\Omega^* = 0$. The strongest zonal flows occur at $\Omega^* = \frac{1}{8}$ in association with the strong Hadley mode present in moist atmospheres.

The meridional balance of zonal momentum, represented by the equation

$$\bar{u}_t = (f - \bar{u}_y)\bar{v} - (\overline{v'u'})_y - c_D\bar{u} \tag{33}$$

involves a Coriolis term that redistributes momentum in the vertical only (it vanishes in the vertically averaged balance), together with cell and eddy flux convergences and a surface drag. The advection term $\bar{v}\bar{u}_y$ provides the main ageostrophic process — when vertical fluxes are negligible — and acts mainly in the Hadley region via the momentum wind; it does not appear in the midlatitudinal QG formalism of § 3.4.

In the vertically averaged balances in Fig. 14, the classical view for the midrange (MSHS70) has the Hadley cell transporting the westerly momentum created by the trade-wind torque upward to maintain the low-latitude (QH) westerlies and,

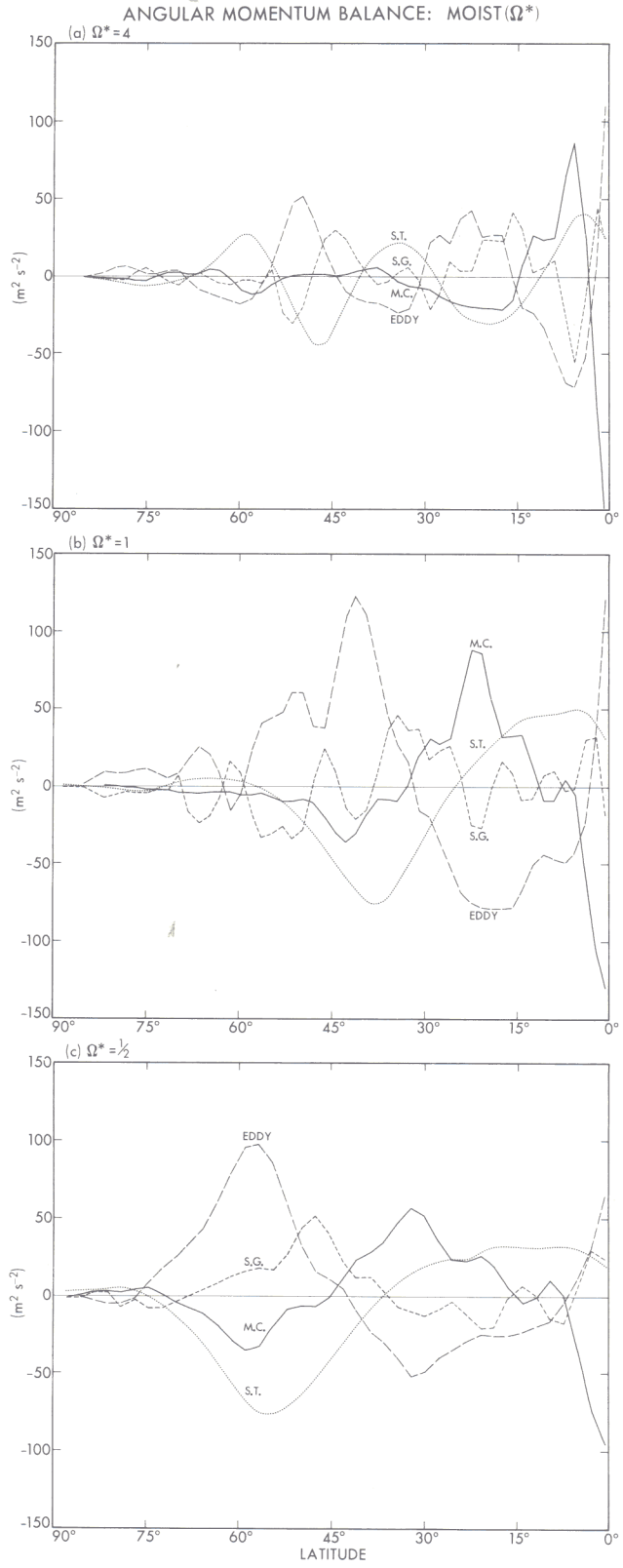

Fig. 14. Latitudinal distribution of the contributions to the mean rate of angular-momentum change by the meridional circulation (M.C.), the eddies (EDDY), the surface torque (S.T.) and the subgrid-scale diffusion (S.G.) in the MOIST model with $\Omega^* = \frac{1}{2}$, 1, and 4

after lateral eddy transport, to maintain the midlatitude (QG_γ) westerlies against their torque and also to produce the equatorial westerlies. A more causal explanation, however, has the midlatitude eddies as the main source of the zonal and meridional flow changes and of the surface torques. In midlatitudes in Fig. 14b and 14c, the eddy-flux acceleration of the (QG_γ) westerlies is balanced by the torque communicated vertically by the (eddy-induced) Ferrel cell. In low latitudes, the eddy fluxes balance the westerly (QH) acceleration produced by (eddy-induced) changes in the Hadley cell and torque. In the high range in Fig. 14a, this form of balance is restricted to the region between $\theta = 0°$ and 35°, with the Hadley cell driving the QH(10°) jet and the eddies driving the $QG_\beta(25°)$ jet (and also the $QG_\beta(50°)$ jet). The similarity between the balances at $\Omega^* = 1$ and 4 supports the idea that midrange flows consist of two overlapping components.

The actions of the cells and eddies in transporting heat and momentum are constrained by the thermal wind balance and must be mutually consistent. In QG regions the eddies act to increase $\bar{u}_z$ via $\overline{v'u'}$ and to decrease $\bar{T}_y$ via $\overline{v'T'}$ and so destroy the thermal wind balance. The Ferrel cell arises to decrease $\bar{u}_z$, by producing easterly momentum aloft and westerly below, and to increase $\bar{T}_y$, by warming on the equatorward side and cooling on the poleward side, and so maintains the thermal wind balance. In QH regions the eddies break the thermal wind balance by decreasing $\bar{u}_z$ and increasing $\bar{T}_y$. The Hadley cell strengthens itself to reduce $\bar{T}_y$, thereby creating the easterly trades and strengthening the westerly jet.

Energy. The parametric variation in the global energy statistics in Table 3 reflects the presence of two strong modes: the eddy kinetic energy peaks at $\Omega^* = 1$ in a compromise between QG eddy size and QH cell size; the mean kinetic energy peaks at $\Omega^* = \frac{1}{8}$ in association with the NH mode; and the minimum value of $\{P{:}K_Z\}$ occurs at $\Omega^* = \frac{1}{2}$ because the Ferrel cell nearly matches the Hadley cell as a potential energy converter when its inducing eddies are at their largest — in the DRY midrange the Ferrel cell actually dominates to give $\{P{:}K_Z\} < 0$.

The kinetic energy spectra in Fig. 15, based on the longitudinal decomposition of instantaneous data averaged over all heights and latitudes, vary from a k^{-2} form at $\Omega^* = 0$ to a k^{-5} form at $\Omega^* = 4$. Although the GCM has too low a numerical resolution and too sparse an energy supply for turbulence studies, its midrange spectra are in line with

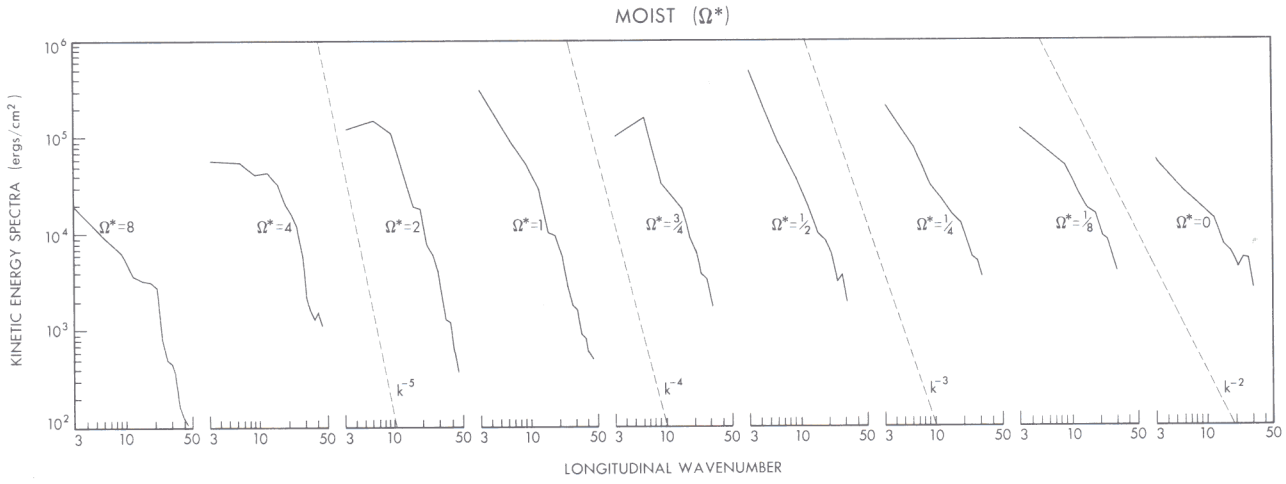

Fig. 15. Instantaneous kinetic energy spectra in terms of the longitudinal wavenumbers for the MOIST model with $\Omega^* = 0$–8

the k^{-3}–k^{-6} enstrophy-cascading forms obtained in recent high-resolution turbulence calculations (Basdevant et al. 1981) (see § 3.2). The steepening of the spectra with increasing Ω^* reflects both the increased intermittency of small eddies and the emergence of the wave regime at larger β (Rhines 1975). Moist convection produces the equipartitioned k^{-2} spectra in the low range;

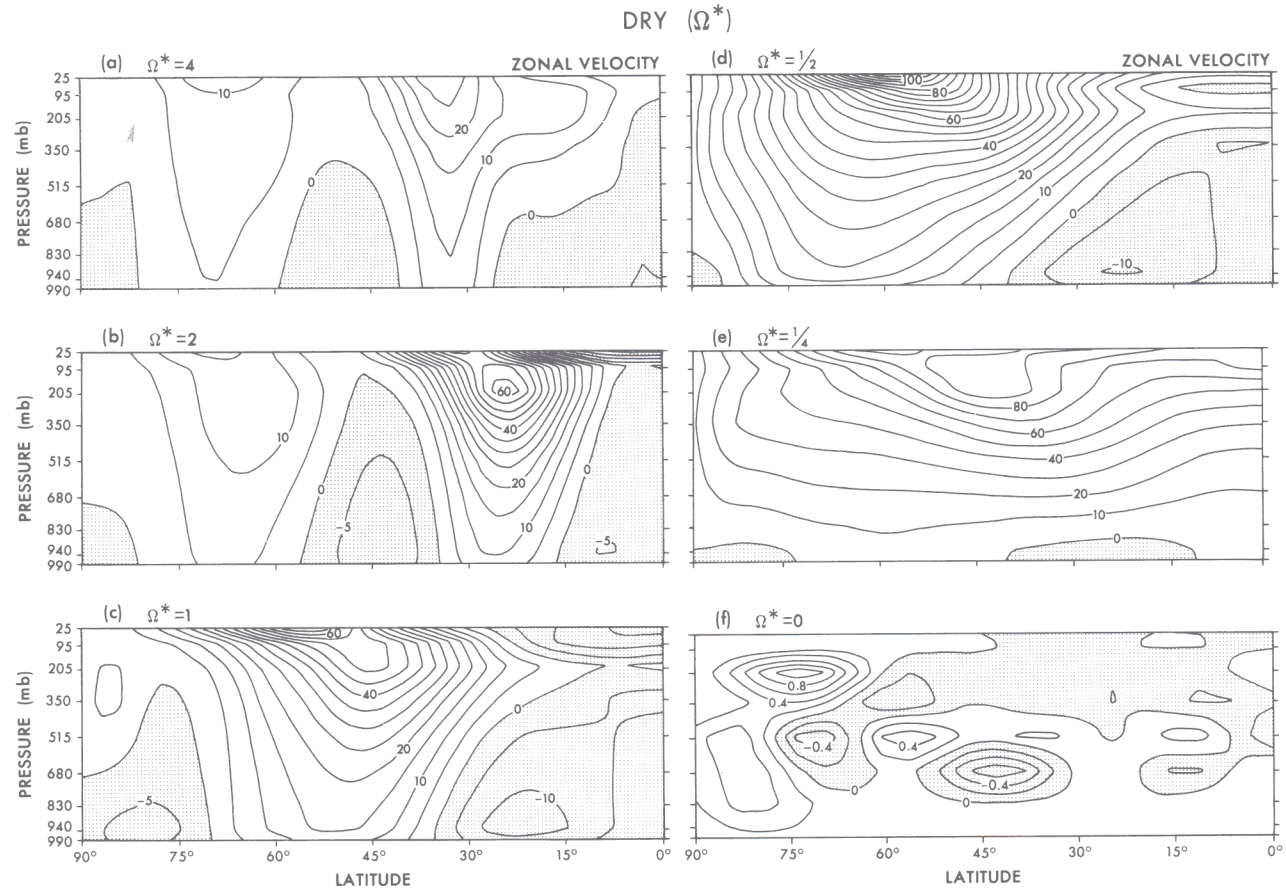

Fig. 16. Meridional distribution of the mean zonal wind for the DRY model with $\Omega^* = 0$–4. Units: m s^{-1}

Table 4. DRY and modified-surface circulations: energy, heat, and momentum integrals

Case		Energy						Heat				Momentum				
Ω^{*e}	Δ	τ_I	K_Z	K_E	$P{:}K_Z$	$P{:}K_E$	$K_Z{:}K_E$	T^a	RAD	$v'T'^c$	$-\omega'T'$	Max[b] torque	$v'M'$	$-\omega'M'$	Max[d] $\lvert u\rvert$	Max $\lvert v\rvert$
4	D	529	34	8	11	79	− 15	251.1	−540	145	136	− 56	31	− 14	30	1.0
2	D	819	156	47	39	180	− 47	252.2	−649	373	346	− 66	46	−198	63	1.7
1	D	409	176	65	− 7	351	−204	251.3	−678	623	649	−106	557	547	70	3.1
½	D	729	371	57	−84	439	−320	252.8	−655	753	817	− 89	646	721	110	4.2
¼	D	1700	105	61	127	175	− 19	251.8	−642	213	465	− 20	− 76	256	98	2.5
1/32	A	860	77	13	58	−14	23	251.8	−452	−18	433	− 9	−122	− 11	39	5.2
0	A	400	3	0.4	7	− 0.1	0.2	250.9	−345	0.1	0	− 0.1	0.7	0.1	1.1	6.0
4, SLIP	E	249	128	20	58	196	− 35	252.7	−908	150	299	—	106	−118	39	5.0
1, SLIP	A	280	275	37	− 7	59	− 7	237.5	−296	335	152	—	73	79	54	2.5
4, HOT	A	440	296	49	56	183	− 43	262.5	−914	436	393	63	203	96	112	2.0
Units		Days	$J\,kg^{-1}$		$10^{-6}\,W\,kg^{-1}$			K	$10^{-8}\,Ks^{-1}$	$10^1\,J\,m\,kg^{-1}\,s^{-1}$	$10^{-2}\,W\,m^{-2}$	$m^2\,s^{-2}$	$10^5\,kg^2\,m^{-2}$	$10^2\,s^{-2}$	$m\,s^{-1}$	

[a] Instantaneous value here only
[b] Max denotes local extreme; global means elsewhere
[c] Eddy integrals are denoted symbolically; sphericity factors are involved
[d] In the troposphere
[e] SLIP, HOT variants denote cases with surface slip and enhanced heating; only SLIP(4) model is moist

τ_I denotes integration period
Δ denotes integration domain and resolution (see Table 1)
RAD denotes radiative heating rate

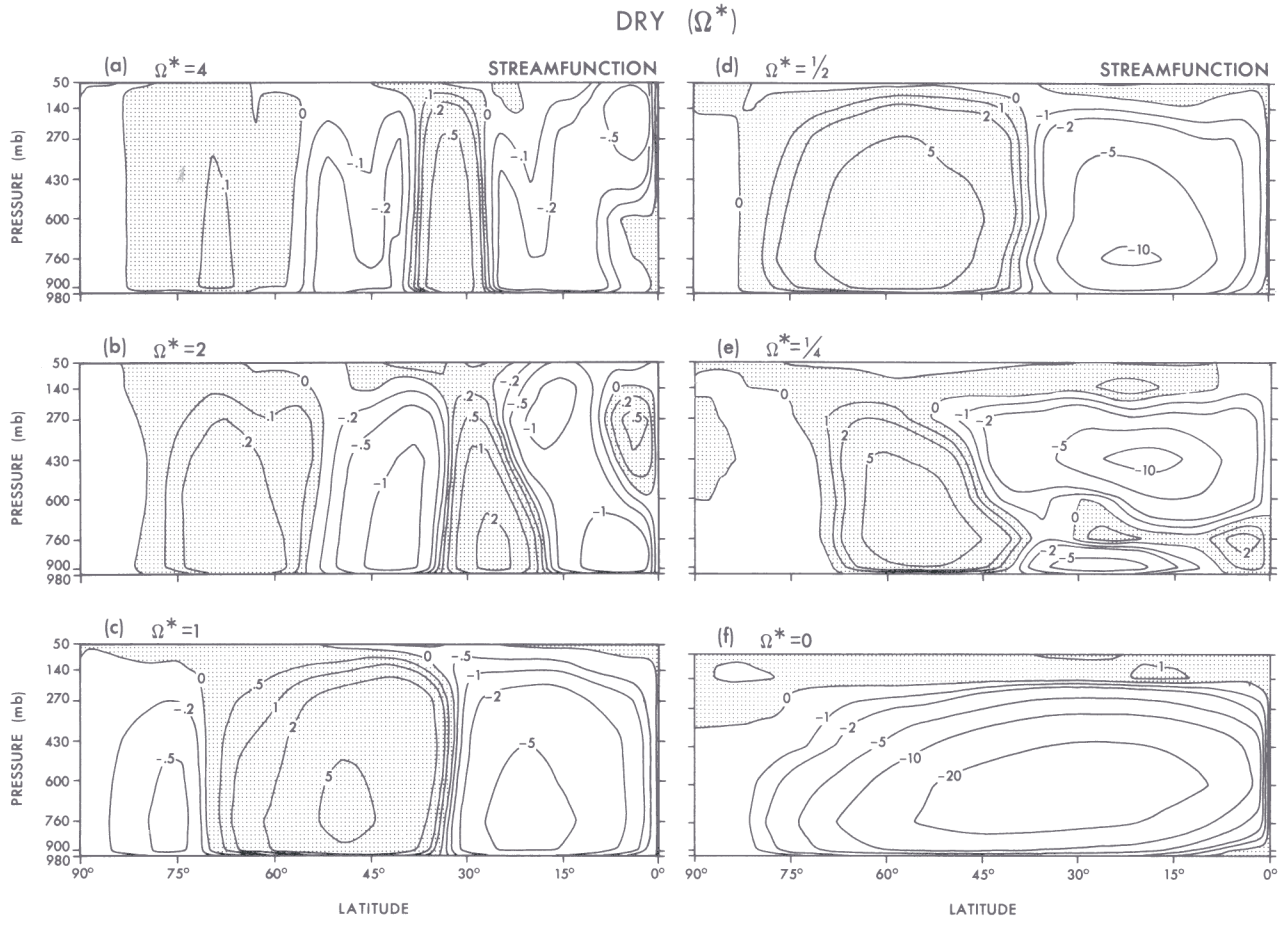

Fig. 17. Meridional distribution of the mean stream function for the DRY model with $\Omega^*=0$–4. Units: $10^{13}\,g\,s^{-1}$

such spectra occur in the tropics when $\Omega^* = 1$ (Gordon and Stern 1982). The DRY spectra are all steeper than k^{-2}.

5 DRY(Ω^*) circulations

To clarify the role of moist dynamical processes in the MOIST(Ω^*) circulations, we exclude them and create a pseudo-dry model. The main virtue of the resulting DRY(Ω^*) solutions is their lack of a QH component in the mid- and high ranges. This allows the GCM to give cleaner examples of nonlinear baroclinic instabilities. In addition, the absence of moist convection leads, in the low range, to weaker wave generation and cleaner examples of NH elements. What goes on in the transition between the stable and unstable flows is also more clearly revealed. The MOIST, DRY, and AXISYMMETRIC circulations have a considerable (but superficial and confusing) similarity to one another when $\Omega^* = 1$, but at other Ω^* their fundamental differences are obvious.

To eliminate the influence of moist dynamics, we no longer predict the mixing ratio and we adopt a pseudo-dry convective adjustment scheme in which the lapse rate is reset to the theoretical moist adiabat whenever it is exceeded (Smagorinsky et al. 1965). Such a scheme produces static stabilities and hence baroclinic eddies comparable with those of the MOIST set. The radiative influence of moisture is retained by prescribing the ($\Omega^* = 1$) climatological mixing ratios in tabular form. Omitting moisture altogether would alter the thermodynamics too much. The pseudo-dry model, however, maintains a close thermodynamical similarity with the moist model only at $\Omega^* = 1$. At other Ω^*, the three fixed gas distributions give only a relative radiative forcing.

The DRY(Ω^*) set is evaluated at six representative values of Ω^*, two per subrange between $\Omega^* = 0$ and 4, together with a supplementary low-range value at $\Omega^* = 1/32$ (Table 4). The R30 spectral resolution is more than adequate for flows that have little energy in the small convective scales.

5.1 *The DRY(Ω^*) progression* (Figs. 16–28)

The DRY circulations progress in Figs. 16–19 and 27 from NH states with one jet and one cell in the low range, to QG_γ states with one jet and two or three cells in the midrange, to paired QG_γ and QG_β jets with four (all eddy-induced) cells in the high range. The easterly trade winds are deeper and more extensive than in the MOIST flows and are associated with the (non-Hadley) direct cells. The QH westerly jet and Hadley cell fail to arise because the QG eddy-forced modes exceed and overwhelm the diabatically driven Hadley modes, whereas in the MOIST case both modes are equally robust and so coexist. Consequently, the DRY(Ω^*) progression is simpler and hybrid flows are confined to the transitional state at $\Omega^* = 1/4$, a state that has remarkably strong equatorial westerlies.

The DRY eddies have little kinetic energy in low latitudes in the absence of moist convection and the presence of deep blocking easterlies (Fig. 19). In the low range, the eddies are confined to their source region in the polar jet (Fig. 27). The DRY eddy heat fluxes parallel the MOIST ones in midlatitudes, being continuously poleward and upward, even for the double-jet states (Figs. 20 and 21). There is, however, almost no equatorward transport into low latitudes because waves cannot penetrate the deep DRY easterlies. The transitional DRY(1/4) fluxes indicate the existence of a semi-shallow instability.

The lateral momentum fluxes in Figs. 22 and 28b progress from traversing equatorward in the low range and traversing poleward in the midrange, to converging on low-latitude jets and traversing high-latitude jets in the high range. The vertical momentum fluxes are appropriately upward in the midrange and bimodal in the high-range low-latitude jets (Fig. 23). The geopotential fluxes in Fig. 28c and 28f — downward and equatorward — confirm that the polar jet is the main energy source for the low-range eddies. In the high range, the geopotential fluxes transfer energy downward into the midlatitude easterlies and upward into the low-latitude jet core, and thence north and south to the jet boundaries (Figs. 24 and 25).

The barotropic conversion $\{K_Z : K_E\} = \bar{u}\nabla \cdot (\overline{\mathbf{v}u'})$ in Fig. 28g also shows the polar jet as sustaining the low-range eddies by weak barotropic wave-wave resonances (Baines 1976). The eddies, however, accelerate the midrange jets and the cores of the high-range jets (Fig. 26). The transitional DRY(1/4) circulation has a mix of low-range and midrange features, with, for example, the eddies energizing the poleward side and de-energizing the equatorward side of the zonal flow in near-equal amounts (Fig. 26e).

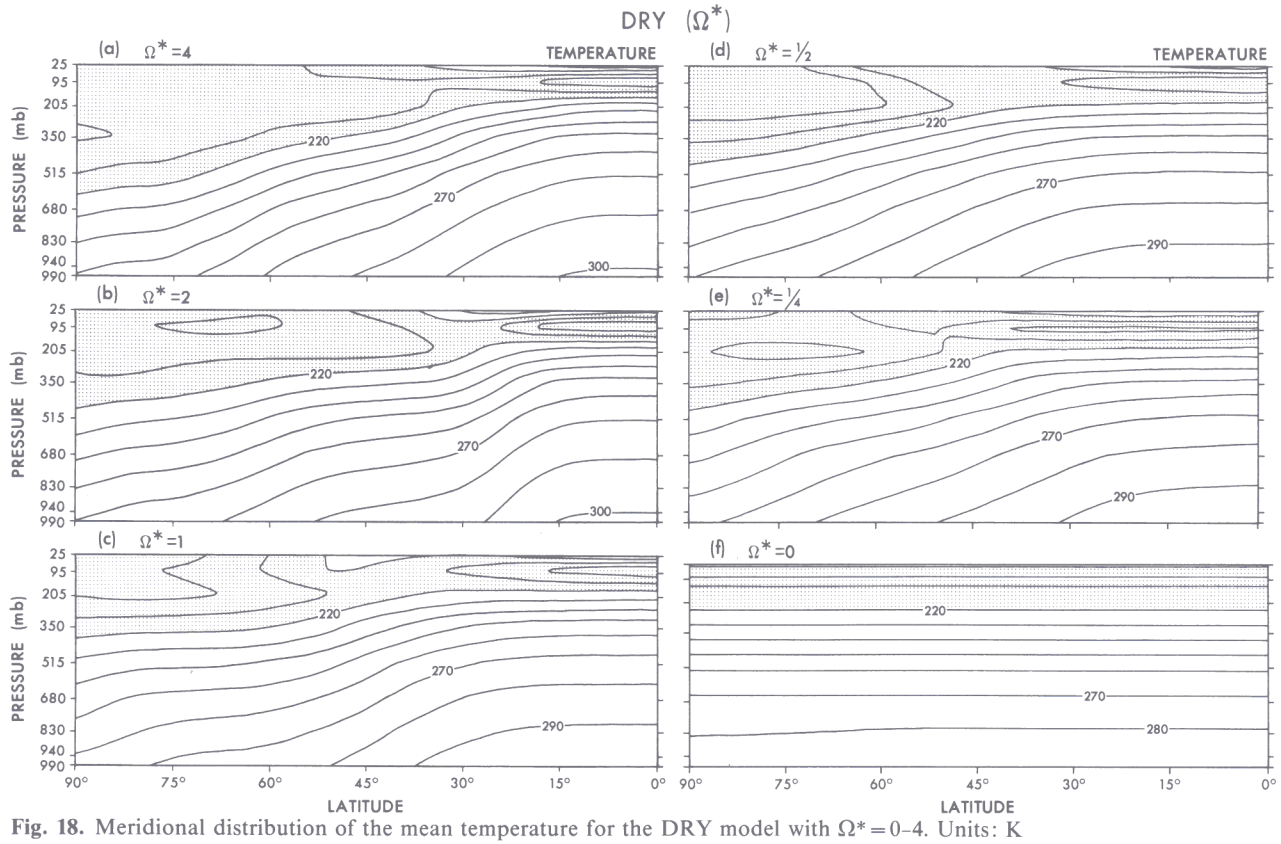

Fig. 18. Meridional distribution of the mean temperature for the DRY model with $\Omega^* = 0$–4. Units: K

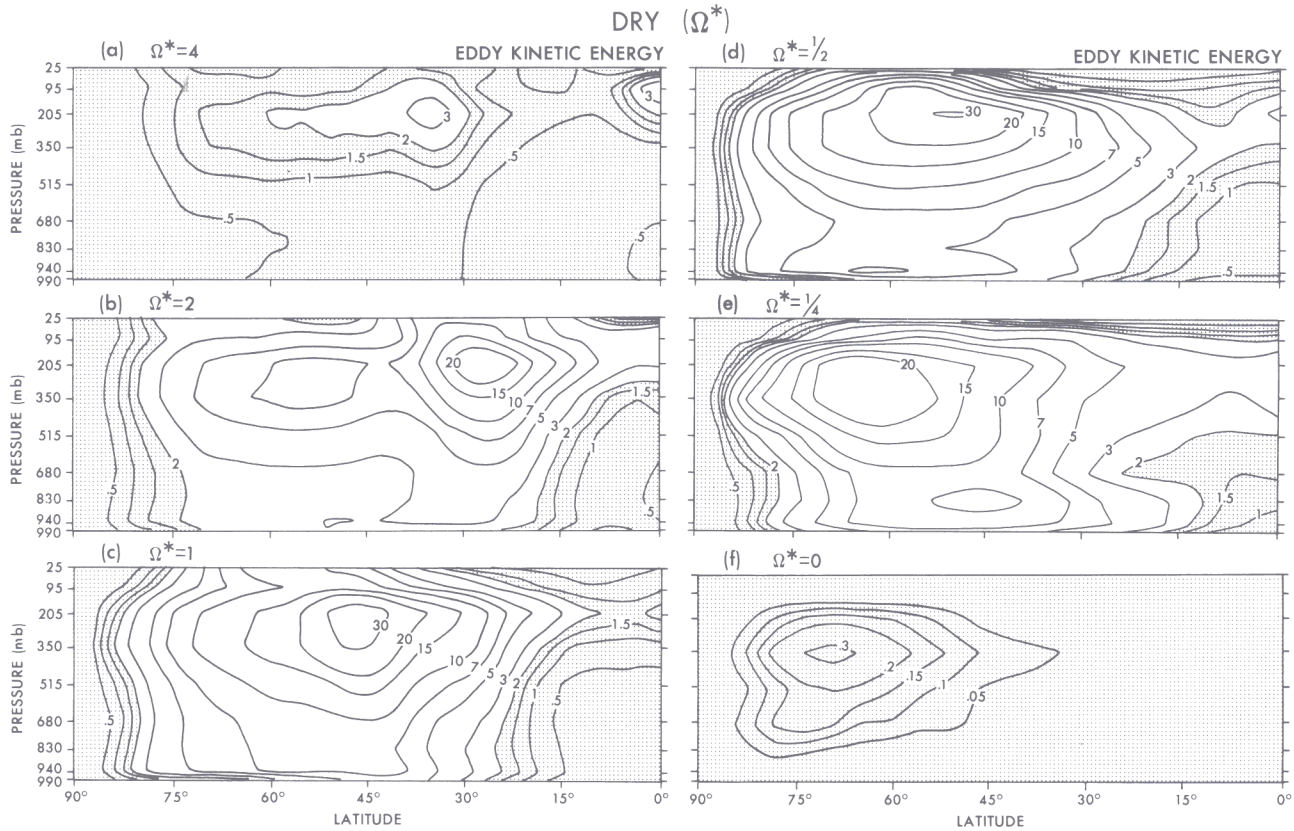

Fig. 19. Meridional distribution of the mean eddy kinetic energy for the DRY model with $\Omega^* = 0$–4. Units: 10 J kg^{-1}

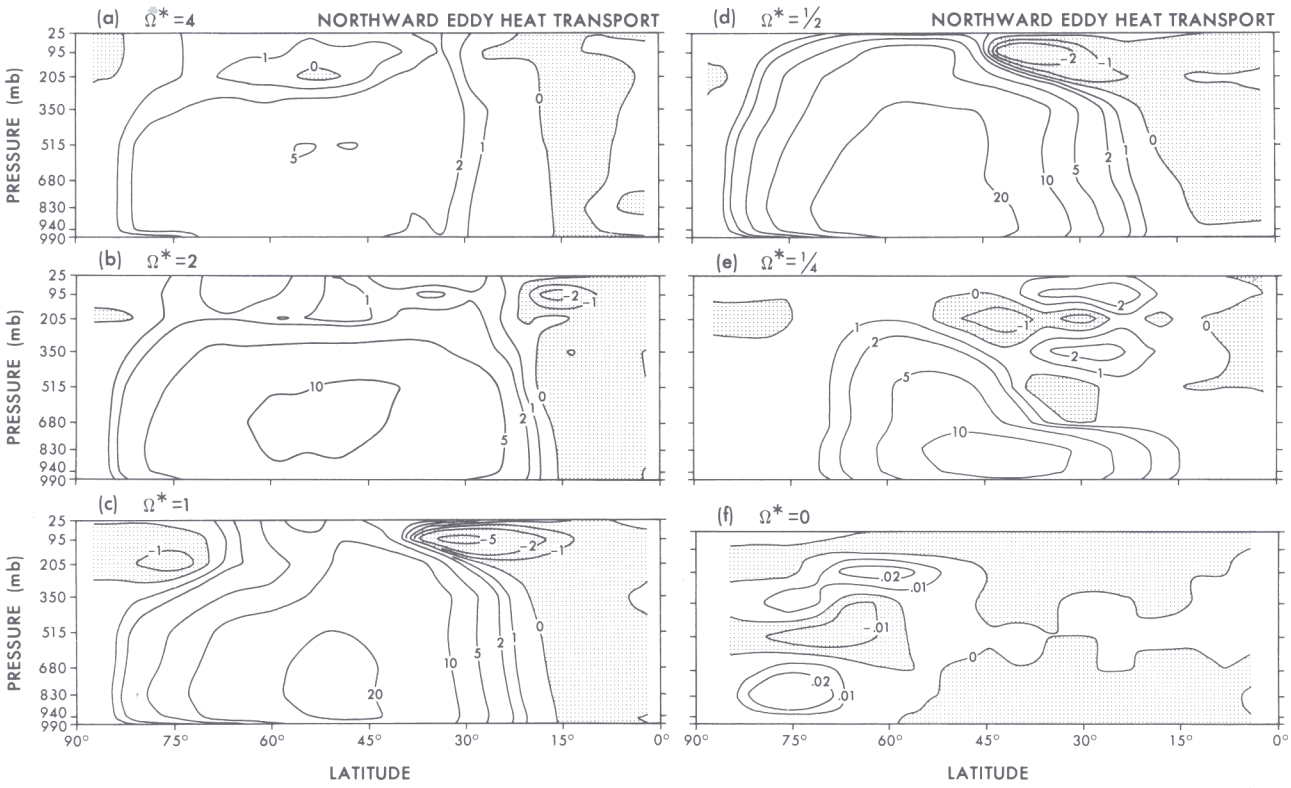

Fig. 20. Meridional distribution of the mean northward transport of heat by the eddies in the DRY model with $\Omega^* = 0$–4. Units: 10^3 J m kg^{-1} s^{-1}

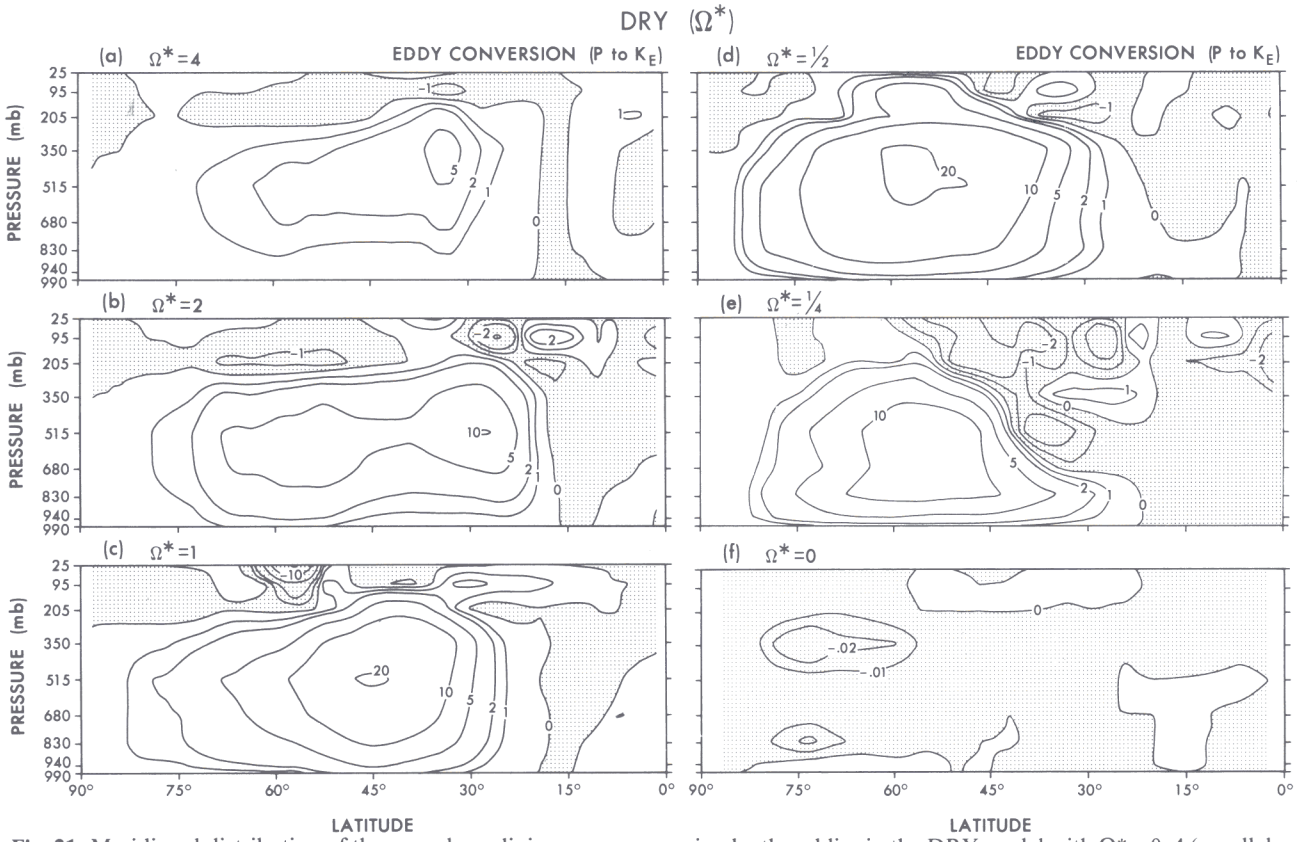

Fig. 21. Meridional distribution of the mean baroclinic energy conversion by the eddies in the DRY model with $\Omega^* = 0$–4 (parallels the vertical eddy heat transport). Units: 10^{-4} W kg^{-1}

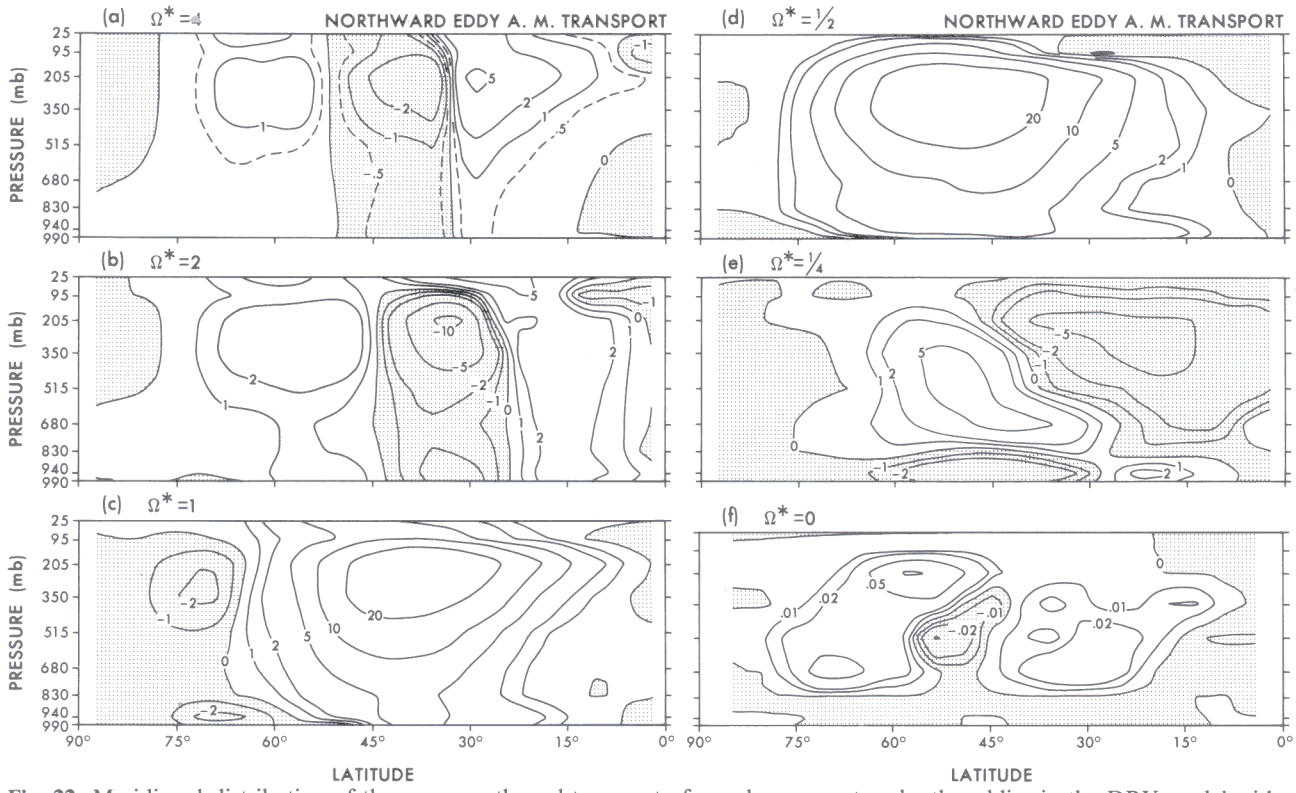

Fig. 22. Meridional distribution of the mean northward transport of angular momentum by the eddies in the DRY model with $\Omega^* = 0$–4. Units: 10^7 m^3 s^{-2}

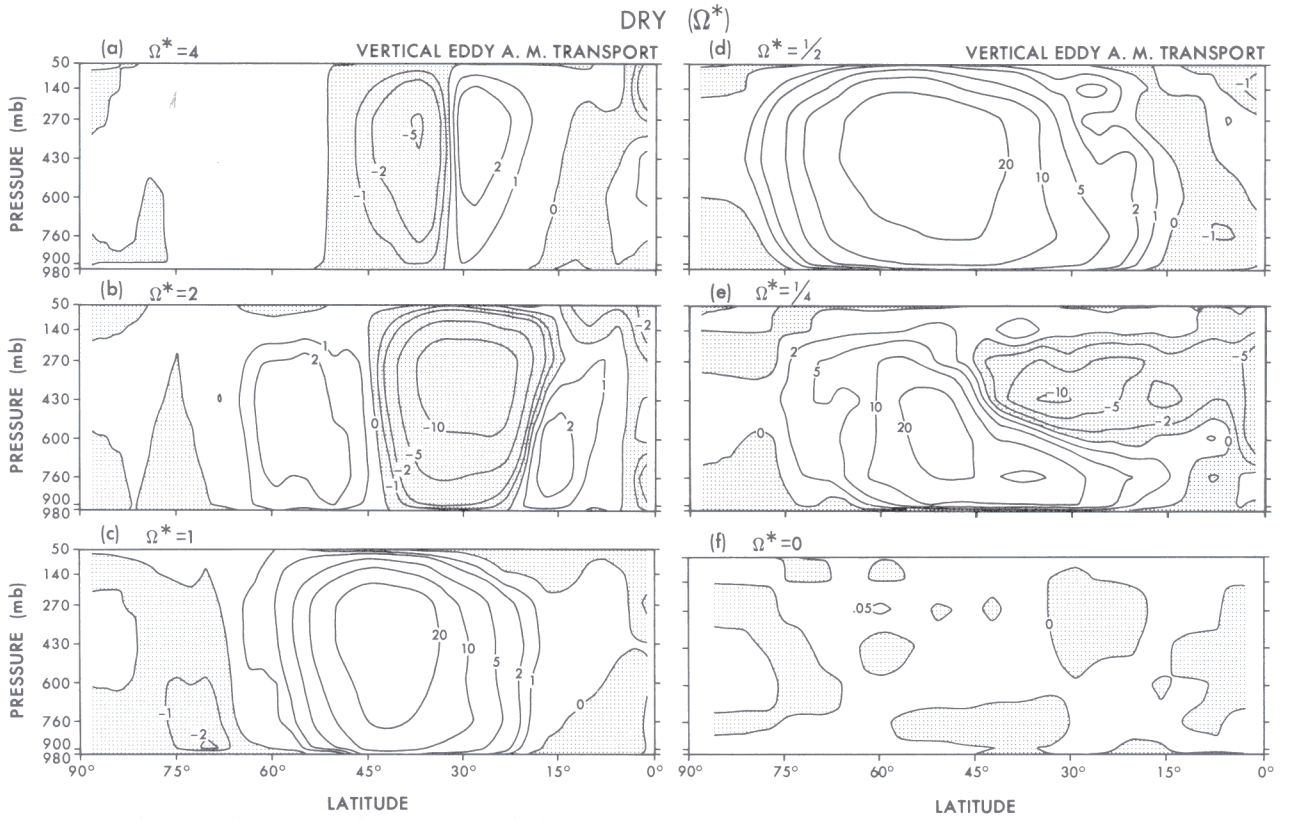

Fig. 23. Meridional distribution of the mean vertical transport of angular momentum by the eddies in the DRY model with $\Omega^* = 0$–4. Units: 10^4 kg s^{-2}

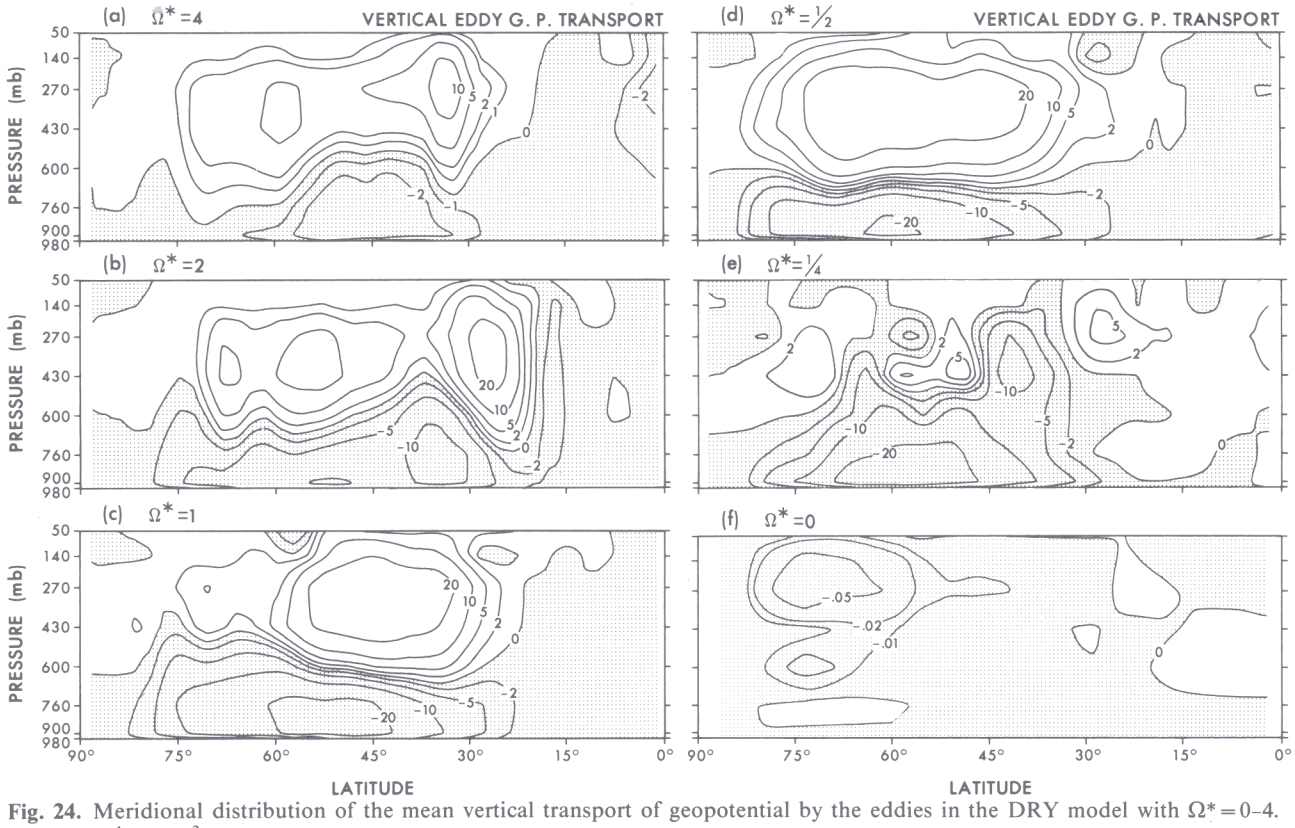

Fig. 24. Meridional distribution of the mean vertical transport of geopotential by the eddies in the DRY model with $\Omega^* = 0$–4. Units: 10^{-1} W m^{-2}

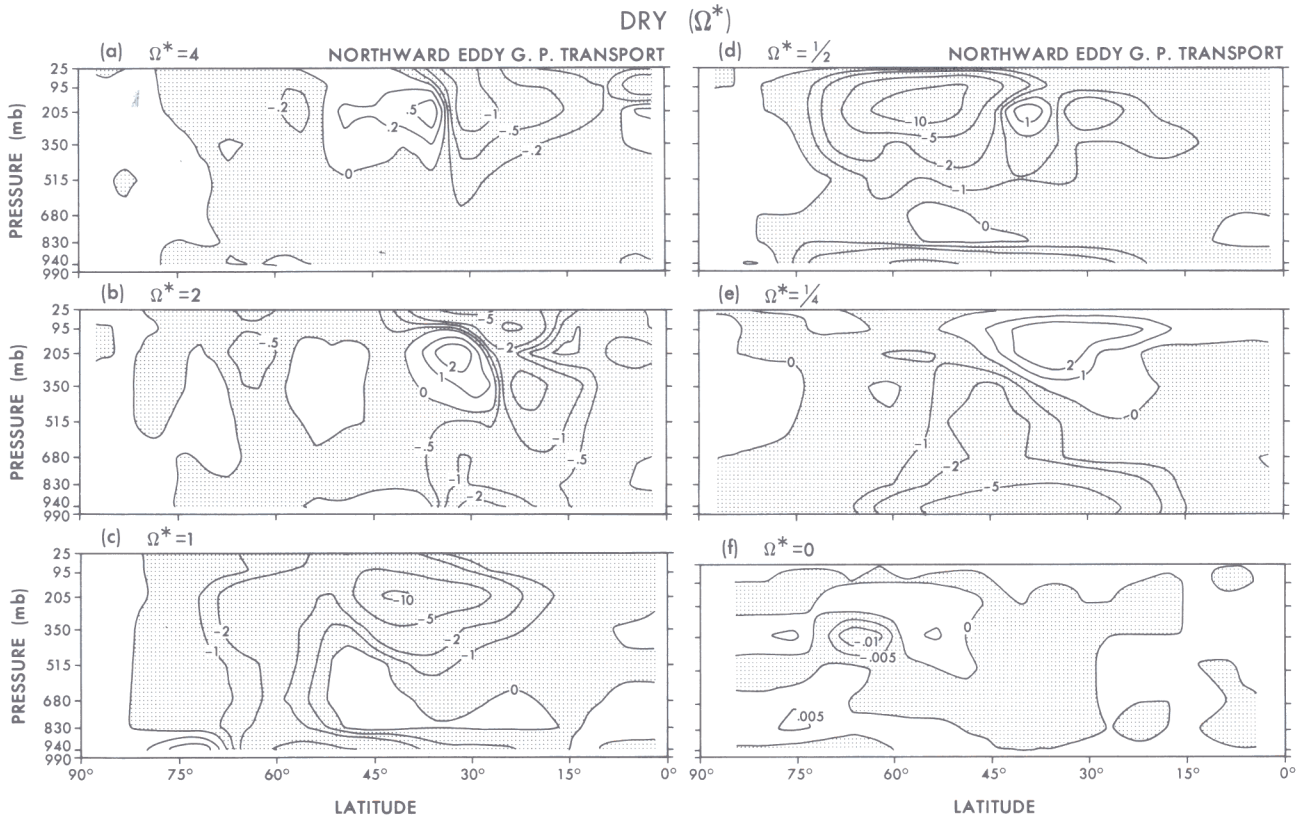

Fig. 25. Meridional distribution of the mean northward transport of geopotential by the eddies in the DRY model with $\Omega^* = 0$–4. Units: 10^2 J m kg^{-1} s^{-1}

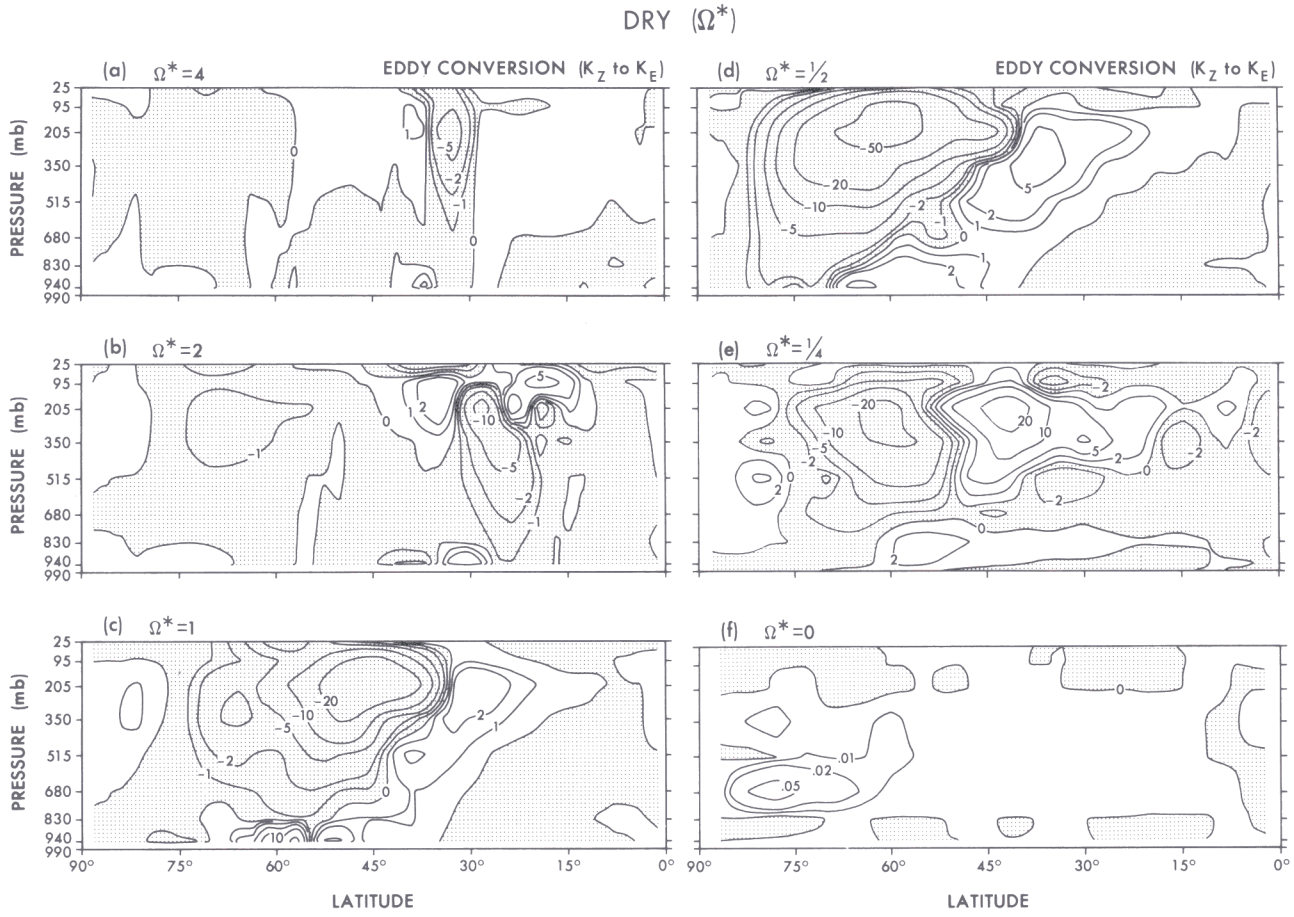

Fig. 26. Meridional distribution of the mean barotropic energy conversion by the eddies in the DRY model with $\Omega^* = 0$–4. Units: 10^{-4} W kg^{-1}

The baroclinically generated eddies clearly dominate the DRY(Ω^*) circulations when $\Omega^* \geqslant \frac{1}{4}$ by forcing zonal and meridional flows that eliminate the Hadley mode. The eddies also produce deep easterly trade winds that block further wave propagation. In the MOIST case, the eddies convert the Hadley mode into a QH element and propagation continues.

5.2 *The low-range circulations*

The DRY low-range circulation in Figs. 27 and 28 has the same mean fields and eddy fluxes as its MOIST counterpart in Figs. 2i–9i, but its waves have a different source. The DRY eddies are generated in the polar jet ($\{K_Z : K_E\} > 0$) and transfer little energy and momentum equatorward, unlike the MOIST eddies which are mainly energized by the tropical convection ($\{P : K_E\} > 0$). Cell upflow is broader in the absence of moisture. Both systems, however, qualify as having NH circulations. The DRY eddy fluxes are weaker but well defined and symptomatic of wave propagation: for example, the $\overline{v'\Phi'}$ flux is latitudinally uniform in keeping with the Eliassen-Palm non-acceleration condition for Rossby waves that $[\overline{v'\Phi'}/(\bar{u}-c)]_y = 0$.

The DRY($\frac{1}{4}$) circulation in Figs. 16e—26e, with its strong semi-shallow instability, is a poor guide to the low range but a good guide to the transition. Two major events can be discerned in this flow: (1) on the poleward side the u_E thermal wind becomes baroclinically unstable and creates strong eddy fluxes; and (2), on the equatorward side the Hadley cell becomes disconnected from the surface because of flow changes forced by the eddies (Fig. 17e). Without the cell upflow to communicate the angular momentum value of the surface to the atmosphere and initialize the u_M wind, the angular-momentum constraint is eliminated and the u_E wind extends to the equator (Fig. 16e).

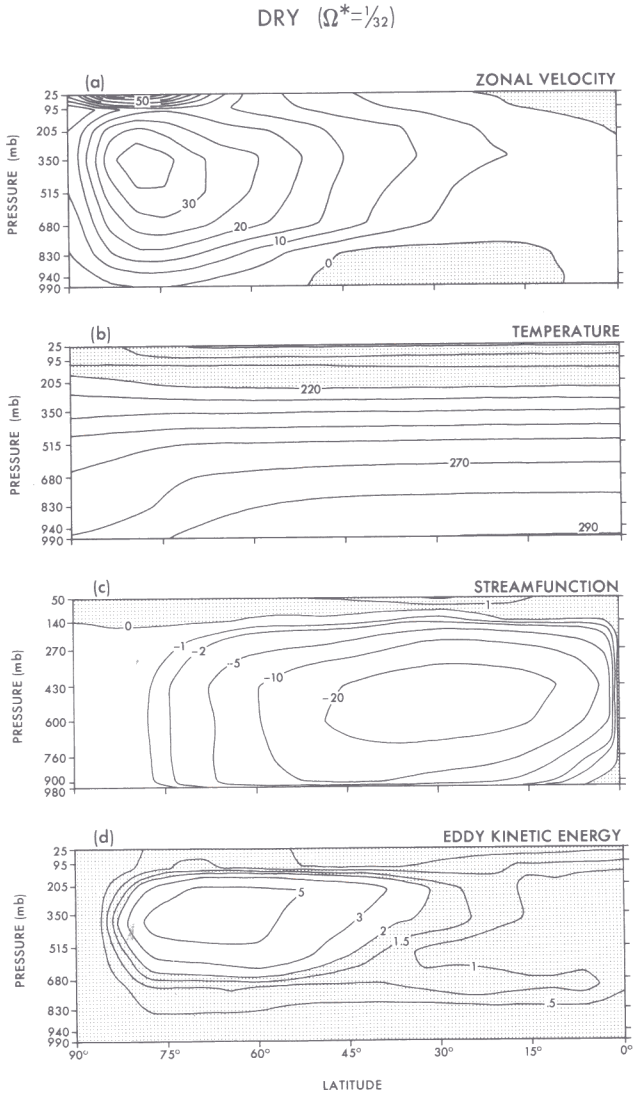

Fig. 27. Meridional distribution of the mean zonal wind, temperature, stream function, and eddy kinetic energy for the DRY model with $\Omega^* = 1/32$. Units: m s^{-1}, K, 10^{13} gs^{-1}, 10 J kg^{-1} in (a)–(d), respectively

The DRY(¼) circulation has QG_γ characteristics on the poleward side but unique (transitional) characteristics on the equatorward side.

The eddies of the semi-shallow instability, like those of Charney's linear theory, transport a lot of heat but not much momentum (cf. Hunt 1979a). The equatorial westerlies come from the thermal wind balance, not the eddy flux. How the eddies disconnect the momentum constraint and extend the thermal wind during this transition from stable NH to unstable QG_γ flow remains a theoretical puzzle. Perhaps the eddies strengthen the Hadley cell aloft or weaken it below, causing it to split into two and switch off the SH mode.

5.3 The midrange circulations

The DRY midrange circulations, being eddy dominated, peak along with the eddy size and strength at $\Omega^* = ½$, whereas the Hadley-dominated MOIST circulations peak in the stable low range, at $\Omega^* = ⅛$ (Fig. 16c and 16d). The eddies induce two cells at $\Omega^* = ½$ and three cells at $\Omega^* = 1$; all cells are wider than their MOIST equivalents because the eddies are larger and because the upflow in the main direct cell is spread over 20° of latitude, not confined to the equator (Fig. 17c and 17d). Compensation between the eddy and cell transports again gives a near-constant net heat flux and surface baroclinicity (35 K) (Fig. 18c and 18d). Both the pole and the equator are about 10 K cooler than in the MOIST system, and a strong stratospheric baroclinicity of −35 K gives a well-defined tropopause gap and polar inversion.

Although the midrange DRY and MOIST circulations have similar amplitudes, they have different structures and dynamical balances. The instability-driven heat flux in Fig. 20c and the wave-driven momentum flux in Fig. 22c — both poleward — define the DRY midrange flows as pure QG_γ elements and, hence, simpler than the hybrid MOIST flows. The baroclinic instability eradicates all trace of the Hadley mode and produces direct and indirect cells affiliated with easterlies and westerlies, respectively. The main direct cell in the DRY midrange is eddy-forced, not diabatically driven, and the weak values of $\{P{:}K_Z\}$ in Table 4 reflect its equality with the Ferrel cell. (The Hadley cell survives in the MOIST midrange because of the localization of the upflow and produces large positive $\{P{:}K_Z\}$ conversions; see Table 3.)

5.4 The high-range circulations

A large transition occurs when Ω^* increases from 1 to 2 and the DRY(1) $QG_\gamma(50°)$ jet narrows, moves equatorward, evolves into a $QG_\beta(25°)$ jet, and allows a second $QG_\gamma(65°)$ jet to arise (Fig. 16b and 16c). A further doubling of Ω^* weakens the two jets but does not alter their width or position (Fig. 16a). Although the jets do narrow as Ω^{-1} between $\Omega^* = 1$ and 2, their constancy between $\Omega^* = 2$ and 4 suggests that some factor other than the eddy scales L_R and L_β controls their width. Jets form under the influence of both eddy forcing and wave dispersion, and it may be the latter that determines the jet scale here. The high-range

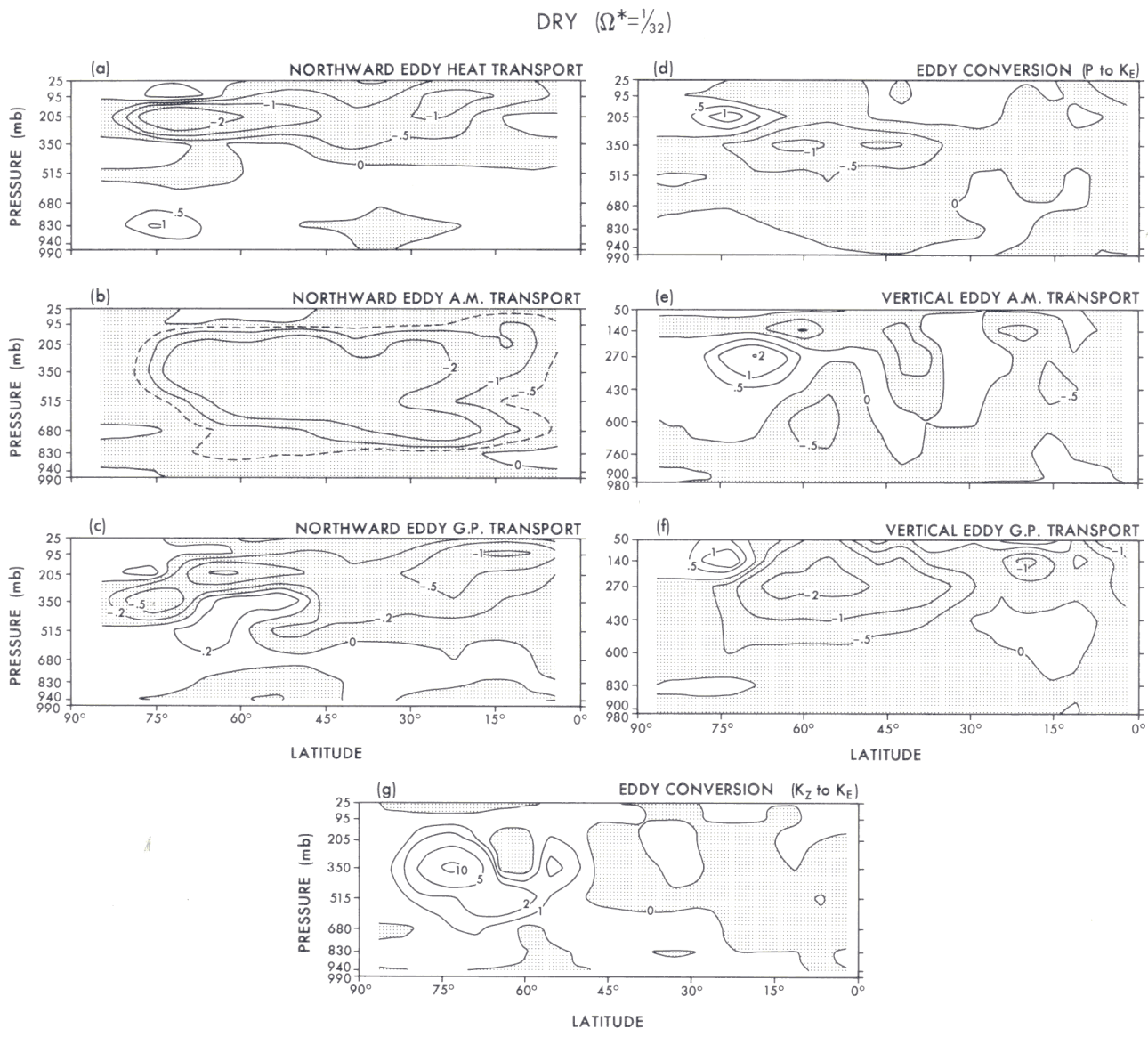

Fig. 28. Meridional distribution of the mean northward heat transport, northward angular-momentum transport, northward geopotential transport, baroclinic energy conversion, vertical angular-momentum transport, vertical geopotential transport, and barotropic energy conversion — all by the eddies — in the DRY model with $\Omega^* = 1/32$. Units: 10^3 J m kg^{-1} s^{-1}, 10^7 m^3 s^{-2}, 10^2 J m kg^{-1} s^{-1}, 10^{-4} W kg^{-1}, 10^4 kg s^{-2}, 10^{-1} W m^{-2}, 10^{-4} W kg^{-1} in (a)–(g), respectively

easterly trade winds are weak and poorly defined compared to their MOIST counterparts because wave propagation is weak in the absence of the QH westerlies.

The high-latitude QG_γ element has two cells, while the low-latitude QG_β element has three cells, but they share one to give high-range flows a total of four cells (Fig. 17a and 17d). Cell sharing, a measure of the interaction between the two elements, can be seen in the DRY(4) bimodal direct cell at $\theta = 45°$ where the two contributions have not merged completely. The main DRY(4) direct cell lacks the simplicity of a diabatically driven Hadley cell and reflects the complexity of wave propagation and eddy induction in the low latitudes (Fig. 17a). All cells correlate closely with the surface zonal winds via the simple momentum balance $f\bar{v} = c_D \bar{u}_s$ for the boundary layer: the Ferrel cells lie in the jet cores, while the direct cells lie in the jet edges and the easterlies in keeping with QG theory.

Quantitative comparisons between the DRY and MOIST solutions are only marginally useful because their radiative forcings differ signifi-

cantly when $\Omega^* \neq 1$. For example, the DRY(4) polar atmosphere is warmer than that of MOIST(4) because, radiatively, it contains more moisture — the observed $\Omega^* = 1$ distribution. The MOIST and DRY cooling rates differ even at $\Omega^* = 1$ because the swamp surface of the former yields more moisture than is observed (Fig. 13a and 13b).

The DRY eddies transport momentum poleward across the high-latitude QG_γ jet and converge it on the low-latitude QG_β jet core in both high-range cases (Fig. 22a and 22b). The DRY(2) convergence, however, is not symmetrical: the equatorward flux is stronger aloft and the poleward flux is independent of height (barotropic). The corresponding bimodal vertical flux is also asymmetric and has a very strong downward component, a feature not covered by the $QG_{\gamma,\beta}$ elements (Fig. 23b). These flux asymmetries suggest that waves disperse poleward more easily than equatorward when deep easterlies have been established in low latitudes. The geopotential flux in Fig. 25b confirms the dispersion preference and shows that the waves propagate only as far as the jet border. In the DRY(4) case the wave dispersion is confined to the upper troposphere and the momentum converges uniformly on the QG_β jet (Fig. 22a). The absence of diverging fluxes in low latitudes confirms that no QH mode exists.

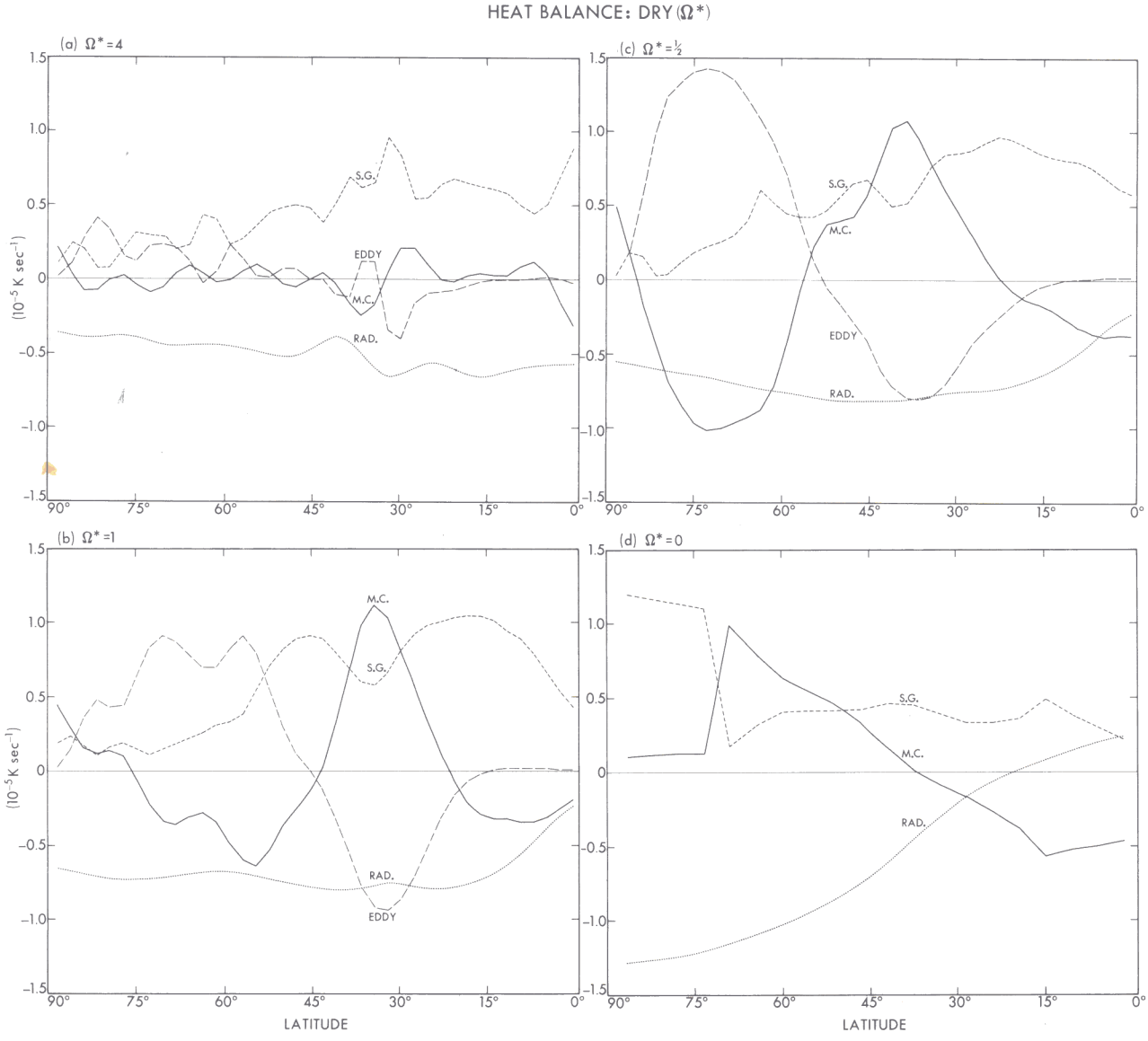

Fig. 29. Latitudinal distribution of the contributions to the mean rate of temperature change by the meridional circulation (M.C.), the radiation (RAD), the eddies (EDDY) and the subgrid-scale exchanges (S.G.) in the DRY model with $\Omega^* = 0$, ½, 1, and 4

5.5 The budgets and balances (Table 4; Figs. 13, 29 and 30)

The heat, momentum and energy balances in the DRY(Ω^*) set involve dynamical variations on the standard DRY(1) theme of Smagorinsky et al. (1965).

Although the DRY global temperatures also remain close to the effective temperature, they involve radiative cooling rates that are generally 50% weaker than the MOIST ones (Table 4). The radiative cooling is especially weak at $\Omega^* = 0$ because the Hadley cell upflow is more effective in cooling low latitudes when it is broad than when it is confined to the equator. According to the heat balance in Fig. 29d, the DRY(0) Hadley cell cools 35° of latitude, whereas the MOIST(0) cell only cools 5° of latitude in Fig. 12d. The cell cools the low-latitude surface so effectively that convection is suppressed and radiation actually produces a net heating of the tropics (in the layer below 700 mb) (Fig. 29d). Clearly, when $\Omega^* = 0$ the radiative-convective approximation to the heat balance is not valid.

The DRY heat balances in Fig. 29 generally lack the complexity and equatorial extremes associated with the MOIST Hadley cells. Furthermore, the dynamical contributions match the radiative-convective amplitude at *all* latitudes, except in the high range. The compensation between the cell and eddy fluxes is most apparent at $\Omega^* = \frac{1}{2}$ and of least consequence at $\Omega^* = 4$. The eddies cool the equatorward side and heat the poleward side of each jet, while the cells do the opposite. The eddies are the main source of heat in high latitudes but are absent from low latitudes where convection balances cooling by radiation and cell upflow. Although the DRY(1) and MOIST(1) radiative coolings in Fig. 13a and 13b are similar, an anomalous surface heating occurs in the DRY tropics because the Hadley cell cools so effectively.

Most properties of the DRY(Ω^*) circulations peak along with the eddy size at $\Omega^* = \frac{1}{2}$, but the strongest surface torques actually occur at $\Omega^* = 1$ because of their direct dependence on the Coriolis force (Table 4). In Fig. 30 the simplicity of the momentum balances in low latitudes again confirms the nonexistence of a Hadley mode. In all cases, it is clear that the eddies accelerate both the westerlies and the easterlies and that the cells create balancing surface torques without advecting much momentum laterally.

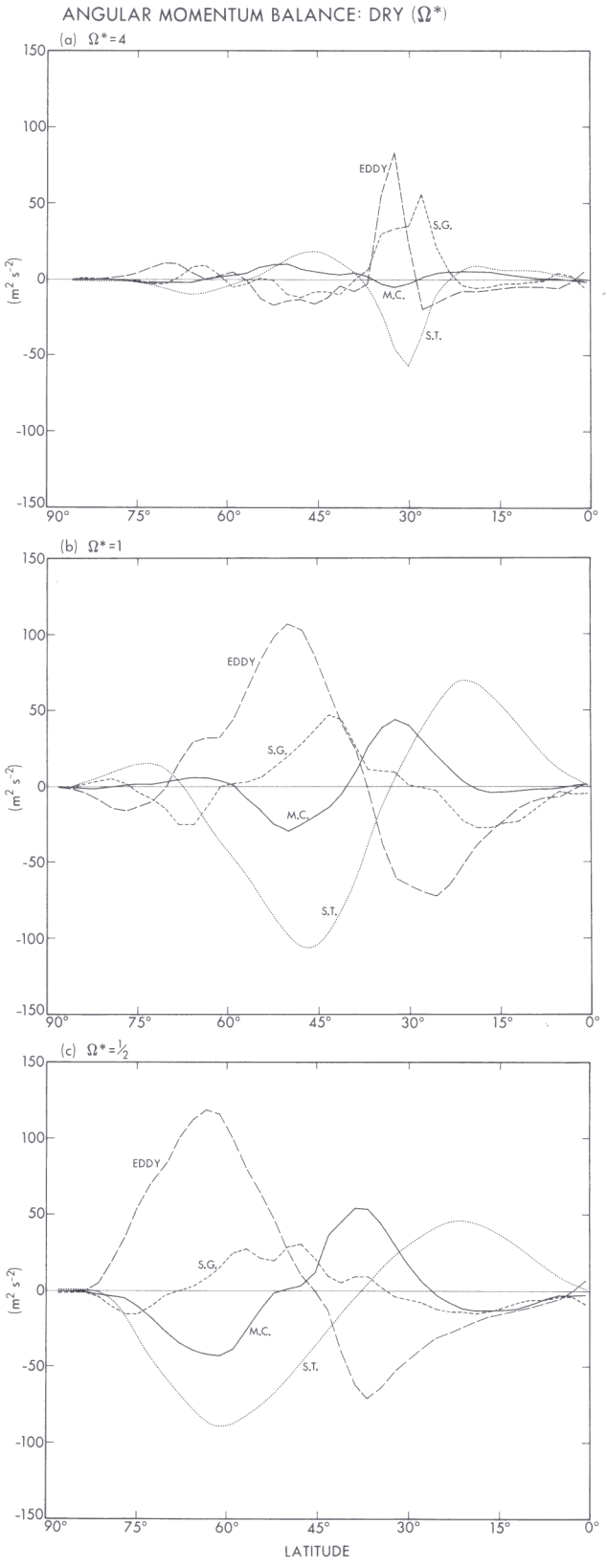

Fig. 30. Latitudinal distribution of the contributions to the mean rate of angular-momentum change by the meridional circulation (M.C.), the eddies (EDDY), the surface torque (S.T.), and the subgrid-scale diffusion (S.G.) in the DRY model with $\Omega^* = \frac{1}{2}$, 1, and 4

6 Modified-surface circulations

We now consider the three special cases that were designed to examine the influence of surface heat and momentum sources on circulation form. In the two SLIP cases, the surface drag is removed from a DRY(1) and a MOIST(4) model and leads to novel flows with a strong barotropic component and powerful tropical easterlies. In the HOT(4D) case, the surface heating is boosted in the low latitudes of a DRY(4) model to see if localized heating imitates latent heating. It does, and an equatorial westerly develops that is in thermal wind balance and is almost axisymmetric. This solution shows that the constraint represented by Hide's (1970) theorem — that an equatorial westerly cannot exist without longitudinal variations — is easily overcome by weak eddies.

6.1 SURFACE-SLIP circulations (Figs. 31 and 32)

To help isolate and identify the QG and QH modes in the MOIST and DRY circulations, we can modify their influence by altering the surface drag. Omitting drag eliminates the surface mo-

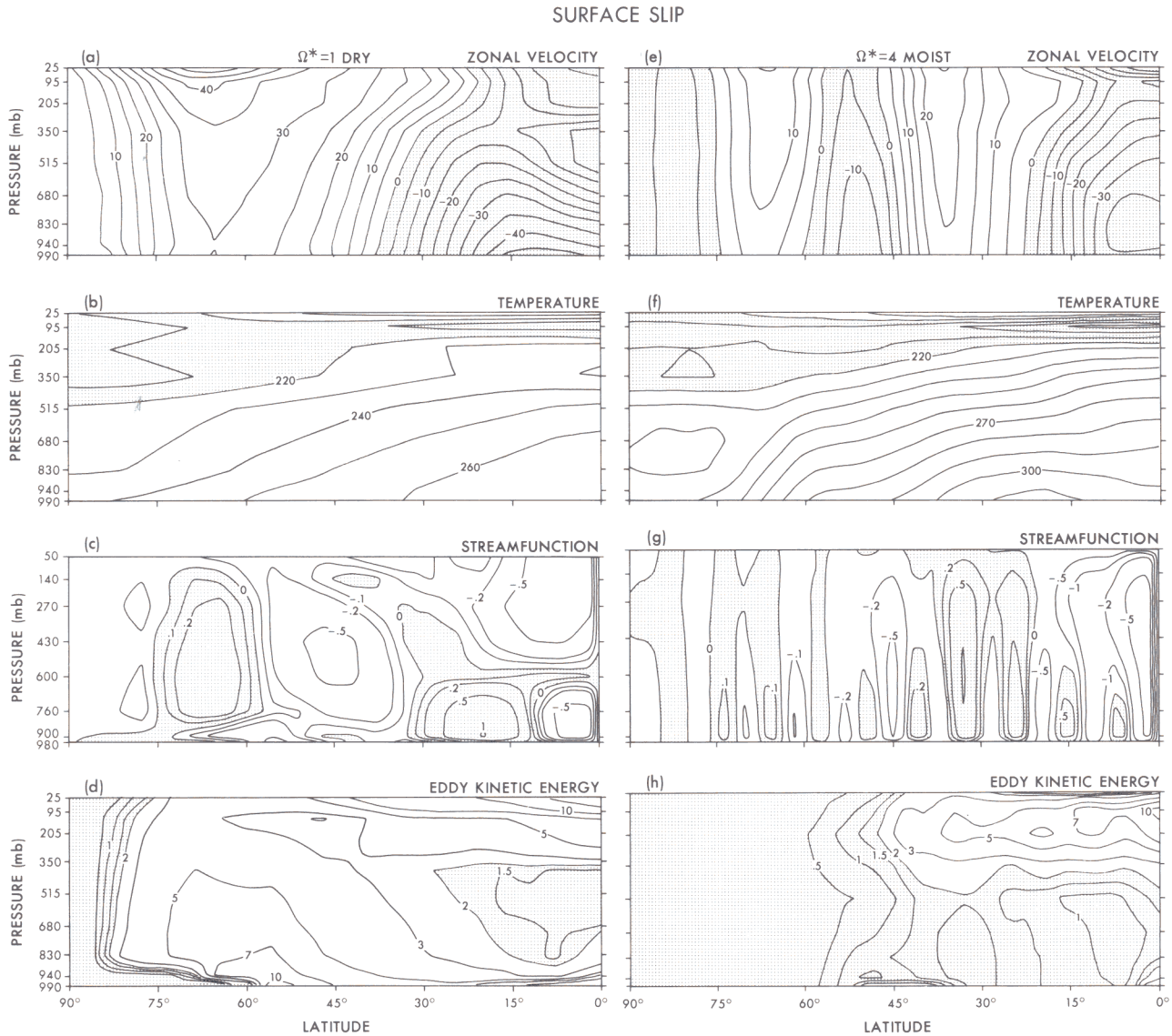

Fig. 31. Meridional distribution of the limited-mean zonal wind, temperature, stream function, and eddy kinetic energy in the DRY-SLIP model with $\Omega^* = 1$ (a–d), and in the MOIST-SLIP model with $\Omega^* = 4$ (e–h). Both models have zero surface drag. Units: m s^{-1}, K, 10^{13} g s^{-1}, 10 J kg^{-1} in (a)–(d) and (e)–(h), respectively

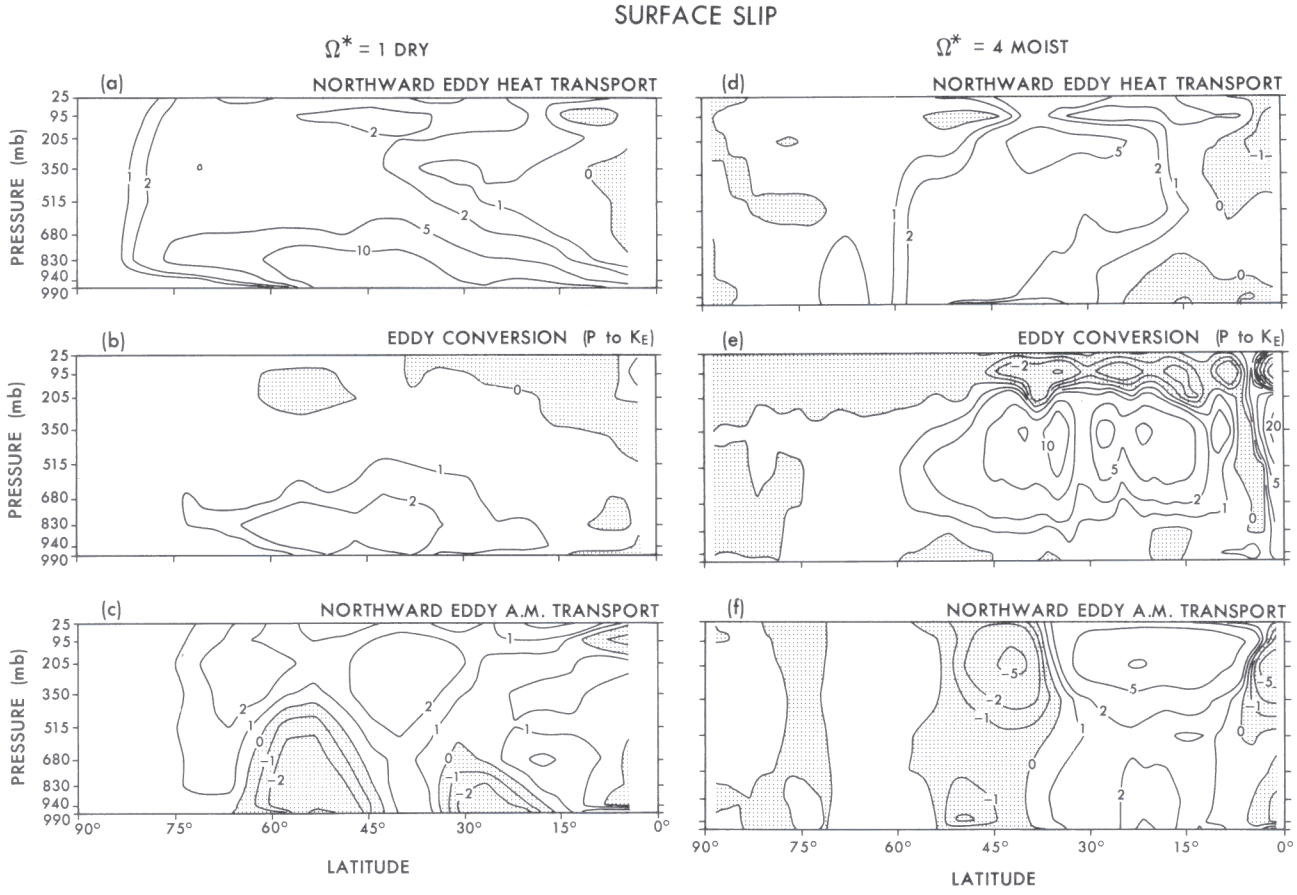

Fig. 32. Meridional distribution of the limited-mean northward heat transport, baroclinic energy conversion, and northward angular-momentum transport — all by the eddies — in the DRY-SLIP model with $\Omega^* = 1$ (a–c) and in the MOIST-SLIP model with $\Omega^* = 4$ (d–f). Both models have zero surface drag. Units: 10^3 J m kg^{-1} s^{-1}, 10^{-4} W kg^{-1}, 10^7 m^3 s^{-2} in (a)–(c) and (d)–(f), respectively

mentum constraint that sustains the QH westerly but liberates the QG westerly from boundary-layer dissipation. Two cases are studied that cover the main range of interest. The SLIP(1D) system uses a DRY(1) model in which the vertical mixing coefficients c_D and κ_V are set to zero for both heat and momentum. The SLIP(4M) system uses a MOIST(4) model in which these coefficients are set to zero only for the momentum exchange; normal values are retained for the heat and moisture exchanges to avoid large changes in the thermodynamical forcing. Neither system equilibrates fully in the 250-day integration period, but the eddy fluxes do level off and the mean flow changes only slowly and only in amplitude, not form.

The SLIP(1D) circulation. The SLIP(1D) zonal flow in Fig. 31a has significant, but not radical, differences from that of DRY(1) in Fig. 16c: the westerly jet lies more poleward but has the same amplitude, and the easterlies are stronger but no more extensive. The westerlies and easterlies have comparable amplitudes and extents and this results in a strong lateral shear and in a zero net internal angular momentum. Such flows also occur in QG_2 and forced barotropic models with slip (Williams 1979b, Fig. 10; 1978, Fig. 8).

The main direct and indirect cells in Fig. 31c lie in the westerly jet and are driven by its baroclinic instability. Because they exist only to compensate the eddy heat flux and not to transfer momentum vertically, they are an order of magnitude weaker than those of DRY(1). A second, shallower, cell pair lies in the easterly jet and is induced either by wave propagation or by a second instability. The planetary eddies have their strongest kinetic energies near the surface — where they are generated but no longer dissipated (Fig. 31d). But without any PBL eddies to mix the heat vertically ($H_s = 0$), the troposphere becomes very stable and cold (Fig. 31b, Table 4).

The strong static stability reduces the QG penetration height $h = f^2 u_z / \beta N^2$ (see § 3.2) and leads to the shallow instability seen in the eddy heat fluxes of Fig. 32a and 32b. The strong lateral shear also stabilizes the westerly jet by increasing the net beta effect $\tilde{\beta} = \beta - \bar{u}_{yy}$. The vertical confinement of the heat fluxes resembles that in the transitional MOIST(¼) state. The instability is not centered on the jet axis but near $\theta = 50°$, and penetrates the easterlies via its lateral heat flux.

The eddy momentum flux in Fig. 32c shows Rossby waves propagating equatorward aloft, transfering easterly momentum to low latitudes as in the DRY(1) case but with a weaker amplitude because of the weaker, shallow source. The negative fluxes in the lower atmosphere are unusual but not unique — they also occur in the transitional DRY(¼) case. They probably reflect the action of shallow linear instabilities in the westerly and easterly jets: the 500-mb synoptic fields show large disturbances near $\theta = 50°$ and smaller ones near $\theta = 30°$. The width of the jets, however, appears to be set more by the domain than by the eddy size.

The main consequence of eliminating the drag is that it allows the barotropic component of the flow to grow and give strong westerly and easterly jets, as in β-turbulence cascades (Williams 1978, 1979b). The thermal wind balance defines the baroclinic component of the flow at all latitudes, so the tropical easterlies peak near the surface. Baroclinic instability generates the eddies whose cascade and propagation produce the barotropic shear. Eventually the lateral shear and vertical stability could become strong enough to suppress the instability and we could end up with steady westerly and easterly jets but with no eddies and no clues as to how the flow originated! Surface drag thus acts to control the barotropic component and, paradoxically, to maintain the instability and the flow history. The influence of drag on other DRY(1) models has been discussed in greater detail by James and Gray (1986).

The SLIP(4M) circulation. Removing drag from the MOIST(4) system while retaining all of the surface heat and moisture exchanges mainly leads to the QH westerly jet being replaced by an eddy-driven easterly jet while the temperature field remains unaltered (Fig. 31e and 31f). In midlatitudes the SLIP(4M) system retains the double jet character of the MOIST(4) state, but with its $QG_\gamma(65°)$ and $QG_\beta(35°)$ jets having a stronger barotropic component and stronger intervening easterlies. The lateral scales remain unaltered, however. A strong direct cell still arises in the tropics but it has a complex form and a dynamics different from that of the SH or QH elements (Fig. 31g). The deep cells and strong eddy fluxes in lower latitudes reflect the strength of the $QG_\beta(35°)$ instability, while the shallow cells and weak eddy fluxes in higher latitudes reflect the weakness of the $QG_\gamma(65°)$ instability (Figs. 31g, h and 32d–f).

Overall, we see that the surface slip has a larger immediate effect on MOIST flows than on DRY, and on low latitudes than on midlatitudes, because it eliminates the Hadley mode but only modifies the QG mode. The barotropic component, with its alternating jets, becomes predominant, so the zonal flow depends less upon whether the instability is strong and deep (as in SLIP(4M)) or weak and shallow (as in SLIP(1D)). Eventually, however, all eddies are suppressed and the midlatitude flows do become fundamentally different. Removing the surface drag shows how much the QH element depends upon it and how much the barotropic mode is suppressed by it. Without drag there is little dynamical difference between the moist and dry systems.

6.2 The ENHANCED-HEATING circulation (Figs. 33–36)

The main differences between moist and dry atmospheres occur in low latitudes because of differences in the nature of their Hadley modes. Moist atmospheres have a strong mode and a tropical westerly jet; dry ones have a weak mode and tropical easterlies. A dry atmosphere might, however, behave more like the moist system if it were subjected to a more-intense, more-local heating in low latitudes. To see if localized heating can imitate latent heating, we add a powerful surface heating to a DRY(4) model with an R15 resolution. This is done by giving Q_e in Eq. (17) an amplitude of 0.25 ly min^{-1} and a form that goes from zero in high latitudes to rapidly increasing values (0.25, 0.5, 0.75, 1.0, 1.0) in low latitudes (20°, 15°, 11°, 7°, 2°). The high rotation is chosen to keep the eddies small and the QG and Hadley processes apart. We refer to the resulting DRY($\Omega^* = 4$, ENHANCED HEATING) solution in Figs. 33–36 as the HOT(4D) case.

The Q_e source produces an intense baroclinicity in low latitudes, eliminates the tropical tropopause, and boosts the global temperature by 10 K (Fig. 33b and Table 4). These changes cause the DRY(4) $QG_\beta(35°)$ jet to move

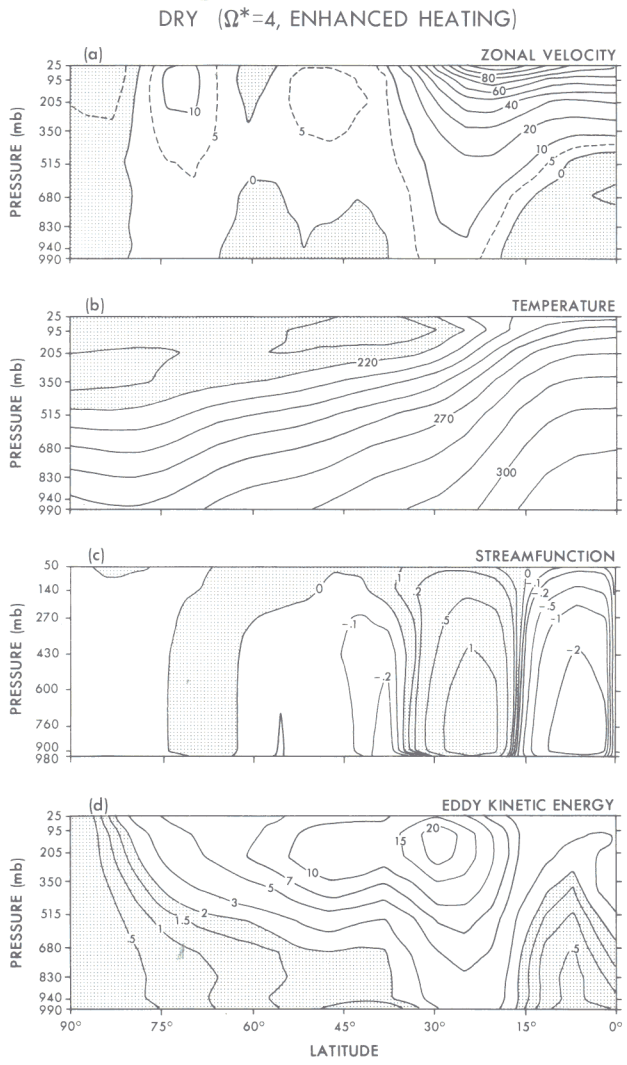

Fig. 33. Meridional distribution of the mean zonal wind, temperature, stream function, and eddy kinetic energy for the DRY model with enhanced surface heating and $\Omega^* = 4$. Units: m s^{-1}, K, 10^{13} g s^{-1}, 10 J kg^{-1} in (a)–(d), respectively

equatorward, evolve into a $QG_\gamma(25°)$ jet, and strengthen from 25 m s^{-1} to 110 m s^{-1} (Fig. 33a). Another big change occurs in low latitudes ($\theta < 15°$) where a strong, latitudinally uniform zonal flow — which we term the Tropical Westerly — arises in the upper atmosphere. The $QG_\gamma(25°)$ jet and the Tropical Westerly merge into a hybrid flow that resembles the low-latitude flows of the MOIST mid- and high ranges. Additional jets form at $\theta = 50°$ and 70°, but are weak.

The Tropical Westerly is associated with a strong direct cell and weak eddies; the $QG_\gamma(25°)$ jet with a strong Ferrel cell and very strong eddies (Fig. 33c and d). The eddies drive the Ferrel cell and the diabatic heating drives the direct cell, a cell that is stronger and better organized than its DRY(4) counterpart. The concentrated vertical flow reflects the strength of the cells, not the heating distribution. The synoptic fields show the strong cyclones and anticyclones centered at $\theta = 25°$ to be 1000 km wide — the smallest scale represented by an R15 model.

The HOT(4D) eddy fluxes in the low latitudes ($\theta < 45°$) of Fig. 34 have much in common with those of the MOIST(1) state, in that: (a) the main release of potential energy occurs in the QG_γ instability; (b) the Rossby waves propagate equatorward into the Tropical Westerly and transfer momentum poleward across the QG_γ jet (thereby defining it); (c) the eddies transport momentum upward in the instability; and (d) the eddies accelerate the QG_γ jet but decelerate the Tropical Westerly. These similarities suggest that the $QG_\gamma(25°)$ jet and the Tropical Westerly have the same dynamics as the hybrid MOIST(1) flow — except near the equator, where the HOT(4D) eddies are much weaker. Elsewhere the HOT(4D) eddies are very strong (but small): their fluxes are on a par with those of the DRY(1) state. The QG_γ form of jet arises even thought the MOIST(4) and DRY(4) systems prefer the QG_β form in low latitudes either because the jet significantly alters the effective $\tilde{\beta}$ or because the waves propagate equatorward so easily in the Tropical Westerly.

The lateral heat balance in Fig. 35 is conventional and resembles that of the MOIST(1) state but without the equatorial extremes: the direct cell cools the tropics and heats the subtropics, while the eddies cool the subtropics and heat the high latitudes. The enhanced surface heat is balanced by a greater radiative cooling in low latitudes. The momentum balance in Fig. 36 also resembles that of MOIST(1) in general but significant differences occur near the equator. In the MOIST(1) case the eddies and surface torque accelerate the equatorial westerlies and are balanced by the lateral cell transport; but in the HOT(4D) case all processes are much weaker and the surface torque alone accelerates the westerly against the eddies, advection, and diffusion. Clearly then, the eddies — explicit or subgrid — do *not* maintain the Tropical Westerly near the equator, at least not directly. Nevertheless, the QG_γ eddies do force the overall momentum balance by accelerating the main jet near $\theta = 25°$ and decelerating the region where the jet and the Tropical Westerly merge near $\theta = 15°$ (Fig. 36). The barotropic conversion in Fig. 34g supports this view of the eddy action.

How then do we explain the existence of the Tropical Westerly, particularly at the equator

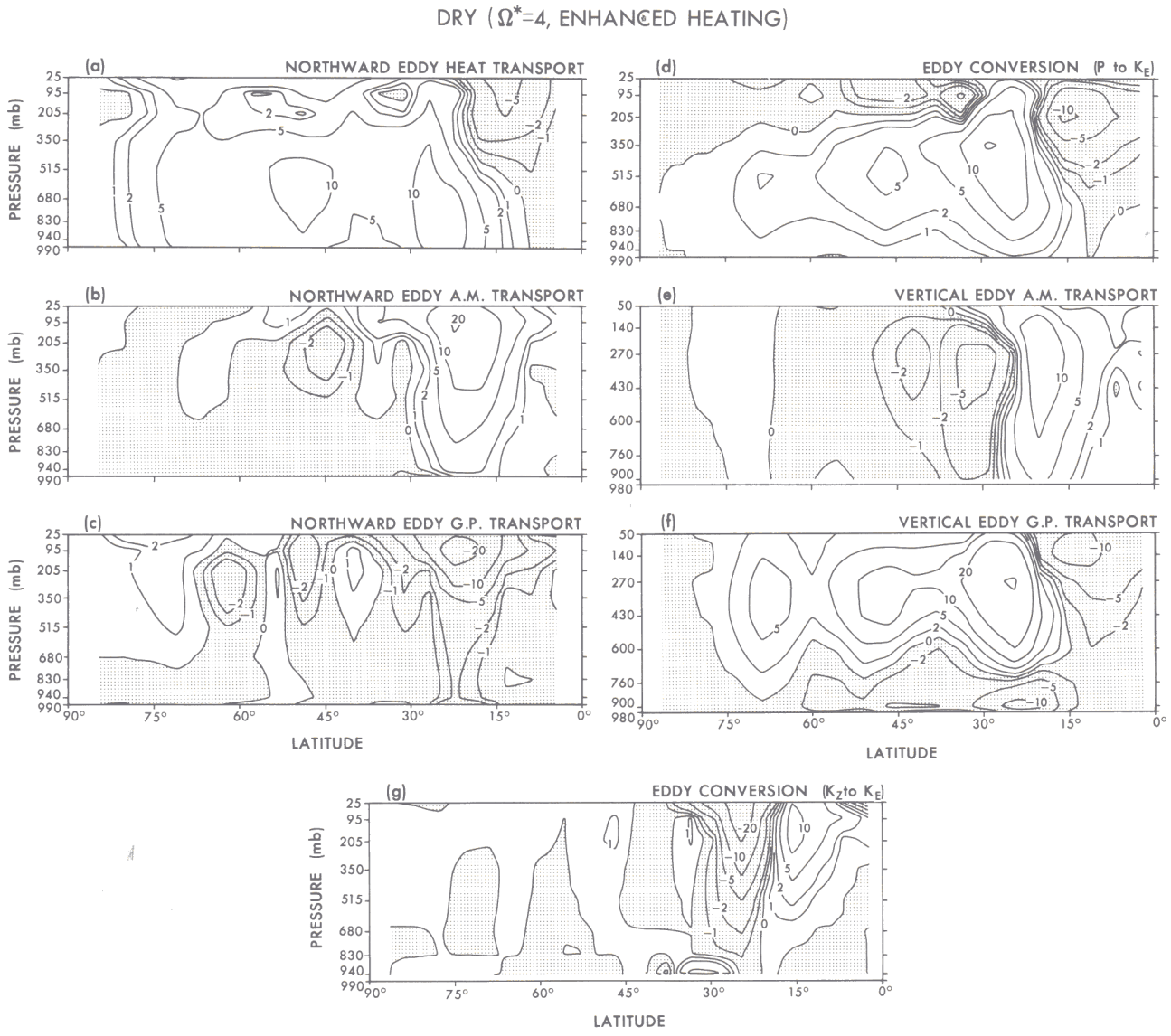

Fig. 34. Meridional distribution of the mean northward heat transport, northward angular-momentum transport, northward geopotential transport, baroclinic energy conversion, vertical angular-momentum transport, vertical geopotential transport, and barotropic energy conversion — all by the eddies — in the DRY model with enhanced surface heating and $\Omega^* = 4$. Units: 10^3 J m kg^{-1} s^{-1}, 10^7 m^3 s^{-2}, 10^2 J m kg^{-1} s^{-1}, 10^{-4} W kg^{-1}, 10^4 kg s^{-2}, 10^{-1} W m^{-2}, 10^{-4} W kg^{-1} in (a)–(g), respectively

where the zonal momentum equation involves only weak terms and gives little guidance? The simplest way is by comparison with the MOIST(1) tropical westerlies. The HOT(4D) Tropical Westerly arises when eddies propagate into low latitudes to create a momentum source in the surface easterlies and when diabatic heating sets up a direct cell strong enough to transport this momentum upward and then poleward. The Tropical Westerly, however, remains relatively free of eddies near the equator, where it is given by the thermal wind balance of the $\bar{v}_t$ equation: $\bar{u}_p = \frac{\hat{R}}{f}\bar{\Theta}_y \to \frac{\hat{R}}{\beta}\bar{\Theta}_{yy}$. Thus the eddies act only indirectly in maintaining the Tropical Westerly by producing the surface momentum source. At the equator weak eddy fluxes are needed to balance the weak $\bar{w}\bar{u}_z$ term in the $\bar{u}_t$ equation, but not to drive the flow itself.

But how can an equatorial westerly that is almost axisymmetric exist without violating Hide's (1970) theorem? In the theory, the axisymmetric angular momentum equation is integrated over an

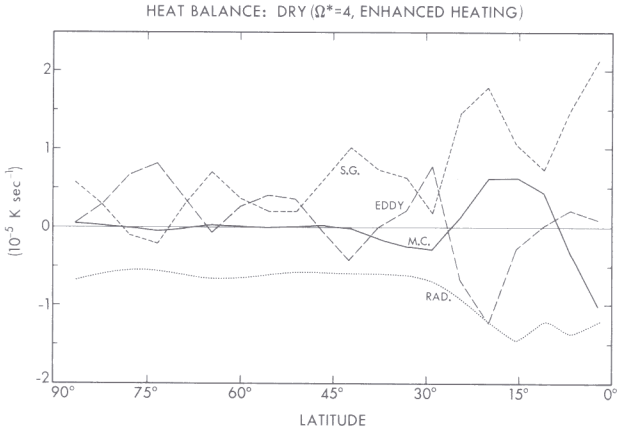

Fig. 35. Latitudinal distribution of the contributions to the mean rate of temperature change by the meridional circulation (M.C.), the eddies (EDDY), the radiation (RAD), and the subgrid-scale exchanges (S.G.) in the DRY model with enhanced surface heating and $\Omega^* = 4$

area enclosing the local angular momentum maximum formed by an upper-level equatorial jet (see Held and Hou 1980). Normally the subgrid diffusive flux out of this region cannot be balanced because the advective flux vanishes, and so such jets cannot exist according to the theorem. The HOT(4D) Tropical Westerly, however, has no lateral shear and has a constant vertical shear and so is nondiffusive for most subgrid-scale formulations. Such profiles are not excluded by the theorem. Furthermore, the constraint represented by the theorem depends on the strength of the subgrid mixing and this is usually weak and easily overcome by weak eddies. Super-rotation occurs in many axisymmetric flows when a thermally driven direct cell passes through a subrotating Ekman layer (Read 1986). The equatorial westerlies seen in many of the GCM solutions are part thermal wind and part eddy forced.

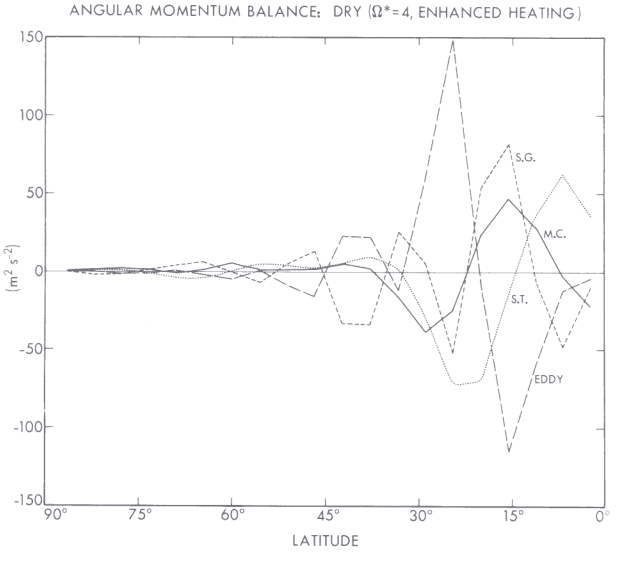

Fig. 36. Latitudinal distribution of the contributions to the mean rate of angular-momentum change by the meridional circulation (M.C.), the eddies (EDDY), the surface torque (S.T.) and the subgrid-scale diffusion (S.G.) in the DRY model with enhanced surface heating and $\Omega^* = 4$

Overall, the various fluxes and balances show the main HOT(4D) flow to be essentially the same as the MOIST(1) flow but with narrower scales and less eddy activity near the equator. The main effect of increasing the surface heating and baroclinicity in the dry system is to strengthen the QG jet and eddies and to produce a diabatically driven Hadley cell and Tropical Westerly. Moisture influences a circulation by making the convective heating more intense, localized, and conditional; effects that strengthen the baroclinicity in the upper-level tropics and drive a strong Hadley cell. Enhanced surface heating in a dry model imitates the first two moisture effects. The third effect cannot be imitated, but the CISK phenomena it produces are not vital to planetary motions. Although moisture is not essential to the generation of equatorial westerlies, it does make it easier.

7 Conclusions

The basic parameter range of global circulations has been derived by varying the rotation rate for moist and dry GCMs. Changing Ω^* is the simplest way of varying the Rossby, Froude, and sphericity numbers that control circulation dynamics by determining the size, strength, and mix of the jets, cells, and eddies. Changing the moisture content alters the strength of the Hadley mode relative to the quasi-geostrophic (QG) modes. Removing the surface drag eliminates the Hadley mode altogether and liberates the QG barotropic mode. The resulting GCM states provide various tests of circulation theory. In Part II, more specialized parameter ranges and the role of various asymmetries are examined.

The basic parametric variability is found to be limited: circulations can be described, to first order, in terms of just four regional components or elements (Fig. 1). At low Ω^* the natural-Hadley (NH) circulation exists with its polar jet, direct cell, and momentum-transferring planetary waves. The waves, driven by tropical moist convection and by polar barotropic cascades, produce a westerly flow in low latitudes. At higher Ω^* baroclinic

instabilities develop in midlatitudes and lead to two forms of QG component: the QG_γ element has an asymmetric (equatorward) wave dispersion and a poleward momentum transport across a diffuse jet; the QG_β element has a symmetric wave dispersion and a momentum convergence into the core of a sharp jet. In low latitudes a quasi-Hadley (QH) component arises with its westerly jet, easterly trade winds and divergent eddy momentum flux, but it survives only in moist atmospheres. The QH eddy fluxes are generated, in part, by a neighboring baroclinic instability and they induce the cell changes that produce the trade winds — such winds are absent and the surface torques are much weaker in the baroclinically stable NH flows.

Circulations in moist atmospheres vary from the single polar jet of the NH element at low Ω^*, to the hybrid jet of the overlapping QG_γ and QH elements at medium Ω^*, to the multiple jets of the polar QG_γ, midlatitudinal QG_β, and tropical QH elements at high Ω^*. Moist circulations are dominated by the Hadley mode and so have their peak kinetic energy at $\Omega^* = 1/8$. The largest QG eddies occur at $\Omega^* = 1/2$ but the largest eddy fluxes occur at $\Omega^* = 1$ because of competition with the Hadley mode. Shallow instabilities occur in the long-wave transition at $\Omega^* = 1/4$, while shallow cells and oscillating jets occur in the short-wave transition at $\Omega^* = 8$. The temperature ranges from near barotropy at $\Omega^* = 0$ to near radiative-convective equilibrium at $\Omega^* = 8$. Moist convection controls the static stability at medium and high Ω^*; cell transport controls it at low Ω^*.

Circulations in dry atmospheres have a similar progression but lack a QH mode and are dominated by QG modes whose kinetic energy and fluxes peak at $\Omega^* = 1/2$. The QG instabilities also generate Rossby waves whose propagation into low latitudes is limited by the easterlies they produce, whereas in moist atmospheres propagation is continuous in the QH westerlies. Circulations without a surface drag develop a strong barotropic component that suppresses instabilities in midlatitudes and produces an easterly jet in low latitudes. Dry atmospheres with a localized low-latitude heating behave like atmospheres with a latent heating, in that similar Hadley cells and tropical westerlies form in both.

Most of the GCM states can be understood in terms of existing circulation theory, beginning with the simple (and isomorphic) two-line geometric descriptions of the SH modes and QG cascades that underlie the mean flows and eddy fluxes of the idealized elements used to simplify the description of the regional and eddy-mean flow interactions. The parallel Ω^*-variation of the MOIST and SH systems suggests that a close connection does exist between the natural and symmetric states, even though it cannot be defined precisely at a particular Ω^* value. At low Ω^*, adding neutral waves to the $SH(R_E > 1)$ mode describes the dynamics of the NH circulation. At medium Ω^*, the thermal-wind part of the $SH(R_E < 1)$ jet becomes unstable and creates a QG_γ jet in midlatitudes by propagating waves into the momentum-wind part, where a QH element forms. At high Ω^*, the thermal-wind part of the $SH(R_E \ll 1)$ mode develops the multiple instabilities that form the polar QG_γ jet and the multiple midlatitudinal QG_β jets while forcing the eddy component of the tropical QH jet. The QH mode prevails in moist circulations because of the robustness imparted to the Hadley cell by its intense, concentrated upflow. The QG mode dominates in dry atmospheres so all cells are then eddy-forced — none are diabatically driven.

The eddy-mean flow interactions within each element can (or could) be understood in terms of the eddy-cycle scenarios describing the linear growth of instabilities and the nonlinear dispersion of planetary waves (see § 3.2). Eddy cycles describe the inhomogeneous form of enstrophy cascade, one more spatial than spectral, that occurs when the turbulent energy supply is sparse and the spectral range narrow. The regional interactions between the eddies and mean flows of adjacent elements are not well defined theoretically. The mean flows could interact in ways that parallel the interplay of the SH momentum and thermal winds. The regional eddy interactions appear to be more baroclinic than barotropic, according to the hemispheric $\overline{v'T'}$ and local $\overline{v'M'}$ fluxes.

Our interpretation of the GCM solutions using standard circulation theory leads us to believe that the theory is well founded, that there are no flaws — only disunity and limits at the extremes of the parameter range. To make the theory more complete, the following fundamental questions need to be addressed:

1) What are the equilibrated eddy cycles like for atmospheres with SH basic states at various Ω^*? (Normal eddy cycles are based on arbitrary zonal flows, lack a Hadley component and do not equilibrate.) Such a study could explain the wave propagation in the NH and QH components, the wave dispersion in the $QG_{\gamma,\beta}$ components, the element interactions, and the connection between the natural and SH states. For the long-wave transition at $\Omega^* = 1/4$, it could explain how the Hadley

cell is disconnected in dry atmospheres by a shallow instability and how thermal winds become hemispheric and give equatorial westerlies. For the short-wave transition at $\Omega^* = 8$, it could explain the oscillation of the QH jet.

2) What are the eddy cycles like for the instabilities of specified zonal flows on equatorial beta-planes? These could explain the switch from symmetric to asymmetric wave dispersion. Baroclinic instability on the equatorial beta-plane has never been studied.

3) What is the baroclinic instability of double jets like? This could explain why the $\overline{v'T'}$ flux is hemispheric and the $\overline{v'M'}$ flux is local, and how QG jets generally interact and coexist.

4) What determines the lateral scale of jets? When do the eddy scale L_R of baroclinic jets and the turbulent scale L_β of barotropic jets prevail? When do the wave dispersion, domain size, and SH mode influence jet widths? Studies of problem (1) could answer some of these questions.

5) How do the planetary waves generated by baroclinic instabilities develop the blocking easterlies of dry atmospheres and the easterly trade winds of moist atmospheres?

6) What is the *numerical* SH state like when cyclostrophy controls the meshing of the thermal and momentum winds at low Ω^*? This could explain the complex cell downflows in the NH and transitional circulations.

7) What is the baroclinic instability of cyclostrophic jets like? The shallow transitional instability at $\Omega^* = \frac{1}{4}$ may be as much cyclostrophic as geostrophic.

8) What are the theoretical and numerical SH states like at large Ω^*, where θ_H is small and the momentum balance nonlinear? This could explain the amplitude oscillation of the circulation for the short-wave transition at $\Omega^* = 8$ and the nature of flows in the limit $\Omega^* \to \infty$.

In Part II, further problems in circulation dynamics arise and concern: (a) the solstitial symmetric-Hadley (SSH) circulation; (b) the eddy cycle for the unstable easterly jet of the SSH summer hemisphere; (c) the role of latent heating in axisymmetric GCM states; (d) the transition between Hadley and Halley circulations for diurnally heated atmospheres; and (e) the influence of vertical structure on circulation form. Solutions to these and other problems may lead eventually to a simpler, more fundamental explanation of multiple circulations than that presented here.

For Earth, whose surface gives it characteristics somewhere between those of the DRY and MOIST systems, the GCM solutions tell us — among other things — that the atmosphere may be close to changing to a double jet system and that transitional phenomena — as yet unidentified — may exist. A question often raised about the midlatitude dynamics of the atmosphere — do the eddies increase or decrease the eddy-free zonal flow — is not a useful one because the answer depends on thermodynamical factors such as the radiative time scale and the surface heat capacity (see Part II, § 2). The eddies do not sense the symmetric state, just as they do not sense the seasonal cycle, because the dynamical time scale of the natural state is much shorter. The relation between the eddies and the zonal mean state, however, is easier to assess: QG turbulence theory tells us that planetary cascades increase the barotropic component of a zonal flow but decrease its baroclinic component. For Earth, the surface drag limits the barotropic growth, while the oceanic and solar heating replenish the baroclinic component. The net result is that the eddies moderately accelerate the mean flow. For Jupiter and other weakly dissipated systems, the barotropic component is liberated and the eddy cascades produce jets that greatly exceed the symmetric ones.

From a planetary perspective, Earth appears to have a complex but relatively limited circulation. Its large-scale motions are restricted by their narrow spectral range and by the size and surface of the planet. Other planets may have more varied and more complete forms of circulation that — like the oceans — press the development of geophysical fluid dynamics and GCMs into new regions of parameter space.

Acknowledgements. This study owes an enormous debt to Leith Holloway for creating the various GCM computer codes with which the calculations were made. Without his legendary programming expertise, this project would not have been feasible. To him, I express my greatest thanks. I am also grateful to Syukuro Manabe for guidance in model design, to Douglas Hahn for analysis advice, to Richard Wetherald for radiation assistance, to the GFDL computer staff for implementing innumberable ASC jobs, to John Wilson for computing an extra CYBER case, to Philip Tunison for co-ordinating the drafting, to John Connor for photography, and to Wendy Marshall and Joan Pege for patient, skillful typing. The difficult task of describing such a slew of circulations was eased by the constructive comments of Larry Gates, Gabriel Lau, and an anonymous reviewer. Preliminary results were presented at the General Circulation Symposium held at Reading University in August, 1981, and at the Venus Circulation Workshop held at NASA-Ames Research Center in November, 1981.

Appendix

Two-level quasi-geostrophic circulations

The Ω-variability of midlatitude circulations, and the role of β processes in their dynamics, is readily given by the two-level

quasi-geostrophic (QG_2) model of Phillips (1956). This model integrates the potential-vorticity equation using finite-difference techniques (Williams 1979a) and standard terrestrial parameter values (case A2, Williams 1979b):
$\Omega = 0.73 \times 10^{-4}\ s^{-1}$, $f_0 = 10^{-4}\ s^{-1}$, $\beta = 0.16 \times 10^{-7}\ km^{-1}\ s^{-1}$, $L_R = 820$ km, $\tau_D = 2.5$ days, $\nu = 0.05\ km^2\ s^{-1}$, $X = 24 \times 10^3$ km, $Y = 10^4$ km, $R = 0.29 \times 10^{-3}\ km^2\ s^{-2}\ K^{-1}$, $a = 6000$ km, $H = 8$ km for the rotation rate, Coriolis term, Coriolis gradient, deformation radius, drag time scale, horizontal diffusion, longitudinal extent, latitudinal extent, specific gas constant, radius, and scale height, respectively. The system is driven by a prescribed latitudinally linear heating function with an amplitude ($H_a = 10^{-9}\ km^2\ s^{-3}$) that heats and cools the extremities of the channel at a rate of $\pm \frac{1}{4}$ K per day. There are 64 grid-points in latitude and 128 in longitude (Table 1).

In column 3 of Fig. 37, Ω^* is varied from ½ to 4 about

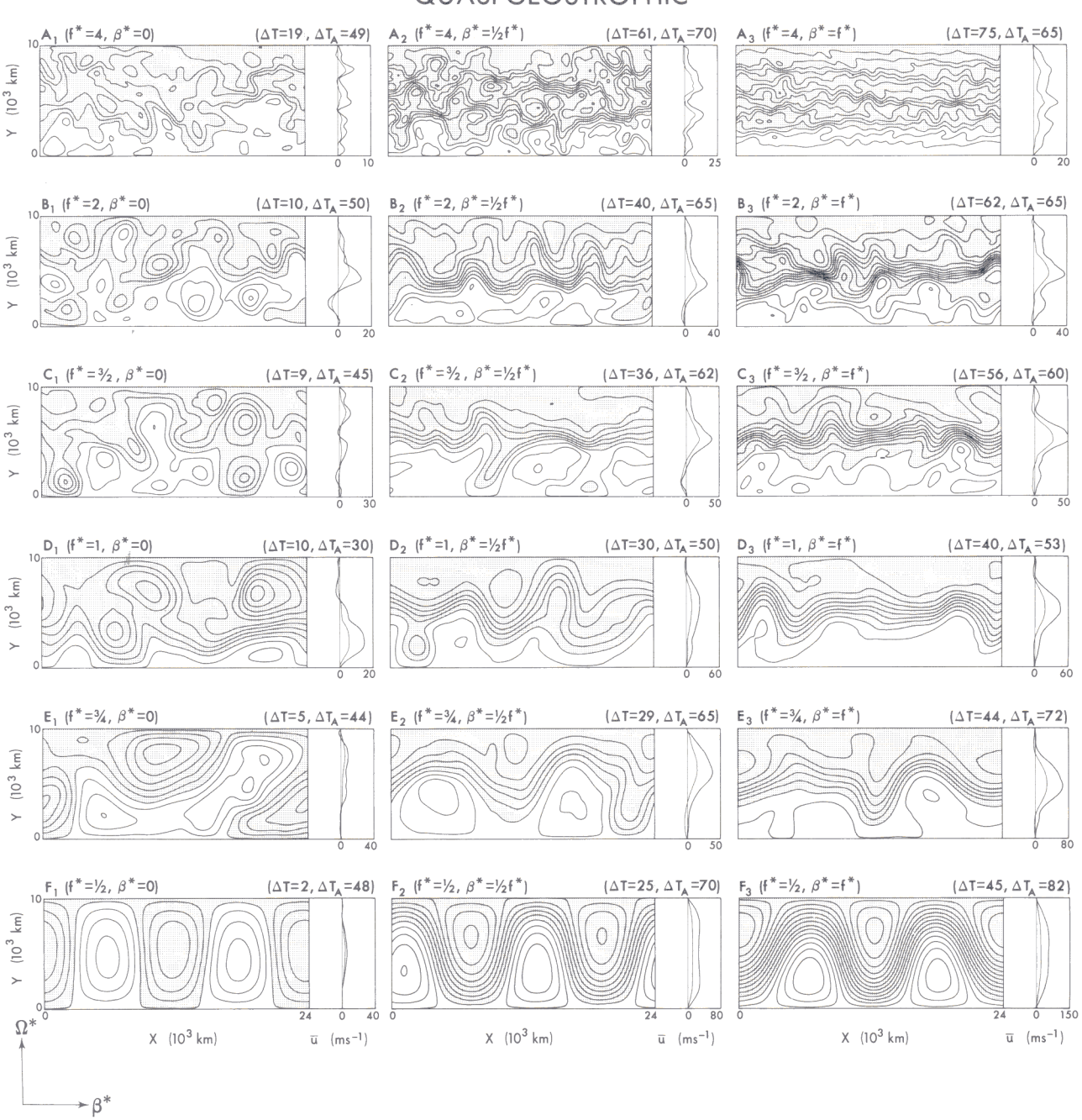

Fig. 37. Quasi-geostrophic circulations as a function of $\Omega^* \equiv (f^*, \beta^*)$ and β^*. In column 1, Ω^* varies from ½ to 4; in column 2, β^* is half of its column 3 values; in column 1, $\beta^* = 0$. Negative values of the upper-layer stream function are *shaded*. Contour intervals, in $km^2\ s^{-1}$, are: 4 for A_1; 6 for A_2; 5 for A_3; 10 for B_1, B_2, B_3, C_1 and D_1; 15 for C_2 and C_3; 20 for D_2, D_3 and E_1; 30 for E_2; 40 for E_3, F_1, F_2 and D_3. Profiles of mean zonal flows at both levels (heavier is upper) are shown at the *right*

the standard terrestrial case, D_3, in the fourth row. The figure shows the instantaneous upper-level flows after 2 months of development from unstable axisymmetric states. When Ω^* increases, the eddies and jets decrease in size, transfer less heat, and allow a larger ambient baroclinicity, ΔT, across the channel. Although three jets form when $\Omega^* = 4$, they are not as well defined as in the drag-free case because the eddy cascade is less complete (cf. Williams 1979b, Fig. 14). When Ω^* decreases, the eddies become as wide as the channel and give a regular flow (F_3) because cascades are limited. Such flows require a larger initial baroclinicity (ΔT_A) to induce instability. Stone's (1978) suggestion that flows adjust toward the critical baroclinicity, ΔT_c ($= 35$ K) given by linear theory, works best when the eddies are efficient but not so large or small that their development is restricted, i.e., when $\Omega^* \sim 1$.

In column 2 of Fig. 37 the β^* values of column 3 have been halved. This makes the circulations more irregular because the eddies are more energetic when ΔT_c is reduced to 18 K. Although more energy is available, the jets are weaker because the β-wave focusing effect is weaker. In column 1 of Fig. 37 with $\beta^* = 0$, the eddies are energized continuously ($\Delta T_c = 0$) and they dominate these f_0-plane flows. Only the strong surface drag prevents the eddies from cascading into domain-size gyres (cf. Williams 1979b, Fig. 11).

The f_0-plane initial states require a large baroclinicity before they become unstable, even though the final values are small. This suggests that the procedure of perturbating an axisymmetric state is not relevant and that the instabilities are of the wave-resonance rather than the Raleigh type (cf. Gill 1974). Baroclinic adjustment is limited by the surface dissipation to a final ΔT of 2 K for the large eddies and 20 K for the small eddies. When the f_0-plane eddies are domain-size at $f^* = \frac{1}{2}$, they produce a regular flow (F_1) but, unlike the corresponding β-plane cases, there is almost no mean flow. Laboratory annulus flows differ from these f_0-plane flows because their thermal boundary layers maintain a stronger axisymmetric component (Williams 1971).

Clearly, zonal currents cannot form without the β-effects that limit the baroclinic energy supply and develop the waves that focus the energy into the zonal mode. Circulation variability in the QG_2 model parallels that in the GCM, with a transition to baroclinic stability near $\Omega^* = \frac{1}{4}$ and to radiative balance near $\Omega^* = 8$.

References

Andrews DG (1985) Wave-mean-flow interaction in the middle atmosphere. Adv Geophys 28A:249–275

Andrews DG, McIntyre ME (1976) Planetary waves in horizontal and vertical shear: The generalized Eliassen-Palm relation and mean flow acceleration. J Atmos Sci 33:2031–2048

Baines PG (1976) The stability of planetary waves on a sphere. J Fluid Mech 73:193–213

Basdevant C, Legras B, Sadourny R, Beland M (1981) A study of barotropic model flows: Intermittency, waves and predictability. J Atmos Sci 38:2305–2326

Charney JG (1947) The dynamics of long waves in a baroclinic westerly current. J Meteor 4:135–163

Dickinson RE (1978) Rossby waves — long period oscillations of oceans and atmospheres. Ann Rev Fluid Mech 10:159–195

Edmon HJ, Hoskins BJ, McIntyre ME (1980) Eliassen-Palm cross-sections for the troposphere. J Atmos Sci 37:2600–2616

Gill AE (1974 The stability of planetary waves on an infinte beta-plane. Geophys Fluid Dyn 6:29–47

Gordon CT, Stern WF (1982) A description of the GFDL global spectral model. Mon Weather Rev 110:625–644

Haltiner GJ, Williams RT (1980) Numerical prediction and dynamic meteorology. Wiley, New York, 477 pp

Hayashi Y (1974) Spectral analysis of tropical disturbances appearing in a GFDL general circulation model. J Atmos Sci 31:180–218

Held IM (1978) The vertical scale of an unstable baroclinic wave and its importance for eddy heat flux parameterizations. J Atmos Sci 35:572–576

Held IM, Andrews DG (1983) On the direction of eddy momentum flux in baroclinic instability. J Atmos Sci 40:2220–2231

Held IM, Hoskins BJ (1985) Large-scale eddies and the general circulation of the troposphere. Adv Geophys 28A:3–31

Held IM, Hou AY (1980) Nonlinear axially symmetric circulations in a nearly inviscid atmosphere. J Atmos Sci 37:515–533

Hide R (1970) Equatorial jets in planetary atmospheres. Nature 225:254

Hollingsworth A (1975) Baroclinic instability of a simple flow on the sphere. Q J Roy Meteorol Soc 101:495–528

Holloway JL, Manabe S (1971) Simulation of climate by a global general circulation model. Mon Weather Rev 99:335–370

Hunt BG (1979a) The influence of the Earth's rotation rate on the general circulation of the atmosphere. J Atmos Sci 36:1392–1408

Hunt BG (1979b) The effects of past variations of the Earth's rotation rate on climate. Nature 281:188–191

Hunt BG (1982) The impact of large variations of the Earth's obliquity on the climate. J Meteorol Soc Japan 60:309–318

James IN, Gray LJ (1986) Concerning the effect of surface drag on the circulation of a baroclinic planetary atmosphere. Q J Roy Meteorol Soc 112:1231–1250

Kraichnan RH (1967) Inertial ranges in two-dimensional turbulence. Phys Fluids 10:1417–1423

Leovy CB (1985) The general circulation of Mars: models and observations. Adv Geophys 28A:327–346

Lorenz EN (1967) The nature and theory of the general circulation of the atmosphere. WMO, No. 218, TP. 115, 161 pp

Lorenz EN (1969) The nature of the global circulation of the atmosphere: a present view. In: Corby GA (ed) The global circulation of the atmosphere, Roy. Meteorol. Soc., London, pp 2–23

Manabe S, Holloway JL (1975) The seasonal variation of the hydrologic cycle as simulated by a global model of the atmosphere. J Geophys Res 80:1617–1649

Manabe S, Strickler RF (1964) Thermal equilibrium of the atmosphere with a convective adjustment. J Atmos Sci 21:361–385

Manabe S, Wetherald RT (1967) Thermal equilibrium of the atmosphere with a given distribution of relative humidity. J Atmos Sci 24:241–259

Manabe S, Smagorinsky J, Strickler RF (1965) Simulated climatology of a general circulation model with a hydrologic cycle. Mon Weather Rev 93:769–798

Manabe S, Holloway JL, Stone HM (1970) Tropical circulation in a time-integration of a global model of the atmosphere. J Atmos Sci 27:580–613

Manabe S, Smagorinsky J, Holloway JL, Stone HM (1970) Simulated climatology of a general circulation model with a hydrologic cycle. Part 3. Effects of increased horizontal computational resolution. Mon Weather Rev 98:175–212

Miyakoda K (1973) Cumulative results of testing a meteorological-mathematical model: Description of the model. Proc Roy Irish Acad 73A:99–130

Phillips NA (1956) The general circulation of the atmosphere: A numerical experiment. Q J Roy Meteorol Soc 82:123–164

Plumb RA (1983) A new look at the energy cycle. J Atmos Sci 40:1669–1688

Plumb RA (1986) Three-dimensional propagation of transient quasi-geostrophic eddies and its relationship with the eddy-forcing of the time-mean flow. J Atmos Sci 43:1657–1678

Read PL (1986) Super-rotation and diffusion of axial angular momentum: II. A review of quasi-axisymmetric models of planetary atmospheres. Q J Roy Meteorol Soc 112:253–272

Rhines PB (1975) Waves and turbulence on a beta plane. J Fluid Mech 69:417–443

Rhines PB (1977) The dynamics of unsteady currents. In: McCave IN, O'Brien JJ, Steele JM (eds) The Sea, Vol. 6. Wiley, New York, pp 189–318

Rossow WB (1985) Atmospheric circulation of Venus. Adv Geophys 28A:347–379

Salmon R (1982) Geostrophic turbulence. In: Topics in ocean physics, Proceedings of the 'Enrico Fermi' Summer School Ital. Phys. Soc., North-Holland Publ., Amsterdam, pp 30–78

Schneider EK (1977) Axially symmetric steady state models of the basic state for instability and climate studies. Part 2. Nonlinear calculations. J Atmos Sci 34:280–296

Simmons AJ (1974) The meridional scale of baroclinic waves. J Atmos Sci 31:1515–1525

Simmons AJ, Hoskins BJ (1976) Baroclinic instability on the sphere: Normal modes of the primitive and quasi-geostrophic equations. J Atmos Sci 33:1454–1477

Simmons AJ, Hoskins BJ (1978) The life cycles of some nonlinear baroclinic waves. J Atmos Sci 35:414–432

Simmons AJ, Hoskins BJ (1980) Barotropic influences on the growth and decay of nonlinear baroclinic waves. J Atmos Sci 37:1679–1684

Smagorinsky J (1963) General circulation experiments with the primitive equations. I. The basic experiment. Mon Weather Rev 91:99–164

Smagorinsky J, Manabe S, Holloway JL (1965) Numerical results from a nine-level general circulation model of the atmosphere. Mon Weather Rev 93:727–768

Stone PH (1978) Baroclinic adjustment. J Atmos Sci 35:561–571

Uryu M (1980) Acceleration of mean zonal flows by planetary waves. Pure Appl Geophys 118:661–693

Wallace JM, Lau N-C (1985) On the role of barotropic energy conversions in the general circulation. Adv Geophys 28A:33–74

Williams GP (1971) Baroclinic annulus waves. J Fluid Mech 49:417–449

Williams GP (1978) Planetary circulations: 1. Barotropic representation of Jovian and terrestrial turbulence. J Atmos Sci 35:1399–1426

Williams GP (1979a) Planetary circulations: 2. The Jovian quasi-geostrophic regime. J Atmos Sci 36:932–968

Williams GP (1979b) Planetary circulations: 3. The terrestrial quasi-geostrophic regime. J Atmos Sci 36:1409–1435

Williams GP (1985) Jovian and comparative atmospheric modeling. Adv Geophys 28A:381–429

Williams GP, Holloway JL (1982) The range and unity of planetary circulations. Nature 297:295–299

Received August 28, 1986/Accepted January 8, 1988